Technical Report

TR-02-27

Formation factor logging in-situ by electrical methods

Background and methodology

Martin Löfgren, Ivars Neretnieks
Department of Chemical Engineering and Technology,
Royal Institute of Technology

October 2002

Svensk Kärnbränslehantering AB
Swedish Nuclear Fuel
and Waste Management Co
Box 5864
SE-102 40 Stockholm Sweden
Tel 08-459 84 00
+46 8 459 84 00
Fax 08-661 57 19
+46 8 661 57 19

Formation factor logging in-situ by electrical methods

Background and methodology

Martin Löfgren, Ivars Neretnieks
Department of Chemical Engineering and Technology,
Royal Institute of Technology

October 2002

Keywords: Matrix diffusion, Formation factor, In-Situ, Geophysical logging, KLX02

Abstract

Matrix diffusion has been identified as one of the most important mechanisms governing the retardation of radionuclides escaping from a deep geological repository for nuclear waste. Radionuclides dissolved in groundwater flowing in water-bearing fractures will diffuse into water filled micropores in the rock. Important parameters governing the matrix diffusion are the formation factor, the surface diffusion and sorption. This report focuses on the formation factor in undisturbed intrusive igneous rock and the possibility of measuring this parameter in-situ. The background to and the methodology of formation factor logging in-situ by electrical methods are given. The formation factor is here defined as a parameter only depending on the geometry of the porous system and not on the diffusing specie. Traditionally the formation factor has been measured by through diffusion experiments on core samples, which are costly and time consuming. It has been shown that the formation factor could also be measured by electrical methods that are faster and less expensive. Previously this has only been done quantitatively in the laboratory on a centimetre or decimetre scale.

When measuring the formation factor in-situ in regions with saline groundwater only the rock resistivity and the pore water resistivity are needed. The rock resistivity could be obtained by a variety of geophysical downhole tools. Water-bearing fractures disturb the measurements and data possibly affected by free water has to be sorted out. This could be done without loosing too much data if the vertical resolution of the tool is high enough. It was found that the rock resistivity tool presently used by SKB are neither quantitative or have a high enough vertical resolution. Therefore the slimhole Dual-Laterolog from Antares was tested with good results. This tool has a high vertical resolution and gives quantitative rock resistivities that need no correction. At present there is no method of directly obtaining the pore water resistivity. Therefore the approximation was made that the pore water is in equilibrium with free groundwater at a corresponding depth. The electrical conductivity of groundwater flowing from isolated fractures was measured with the Posiva difference flow meter.

In order to test the proposed methodology all necessary logs were obtained by SKB from the 1.7 km deep borehole KLX02 in Laxemar, Sweden. The report contains many examples of these logs and also describes the tools. From the logs a step by step procedure how to obtain a formation factor log is shown. In order to verify that the obtained in-situ formation factor log was quantitative a great number samples were taken from the borehole core. The formation factor of these bore core samples was measured in the laboratory with electrical methods. The comparison between the in-situ and laboratory formation factor logs was encouraging. Both logs clearly displayed the same geological features in a similar manner. The in-situ formation factors were on average about 1/3 of the laboratory formation factors, which is consistent with earlier work on rock stress effects on cores.

Extensive summary

When making a safety assessment for a deep geological repository for nuclear waste, radionuclide transport through rock is of great importance. Lately matrix diffusion has been identified as one of the most important mechanisms governing the retardation of the radionuclide transport in rock. Radionuclides that have escaped from a repository will mainly be transported in water-bearing fractures through the rock. The surrounding rock is porous and the radionuclides will diffuse into the water filled micropores and thus be withdrawn from the water flow that could otherwise carry them to the biosphere. Important parameters governing the matrix diffusion are the formation factor, surface diffusion and sorption. This report focuses on the formation factor in undisturbed intrusive igneous rock and the possibility of measuring it in-situ. The formation factor is here defined to depend only on the geometry of the porous system and not of the diffusing specie.

Traditionally the formation factor has been measured by through diffusion experiments on bore core samples, which are costly and time consuming. It has been shown that the formation factor could also be measured by electrical methods that are faster and less expensive. Previously this has only been done quantitatively in the laboratory and in a centimetre or decimetre scale, typically on core samples from core drilled boreholes. Three key parameters are needed in obtaining the formation factor: the undisturbed rock resistivity, the pore water resistivity, and the contribution from surface conduction. The contribution from surface conduction becomes small in saline environments. A new method of obtaining formation factors in-situ would be valuable as one would be able to obtain formation factor logs with a high vertical resolution both time and cost effectively, even in comparison with electrical methods in the laboratory. This would also give formation factors at natural conditions, such as the rock stress. The drawback is that one loses the ability of controlling the chemical composition of the pore water. Another drawback is that the sampling volume is less defined in-situ. In addition it would be hard to measure the formation factor in alteration zones around water-bearing fractures as the free water disturbs the measurements.

The aim of this report is to give the background of formation factor logging in-situ by electrical methods but also to present a recently developed methodology. An introduction to the theory of diffusion, electrical conduction and electrical field are given. Furthermore some elementary geology and groundwater chemistry are presented. An overview of useful geophysical tools, especially rock resistivity tools, are given. Modern tools are compared with the tools used by SKB at present. Especially the usefulness, or rather lack of usefulness, of the rock resistivity tool used by SKB at present has been investigated, both by examining the theory that they are based on and also by examining data from in-situ campaigns.

Data from two newly performed in-situ logging campaigns in the borehole KLX02 in Laxemar, Sweden is presented. Rock resistivity data was obtained with the slimhole Dual-Laterolog from Antares during September 2000 and groundwater flow and groundwater electrical conductivity data was obtained with the Difference flow meter from Posiva during spring 2000. Furthermore, data from SICADA has been used. When obtaining the rock resistivity, not only the accuracy of the measurements but also the vertical resolution is of greatest importance. Water-bearing fractures will greatly affect the rock resistivity measurements and therefore data possibly affected by fractures have to be sorted out. In identifying this data, information from the core log and the caliper log has been used in combination with groundwater flow data. It is shown that when the vertical resolution of the rock resistivity tool is only a few decimetres, the data affected by water-bearing fractures could effectively be sorted out without loosing too much data even in fractured rock.

At present it is not possible to directly measure the pore water resistivity in-situ. In earlier work the borehole fluid resistivity has been used as an approximation of the pore water resistivity at a corresponding depth. This approximation is not valid in general. Instead another approximation has been made that the pore water is in equilibrium with groundwater withdrawn from fractures at a corresponding depth. It is not clear how the drilling of a borehole and extensive pumping disturbs the natural groundwater situation in the fractures and therefore care should be taken when using this approximation. The Posiva difference flow meter can isolate a single fracture from where groundwater is withdrawn. The electrical conductivity of this groundwater (fracture specific EC) is then measured. This was done in the borehole KLX02 in Laxemar, Sweden. The fracture specific EC was only measured in fractures with a flow higher than 1.5 l/h. In regions with many fractures having a flow higher than this, a reasonable groundwater conductivity profile could be obtained. In other sections where most or all of the fractures had a flow lower than 1.5 l/h no fracture specific EC was measured and creating groundwater electric conductivity profiles became quite speculative. This shows the necessity of choosing fractures not only on the basis of the flow but also on their position. It also shows the necessity of further developing the tool in order to lower the flow limit where fracture specific EC could be measured.

From the above-mentioned campaigns and from the bore core log of KLX02, a formation factor log of the section 349-400 m was created. A step by step procedure of how this was done is shown. Surface conduction was not taken into account when making the formation factor log. The obtained in-situ log seemed very reasonable, as the formation factors of granite were comparable with values in previous works (in the order 10^{-5} - 10^{-4}) and the log clearly follows geological features such as rock type changes. In order to validate the in-situ method a great number of rock samples were taken from the borehole core. The formation factor of these samples was measured in the laboratory by electrical methods. The comparison of the in-situ and laboratory formation factor logs was quite encouraging showing that the in-situ log was quantitative, perhaps with a systematic error. The in-situ formation factors were found to be about 35% of the laboratory formation factors, even if the figure is quite uncertain it is consistent earlier work on rock stress effects on the formation factor.

Although this report contains a great number of results and graphs, their purpose are to show important features in formation factor logging. Therefore, when reading this report it should be kept in mind that the focus has been on the methodology and not on the results.

Sammanfattning

Matrisdiffusion har identifierats som en av de viktigaste retardationsmekanismerna för radionuklider som transporteras från ett geologiskt djupförvar för utbränt kärnbränsle till biosfären. Radionuklider lösta i grundvatten som flödar i öppna sprickor kommer diffundera in i vattenfyllda mikroporer i bergmatrisen. Matrisdiffusionen är bl. a. beroende av bergets formationsfaktor, ytdiffusion och sorbtion. Den här rapporten fokuserar på formationsfaktorn i ostört magmatiskt berg och möjligheten att mäta denna parameter in-situ. Här ges bakgrunden till och metodiken för formationsfaktorloggning in-situ med elektriska metoder. Formationsfaktorn definieras här som en parameter enbart beroende av porsystemets geometri och inte av den diffunderande specien. Traditionellt har formationsfaktorn mätts med genomdiffusionsförsök där prov från borrkärnor har använts, vilket är kostsamt och tidsödande. Det har tidigare visats att formationsfaktorn kan mätas med elektriska metoder vilka är snabbare och kostnadseffektivare. Detta har fram till nu endast gjorts kvantitativt i laboratoriet på en centimeter eller decimeter skala.

För att erhålla formationsfaktorn in-situ i områden med salthaltigt grundvatten behövs endast mätningar av bergets och grundvattnets elektriska resistivitet. Bergets resistivitet kan mätas med ett antal geofysiska borrhålsverktyg. Vattenbärande sprickor stör mätningarna och mätpunkter som kan ha blivit påverkade av fritt flödande vatten måste sorteras bort. Detta kan göras utan att förlora substantiella mängder data om mätningarnas vertikala upplösning är hög nog. I rapporten visas att det verktyg som används för nuvarande av SKB för att mäta bergets resistivitet generellt varken är kvantitativt eller har en tillräkligt hög vertikal upplösning. Ett nytt verktyg för att erhålla bergets resistivitet, Antares slimhole Dual-Laterolog, testades med ett gott resultat. Detta verktyg har en hög vertikal upplösning och är kvantitativt utan behov av korrigeringar. För nuvarande finns ingen metod där man direkt kan erhålla porvattnets resistivitet. Därför gjordes approximationen att porvattnet står i jämvikt med fritt rinnande grundvatten på ett motsvarande djup. Den elektriska konduktiviteten av grundvatten som flödande från isolerade sprickor mättes med Posivas Difference flow meter.

För att testa den föreslagna metodiken utfördes nya loggningarna av SKB i det 1.7 km djupa borrhålet KLX02 i Laxemar i Sverige. Även tidigare erhållna loggar användes. Rapporten innehåller många exempel på dessa loggar och beskriver även verktygen med vilka de erhölls. Dessutom visas en stegvis metod för att erhålla formationsfaktorn från olika loggar. För att verifiera att den erhållna in-situ formationsfaktorloggen var kvantitativ så togs ett stort antal prover från borrkärnan. Dessa provs formationsfaktor mättes i laboratoriet med elektriska metoder. Jämförelsen mellan formationsfaktorloggarna erhållna in-situ och i laboratoriet visade att in-situ metoden är lovande. Båda loggarna uppvisar ett liknande och tydligt gensvar på olika geologiska formationer. Formationsfaktorerna erhålla in-situ var ca. 1/3 av de erhållna i laboratoriet, vilket är förenligt med resultaten från tidigare mätningar där belastningseffekter på borrkärnor studerats.

Contents

1 Introduction

The rock matrix diffusion is central in assessing the transport of radionuclides through rock (Neretnieks, 1980, Andersson et. al, 1997, SKB, 2001). Therefore it is of utmost importance in a defective canister scenario when making a safety assessment for a deep geological nuclear waste repository. If radionuclides escape through the mechanical barriers of a repository they will still have to be transported through the natural barrier, the rock, before they can reach the biosphere. This transport will mainly occur in water-bearing fractures. The rock surrounding these fractures is however slightly porous and the micropores are filled with groundwater. As there are very small concentrations of naturally occurring radionuclides in the pore water there will be a concentration gradient from the fracture, where the radionuclides are dissolved in the groundwater, towards the micropores. The radionuclides will diffuse into the pores and be withdrawn from the water flow that otherwise could carry them to the biosphere. In the micropore system the radionuclides may sorb on the mineral surfaces or be stored in the pore water until they diffuses out of the pores and into the fracture again. Eventually the radionuclides will reach the biosphere. The radioactivity would have declined, preferably to natural levels, by this time.

Matrix diffusion has been studied quantitatively in laboratory experiments, as well as qualitatively in in-situ investigations, during the last 20 years. Diffusion experiments are time-consuming and also expensive if a large number of samples are used, and it is difficult to use samples that are large enough to represent the intact rock. For laboratory samples electrical conductivity measurements, where the two key parameters are the rock resistivity and pore water resistivity, have proven a good alternative to traditional diffusion experiments (Ohlsson, 2000, Ildefonse and Pezard, 2001, Löfgren, 2001). The electrical method is both faster, simpler and more cost effective than through diffusion experiments. Also larger samples on the decimetre scale can be used. Important parameters governing the matrix diffusion (except for the concentration gradient and the diffusivity) are the formation factor, the surface diffusion and sorption. This report will focus on the formation factor of undisturbed intrusive igneous rock and the possibility of measuring this parameter in-situ.

When making a safety assessment for a deep geological repository typically one km^3 of rock is studied. It is clearly that the porous system of this large rock volume can not be characterised by a few rock samples each having a volume of a fraction of a dm^3. To get a three-dimensional "map" of the rock a number of boreholes have to be drilled. From the bore cores and from different geophysical methods a geological characterisation of the rock volumes can be obtained. By logging the formation factor of the rock in the vicinity of the boreholes or of the bore cores and by combining this information with the geological characterisation a three-dimensional "formation factor map" could possibly be obtained.

In the oil industry formation factor logs in-situ have been obtained, mostly in sedimentary rock, by electrical methods for decades (Archie, 1942, Dakhnov, 1959, Keller and Frischknecht, 1966, Desbrandes, 1985). Here the main interest has, however, not been to obtain the matrix diffusivity of the rock but rather the porosity and the fraction of the porosity that is saturated with hydrocarbons (Bryant and Pallatt, 1996).

Logging the formation factor of a few deep boreholes with high vertical resolution in the laboratory performing measurements on the bore core would be extremely time-consuming and costly, as hundreds or thousands of samples might be needed. Therefore it has been so far been unrealistic to obtain a high-resolution three-dimensional formation factor characterisation that focus on the matrix diffusion. By applying some of the concepts used in the oil industry it would be possible to obtain in-situ formation factors of igneous rock that later could be used in matrix diffusion calculations. As this method is very fast and cost effective it would almost be a revolution in the area. In addition the rock would be subjected to the natural rock stress and groundwater chemistry.

The aim of this report has not only been to show that formation factor logging in-situ is doable but also to give the reader a chance to understand how formation factor logging by electrical methods is performed and even a platform to further develop the method. Therefore the importance of a number of different areas has been pointed out and the areas are briefly discussed. Also tools are described and their usefulness is discussed. At the end of the report a step-by-step procedure in obtaining an in-situ formation factor log is shown. This is done by using data form the borehole KLX02 in Laxemar, Sweden. Logging campaigns in the borehole performed during 2000 have given the data needed for this exercise. In order to validate the in-situ formation factor log a great number of samples from the core of KLX02 have been taken and their formation factors have been measured in the laboratory by electrical methods. At the end of the report the in-situ and laboratory formation factor logs are compared. When obtaining the formation factor logs surface conduction has been neglected as the pore water is fairly saline. The influence of surface conduction is under investigation.

In this report the terms electrical conductivity (S/m) and resistivity (ohm.m) are frequently used. The reason is that chemists traditionally use the electrical conductivity while resistivity traditionally is used within geophysics. This could cause some confusion but is should be kept in mind that the electrical conductivity is only the reciprocity of the resistivity.

2 The rock matrix

2.1 Introduction

Before discussing transport of species trough solid rock a brief introduction to the rock matrix is needed. The introduction will be focused on intrusive igneous rock common in Sweden. It should be noted that all methods described in this report are applicable in metamorphic rock even though the result may be harder to interpret if the rock is anisotropic. At present, SKB have no plans of building a repository in sedimentary rock.

2.2 Composition of the earth's crust

Table 2-1 gives the relative abundance of elements in the Earth's crust. If all the silicon, aluminium and iron were fully oxidised to SiO_2, Al_2O_3 and Fe_2O_3 a simple mole balance shows that 93% of the available oxygen in the continental crust would have been consumed. In reality the oxides are not separated and the oxidised cations are mixed in lattices. The average chemical formula of rock would from a mole balance, according to Table 2-1, be $X_8Al_6Si_{23}O_{63}$ where X stands for cations other than silicon and aluminium. Simplifying this one would approximately get $XAlSi_3O_8$, which is the chemical composition of orthoclase and some plagioclase feldspar. These minerals are very abundant.

Table 2-1 Relative abundance of elements in earth crust

Element	Continents		Oceans	
	weight-%	mole-%	weight-%	mole-%
O	46.8	62.5	44.0	61.0
Si	30.6	23.3	23.2	18.3
Al	7.9	6.3	8.9	7.3
Fe	3.3	1.3	6.8	2.7
Ca	3.0	1.6	8.4	4.6
Na	2.7	2.5	2.0	1.9
K	2.7	1.5	0.2	0.1
Mg	1.3	1.1	4.3	3.9
Others	1.7	excluded	2.2	excluded

(Data from Fredén, 1998)

2.3 Igneous rock

Igneous rock is categorised by its chemical composition, ranging from felsic to ultra mafic, and if it is intrusive or extrusive. Intrusive rock has cooled slowly from a liquid

magma melt tens of kilometres deep within the rock, allowing for greater crystals to grow. As the crystals cooled they contracted and micropores formed at the grain boundaries. Extrusive rock, on the other hand, has cooled quickly on the surface of earth or in the oceans after volcanic eruptions and is therefore fine-grained. Felsic rock is poor in iron and magnesium and rich in minerals with a high content of silicon, such as quartz and orthoclase feldspar. The best-known felsic rock, and also the most abundant intrusive igneous rock, is granite containing about 70% of silica. The extrusive equivalent to granite is rhyolite having the same chemical composition. Between felsic and mafic rock the intermediate rocks are found. On the intrusive side granodiorite is more felsic than diorite and on the extrusive side dacite is more felsic than andesite. In the intermediate rocks plagioclase feldspar becomes more abundant at the cost of orthoclase feldspar compared to felsic rock. They also contain more mafic minerals such as biotite, amphibole, and pyroxene. The mafic rocks, gabbro on the intrusive side and basalt on the extrusive side, are high in pyroxene and olivine and thus rich in magnesium and iron but poor in silica. Ultra mafic rock is very poor in silica, only 45%, and rarely found as extrusive rock. The intrusive from is peridotite. Figure 2-1 illustrates in a simplified way how igneous rock is classified and Table 2-2 gives the chemical composition of some common igneous minerals. For further reading Press and Siever, 1998, is recommended.

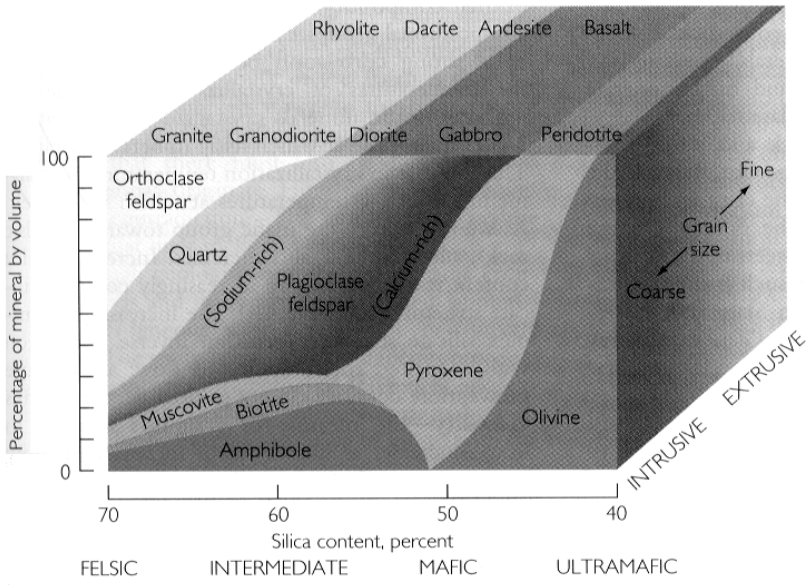

Figure 2-1 Classification of igneous rock. (From Press and Siever, 1998.)

Table 2-2 Chemical composition and structure of common igneous minerals

Mineral	Chemical composition	Lattice type
Orthoclase feldspar	$KalSi_3O_8$	Framework
Quartz	SiO_2	Framework
Plagioclase feldspar	$(Na,Ca)(Al,Si)Si_2O_8$	Framework
Muscovite	$KAl_3Si_3O_{10}(OH)_2$	Sheet
Biotite	$(K,Mg,Fe,Al)_xSi_3O_{10}(OH)_2$	Sheet
Amphibole Hornblende	Ca-Mg-Fe silicate $Ca(Mg,Fe)_4Al(Si_7Al)O_{22}(OH,F)$	Double chain
Pyroxene Enstatite	Mg-Fe silicate $(Fe,Mg)SiO_3$	Single chain
Olivine	$(Mg, Fe)_2SiO_4$	Isolated

(Data from From Press and Siever, 1998.)

2.4 Isotropic and anisotropic rock

The structural unit of the silicates is the $(SiO_4)^{-4}$ tetrahedron shaped group. As the oxygen atoms still have half their bonding energy left when formed they can bind to another tetrahedron, forming lattices (Figure 2-2). The framework structure, where each tetrahedron shares all its oxygen with other tetrahedrons, is not included in Figure 2-2.

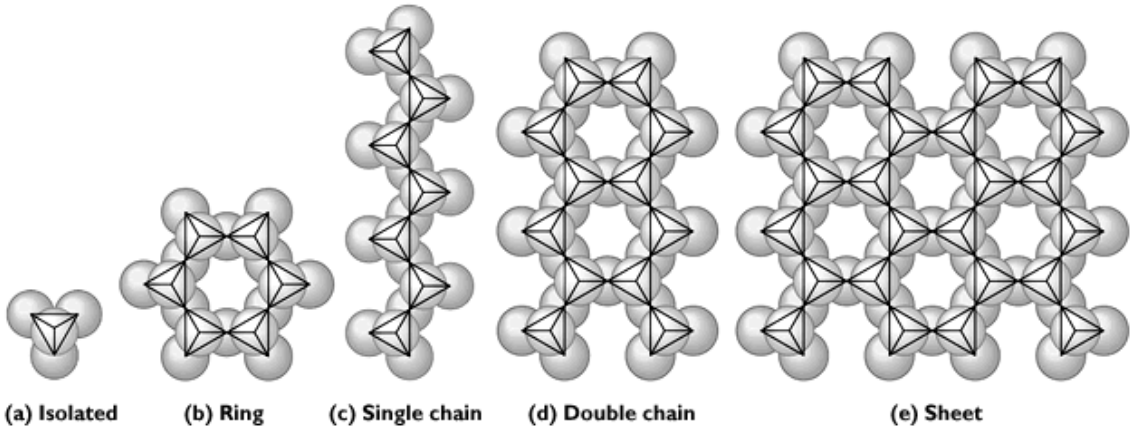

Figure 2-2 Different forms of lattices in slilcate minerals, framework is missing. (From Press and Siever, 1998.)

Depending on the lattice structure, minerals can have different properties in different directions. Mica, for example, has a sheet structure with stronger chemical bounds within the sheet than between the sheets. Therefore, as an example, the cleavage is good in the direction along the sheets but poor perpendicular to the sheets. Minerals with different properties in different directions are anisotropic. Quartz, on the other hand, has a framework structure where all chemical bounds are equally strong. Quartz has no cleavage and, generally speaking, no other properties depending on the direction and is isotropic.

Rock is seldom made of pure mineral but is rather a mixture of different minerals as shown by Figure 2-1. From a uniform magma melt that cools slowly deep in the earth crust, different minerals crystallise at different temperatures. The crystallisation of different minerals could either be continuos or discontinuous. When plagioclase feldspar crystallises, the first crystals formed are rich in calcium. This depletes the melt of calcium. As a result the crystals forming at a lower temperature is rich in sodium. At the same time calcium-rich crystals react with sodium-rich crystals and if the cooling is so slow that the different crystals equilibrates, the result will be a rock with only one mineral type having the same chemical composition as the original melt. If the melt cools faster, the rock will be built out of crystals with different chemical composition. When mafic mineral crystallises, olivine is first formed. When the melt is cooled below a certain degree, pyroxene will form abruptly and all the olivine will convert to pyroxene. However, before the melt has cooled to the point where pyroxene is formed, olivine that is denser than the melt may settle and be withdrawn from the melt creating differences in the final mineral composition. In addition the original melt may not be homogenous, as magmas origin from different rock may be immiscible. Crystallisation of magma is described in Press and Siever, 1998.

Crystals do not normally grow in a spherical manner and therefore rock does not consist of mineral spheres. More than 80% of the crystalline elements and very simple inorganic compounds belong to the regular and hexagonal systems and 60% of the natural minerals belong to orthorhombic or monoclinic systems. Crystals can grow more rapidly, or be stunted, in one direction. Therefore crystals can be needle-shaped, tabular or prismatic. The unlimited crystal growth depend more on the chemical bounds and the properties of the structural unit and cell unit than on outer circumstances, such as the temperature or pressure gradient. Before a crystal starts to grow a nucleus has to be present. If there are no nuclei present they will be created when the solution becomes over saturated enough. These nuclei are created when a number of molecules, driven by random motions, come close enough to form a cluster of a number of structural units. During the crystal growth more structural units are added to the structural units in the cluster. As the clusters were formed by molecules driven by random motion there is little probability that they all should face in the same direction. Furthermore the directions of the crystals will change if there is mixing. Therefore it is a normal behaviour that crystals in a reaction vessel will face in more or less random directions after the crystallisation, even if they all have same shape. When an intrusive melt cools, there are often temperature and pressure gradients over a mineral grain. Therefore the crystals do not have to be completely randomly organised. This possible feature of organisation would however only be minor. In addition crystal growth will be hindered, as the melt becomes denser in crystals. Therefore, as a first approximation, it is reasonable to say that even if most intrusive igneous rock is made up of a number of mineral crystals with a number of shapes, these crystals are to a large extent randomly organised. Even if all minerals are not isotropic, and even if the rock may not be isotropic on a millimetre scale, most intrusive igneous rock would then be isotropic on a lager scale. For further reading on crystallisation Mullin, 1993, is recommended.

2.4.1 Metamorphic rock

The reasoning above is not valid for metamorphic rock as it do not crystallise from a melt but re-crystallise in a solid state, usually under great pressure and/or temperature gradients. Igneous and sedimentary rocks undergo metamorphosis at high temperatures and pressures tens of kilometres below the surface. During the metamorphosis the mineralogy, chemical composition and crystalline texture may be altered even though the rock remains solid. Metamorphism is a consequence of three forces:

- The internal heat of the Earth.
- The weight of overlaying rock.
- The horizontal pressure developed as rock becomes deformed.

When rock is subjected to a change in temperature and pressure it will strive to equilibrate with the new conditions. The greater the changes, a bit simplified the deeper the rock is brought into earth, the faster the metamorphism will be. Most metamorphism occurs regionally but contact and cataclastic metamorphism occurs locally. Contact metamorphism occurs in the near vicinity of an igneous intrusion mainly due to the high temperature but also to the pressure of the magma. Cataclastic metamorphism occurs along faults where the sheer stress causes the rock to undergo changes. Pressure may cause the crystals in originally isotropic rock to become flattened in a preferred orientation (Figure 2-3).

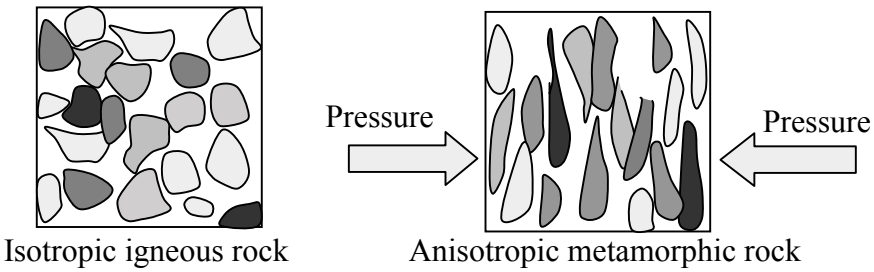

Figure 2-3 Metamorphism by pressure creating an anisotropic rock.

As a consequence of the metamorphism, one can not as a first approximation say that metamorphic rock is isotropic. Formation factor logs in anisotropic rock may be hard to interpret. Especially as it is the rock surrounding water-bearing fractures, that could be more or less randomly orientated, that is of interest in a safety assessment.

2.5 Complexity of intrusive igneous rock

Intrusive igneous rock is far from homogenous. It has formed from a melt deep below the surface, which may or may not have been homogenous. During the cooling of the melt it undergoes different crystallisation processes where different minerals are formed at different temperatures. Different cooling rates also give a different grain size distribution. When the rock is uplifted towards the surface the pressure is released. The

stress field may change gradually or abruptly and fractures are created. The rock could be uplifted or subsided many times before reaching the surface. Igneous intrusions often occur in these fractures creating sills and dikes. The rock in contact to the intrusions is metamorphosed due to the heat and pressures. On top of this, tectonic movements create forces further metamorphosing the rock. When the rock has reached the upper crust it interacts with the groundwater and chemical processes occur. Some minerals are dissolved in the groundwater and some are precipitated, thereby sealing fractures. It is very important to remember that a small area where experiments are made seldom represents a larger area.

2.6 Current conducting properties of solid rock

Most rock types are insulators in a dry state as their minerals are highly resistive. Exceptions are elements, sulphides, semiconductors and metals. Table 2-3 shows the resistivity of some common minerals.

Table 2-3 Resistivity of common minerals.

Mineral (Silicates)	**Resistivity** (ohm.m)	**Mineral** (Others)	**Resistivity** (ohm.m)
Orthoclase feldspar	$1.4 \cdot 10^{12}$	Halite	10^{10} - 10^{13}
Quartz	10^{12} - $2 \cdot 10^{14}$	Calcite	10^{12} - 10^{13}
Plagioclase feldspar	10^{8} - 10^{12}	Gypsum	$1.05 \cdot 10^{11}$
Muscovite	10^{12} - 10^{14}	Pyrite	$1 \cdot 10^{-4}$ - 10^{-1}
Biotite	$8.3 \cdot 10^{10}$	Graphite	$1.4 \cdot 10^{-5}$
Amphibole	$4.8 \cdot 10^{10}$	Hematite	10^{-2} - 10^{6}

(Data from Schön, 1996)

In nature rock at depth almost always holds some interstitial water in micropores containing ions from dissolved minerals. In an electric field, these ions will be transported due to electro-migration (in addition to the natural diffusion in case of any concentration gradient). Therefore an ionic conductivity will arise and the resistivity of the rock will decrease, sometimes substantially. The magnitude of the ionic conductivity depends on the number of current-bearing ions, which in turn is mainly dependent on the ion concentration and on the volume of water that the ions could be effectively transported in. If the ion concentration is constant the resistivity of the rock becomes mainly dependent of this water volume and on the geometry of the pores. Typical resistivities of unweathered granite are 10^{4}-10^{5} times the groundwater resistivity (having the typical resistivity range of 10^{-1}-10^{2} ohm.m at sites in Sweden investigated by SKB (SICADA)). As the current conducting capacity of wet rock is so much larger than that of dry rock, one may assume that all current is conducted in the pore water. There is however a question if even small amounts of highly conducting minerals, such as pyrite and hematite, may increase the conductivity of wet rock. Measurements suggest that this is not the case in the granite at KLX02 in Laxemar, Sweden (Löfgren, 2001). There is also a question if silicates having for example the sheets structure have a lower dry rock resistivity along the sheets than across them.

2.7 Sorbing properties of rock

The structural unit of silicate minerals is the SiO_4^{2-} tetrahedron. The mineral quartz (SO_2) is built only by this structural unit. Table 2-1 shows that aluminium is a very abundant metal in rock and when quartz crystallises in nature a few divalent SiO_4^{2-} tetrahedrons may be replaced by a few trivalent AlO_4^{3-} tetrahedrons. This creates a negatively charged lattice (Figure 2-4)

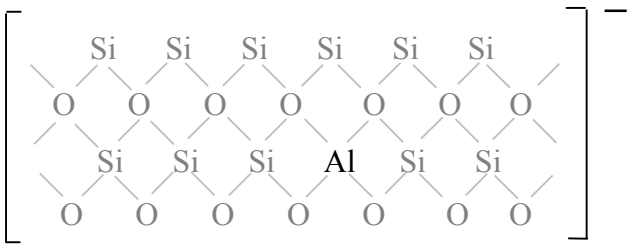

Figure 2-4 Illustration of isomorphous replacement in quartz.

In the same way as silicon can be exchanged by aluminium, aluminium may be exchanged by iron in feldspar and other minerals. This phenomenon is called isomorphous replacement and normally causes the rock to become negatively charged. It is not common that the lattice become positively charged, as replacement of a less positively charged ion to a more positively charged ion would be sterically hindered, as more positively charged ions often are larger. The oxygen ions of the tetrahedron facing toward the surface are often bound to hydrogen. As shown by Equation 2-1 the functional group at the mineral surface in a silicate, ≡Si-O$^-$, is amphoteric. Therefore the surface charge is not only dependent on the isomorphous replacement but also on the pH of the pore water.

$$\equiv S\text{-}OH_2^+ \overset{K1}{\Leftrightarrow} \equiv S\text{-}OH \overset{K2}{\Leftrightarrow} \equiv S\text{-}O^- \qquad 2\text{-}1$$

In silicates not having a framework structure sheets or chains etc. may be negatively charged and counterbalanced by surrounding cations. Mica, as an example, has a Si-Al-O sheets counterbalanced by intermediate cations such as K^+. Figure 2-5 shows the surface charge of a few minerals as a function of the pH.

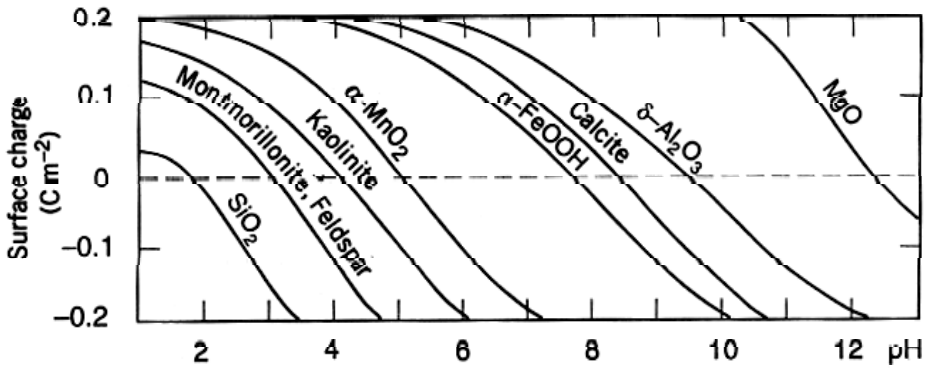

Figure 2-5 The surface charge of a few mineral as a function of pH. (From Stumm and Morgan, 1996.)

Figure 2-5 shows that both quartz and feldspar, the most abundant minerals in felsic igneous rock, has a negative surface charge at pH values of naturally existing groundwater. Normally ions such as Na^+, K^+, Ca^{2+}, and Mg^{2+} exist in the pore water. These ions can take part in ion exchange reactions with the ≡Si-OH group at the mineral surface. Equation 2-2 shows a reaction where the surface charge remains the same and Equation 2-3 show a reaction where the surface charge is altered.

$$\equiv S\text{-}OH + Cs^+ \Leftrightarrow \equiv S\text{-}OCs + H^+ \qquad 2\text{-}2$$

$$\equiv S\text{-}OH + Cu^{2+} \Leftrightarrow \equiv S\text{-}OCu^+ + H^+ \qquad 2\text{-}3$$

The pH at which the proton dependent surface charge is zero is called pH_{pznpc} (point of zero net proton charge) and the pH at which the total surface charge (due to isomorphous replacement, ion exchange reactions, surface complexation, and so on) is zero is called pH_{pzc} (point of zero charge).

Cations can adsorb to a specific adsorption site on a silicate mineral surface in two different ways, as an inner-sphere or outer-sphere complex (Figure 2-6). In the first case, a covalent bond is formed between the cation and the electron-donating ≡S-O^- group. In the second case the cation is separated from the surface by at least one water molecule and is held there by electrostatic forces. Although the cation is separated from the surface, the distance is so short that the electrostatic attraction force influencing the cation origin mainly from one or a few functional groups. It is not yet clear where to draw the line between inner- and outer-sphere complexes and outer-sphere complexes and the diffuse layer. The issue is under debate.

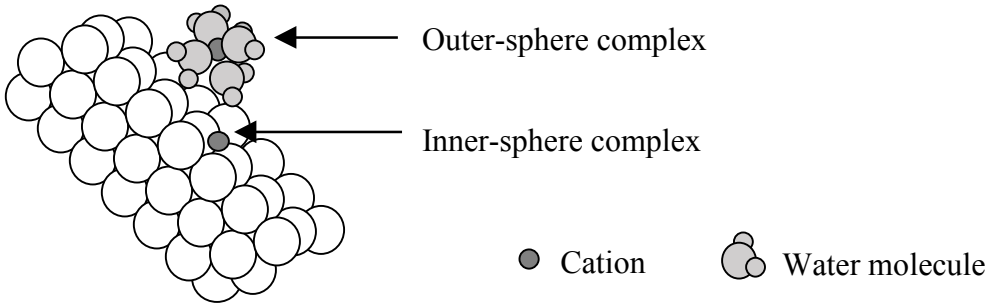

Figure 2-6 Inner- and outer-sphere complexes at a mineral surface. (Drawn from Stumm and Morgan, 1996.)

As seen from Figure 2-5 the negative surface charge of quarts and feldspar is quite high at a neutral pH. This charge is both due to the structure of the mineral, isomorphous replacement and the equilibrium between the functional group and the cations, for example ≡S-O^- ⇔ S-OH. All this charge has to be counterbalanced by cations at the surface or in the pore water. If the negative charge is not counterbalanced at the surface an electric field will be established affecting the ions in the pore water outside the outer-sphere complexes. The consequence is that the cations and anions in the pore water will be attracted or repelled by the surface and a positive layer, containing more cations than

anions, will form (Figure 2-7). This layer is called the diffuse layer or the electrical double layer. The cations are mobile and not sorbed site specifically at the surface, as diffusive forces counteract the electrostatic forces.

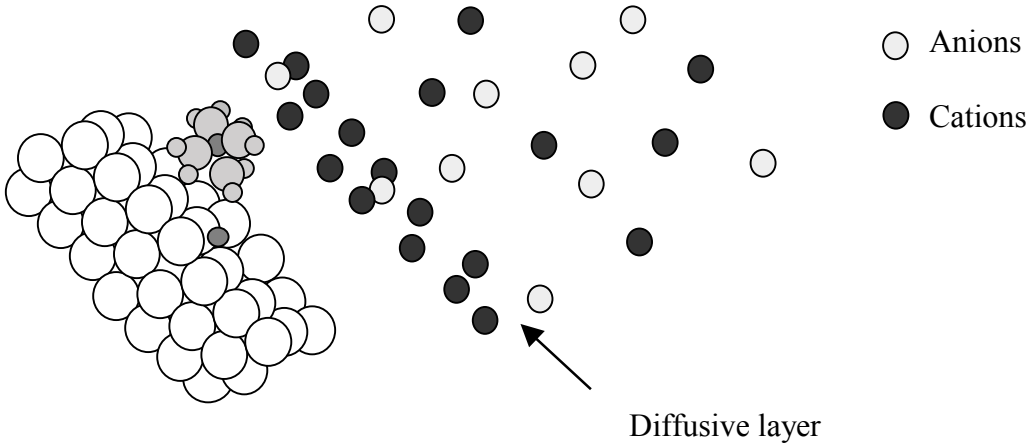

Figure 2-7 Diffusive layer of positively charged ions at a mineral surface.

This report discusses applications where a current is transported by the ions in the pore water through rock. If one would try to run a current through a rock sample where the pore water had been exchanged by deionised water one might except that the current would be transported in the mineral grains or by the protons and hydroxyl ions created by autoprotolysis. The current would in fact be hundreds of times larger than expected. The reason is that the cations in the diffusive layer will remain even if the pore water is exchanged, as they are needed to counterbalance the negative surface charge. Most of the current will then be transported by these cations. This may lead to misinterpretations of the porous system. More will be discussed about electrical applications in the following chapters. At this point it is only noted that the errors due to the diffuse layer are minor in intrusive igneous rock when the pore water has a resistivity in the order of 10^{-1} ohm.m, moderate at 10^{0} ohm.m, and large at 10^{1} ohm.m. (Ohlsson et. al, 2001). The surface conduction in granite from Laxemar, Sweden, is in the order of 10^{-5} S/m (Löfgren, 2001). If using the typical formation factor of 10^{-4} this means that surface and pore conduction would be equal in magnitude if the pore water resistivity was around 10 ohm.m.

3 Theory of matrix diffusion and conduction

3.1 Introduction

The main transport mechanism for radionuclides in solid crystalline rock without fractures is molecular diffusion in the water filled micropores between the mineral grains. As the water in the micropores is practically stagnant the transport of dissolved species by hydraulic conduction could be neglected. Non-sorbing species will mainly be transported in the bulk pore volume while sorbing species could be transported both in the bulk pore volume and in the diffusive layer at the pore surface. Sorbing species could also sorb as inner- or outer-sphere complexes on the mineral surface and therefore partly be withdrawn from the transport. Conduction of an electrical current in solid rock could both be due to transport of ions in the pore water and on the mineral surfaces and to electron transfer in conductive mineral grains. In silicates the dry rock electrical conductivity is normally many order of magnitudes less than the conductivity due to ion transport in the pores.

3.2 Pore diffusion of non-sorbing species

3.2.1 Fick's first law of diffusion

Fick's first law of diffusion states that whenever there is a concentration gradient, there will be a diffusive flow from the high concentration region to the low concentration region. The momentary magnitude of the diffusive flux will depend on the concentration gradient, properties of the diffusing specie, and properties of the surrounding media.

$$N = -D\frac{dC}{dx} \qquad 3\text{-}1$$

where N is the diffusive flux (mol/m^2.s), D is the molecular diffusion coefficient (also called diffusivity) for the diffusing specie in the media under prevailing circumstances (m^2/s) and dC/dx is the concentration gradient (mol/dm^3.m).

3.2.2 Fick's first law - pore diffusion

When the diffusion takes place in rock the only pass ways available are the groundwater filled micropores. This reduces the transport volume considerably (Figure 3-1 a) as the porosity ε in crystalline rock is in the order of 10^{-3} (Skagius, 1986, Ohlsson, 2000, Löfgren 2001, Ildefonse and Pezard, 2001). A pore could either be a dead end pore or be connected to the micropore network. The major material transport takes place in the pores connected to the network. Still, in a transient state, species could diffuse into a

dead end pore if there was a concentration gradient and then be stored there. The porosity is therefore divided into transport porosity (network pores), ε_t, and storage porosity (dead end porosity), ε_d. Furthermore the micropores are tortuous, so species diffusing from point A to B have to be transported an extra long distance (Figure 3-1 b). Finally the cross section area varies along the pores. As the most constricted part of the pore limits the diffusive flux, all of the pore volume could not be effectively used for transport (Figure 3-1c).

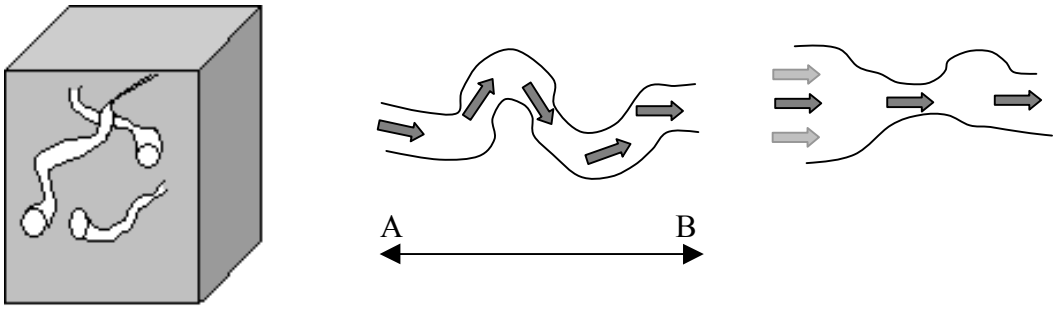

Figure 3-1 Illustration of the importance of a) porosity, b) tortuosity, and c) constrictivity on matrix diffusion.

The transport porosity, ε_t, the tortuosity, τ^2, and the constrictivity, δ_D, are included in Fick's first law for diffusive flux through a porous media (Ohlsson and Neretnieks, 1995):

$$N_{p,i} = -D_{w,i}\varepsilon_t \frac{\delta_D}{\tau^2}\frac{dC_{p,i}}{dx} \qquad 3\text{-}2$$

where i is the index of the diffusing specie, N_p is the diffusive flux through the porous medium, D_w is the molecular diffusion coefficient in free pore water and dC_p/dx is the concentration gradient on a larger scale (from point A to B in Figure 3-1 b). The porosity, the tortuosity, and the constrictivity do not have to be analysed separately as they all could be included in the formation factor.

$$F_f = \varepsilon_t \frac{\delta_D}{\tau^2} \qquad 3\text{-}3$$

The formation factor characterises the reduction in transport rate in an inert porous media compared to transport in a free liquid (as long as there is no surface diffusion). The idea is that the formation factor only depends on the geometry of the pore system and therefore is independent of the diffusing specie. This is not entirely true as the constrictivity can be influenced by the molecule size where large molecules may be more hindered than small molecules in constricted pores. In addition there may be ion exclusion as the surfaces are charged.

The formation factor differs from rock to rock depending on the mineral composition, the grain size distribution and how closely the mineral grains are packed. In the laboratory one can easily determine the porosity of a rock sample. Often it is approximated that the transport porosity could be set equal to the total porosity and the constrictivity-tortuosity ratio could be calculated from the formation factor. By multiplying this ratio with the diffusivity in free pore water, the pore diffusivity, D_p, could be calculated:

$$D_p = D_w \frac{\delta_D}{\tau^2} \qquad 3\text{-}4$$

The diffusive flux through a porous medium could be written in a shorter from by combining Equation 3-2 and Equation 3-3:

$$N_{p,i} = -D_{w,i} F_f \frac{dC_{p,i}}{dx} \qquad 3\text{-}5$$

This means that the matrix diffusion for any non-sorbing specie could be calculated by knowing the concentration gradient, the molecular diffusion coefficient in the free pore water of the specie and the formation factor.

3.2.3 Fick's second law of diffusion

Transient mass transport by molecular diffusion in one direction can generally be described by Fick's second law:

$$\frac{\partial C}{\partial t} = D \frac{\partial^2 C}{\partial x^2} \qquad 3\text{-}6$$

where t is the time (s) and all the other symbols are the same as Equation 3-1.

3.2.4 Fick's second law - pore diffusion

If the transient diffusion of non-sorbing species takes place in a porous material Equation 3-6 has to be modified:

$$\frac{\partial C_p}{\partial t} \varepsilon = D_w F_f \frac{\partial^2 C_p}{\partial x^2} \qquad 3\text{-}7$$

On the left-hand side of Equation 3-7, which is the accumulation part, the total porosity has to be included as species only could accumulate in the pore volume of the porous media. On the right hand side, the transport part, the formation factor has been included.

3.3 Surface diffusion of sorbing species

Many surfaces are naturally charged. Silicates often have a negative surface charge as discussed in previous sections. This negative charge has to be counter balanced by cations sorbed as inner- or outer-complexes or in the diffuse layer. Sorption is often described by the ratio of the concentration of sorbed ions to non-sorbed ions. This is convenient, as it is normally easy to measure the concentration of the non-sorbed ions in the solution around the sorbent. The simplest to way describe the equilibrium between sorbed and non-sorbed ions is the linear isotherm:

$$S = K_d C_p \qquad 3\text{-}8$$

where S is the amount of adsorbed specie per mass of solid matter (mol/kg) and K_d is the sorption coefficient (dm^3 solution/kg sorbent). This can also be expressed as:

$$\varepsilon_s C_s = \rho K_d C_p \qquad 3\text{-}9$$

where ε_s is the hypothetical volume fraction of the sorbing layer, C_s is the concentration in the sorbing layer (mol/dm^3), and ρ is the density of the solid matter (kg/m^3). Ideally K_d is a constant but in practice it is influenced by several factors including the concentration of the sorbing specie, the pH, and the ionic strength.

3.3.1 Fick's first law - surface diffusion

Steady state surface diffusion in the sorbed layer is described by:

$$N_s = -D_s \varepsilon_s \frac{dC_s}{dx} \qquad 3\text{-}10$$

where N_s is the diffusive flux at the surface ($mol/s.m^2$) and D_s is the molecular diffusion constant at the surface (m^2/s). Assuming that there is a linear equilibrium between the ions in the sorbing layer and the ions in the bulk pore water and by combining Equation 3-10 and Equation 3-9 Fick's first law for surface diffusion is obtained:

$$N_s = -D_s \rho K_d \frac{dC_p}{dx} \qquad 3\text{-}11$$

3.3.2 Fick's second law - surface diffusion

For surface diffusion in a porous material Equation 3-6 has to be modified:

$$\frac{\partial C_s}{\partial t} \varepsilon_s = D_s \varepsilon_s \frac{\partial^2 C_s}{\partial x^2} \qquad 3\text{-}12$$

Assuming as before that there is a linear equilibrium between the ions in the sorbing layer and ions in the bulk pore water and by combining Equation 3-12 and Equation 3-9 Fick's second law for surface diffusion is obtained:

$$\frac{\partial C_p}{\partial t}\rho K_d = D_s \rho K_d \frac{\partial^2 C_p}{\partial x^2} \qquad 3\text{-}13$$

Note that our assumption implies that all the sorbed species are mobile. This may not be true and then only the mobile part of the sorbed species must be accounted for on the right side hand of Equation 3-13. Alternatively one can consider D_s to be an average value of the diffusivity of all sorbed species, including both the mobile and non-mobile part.

3.4 Total matrix diffusion

In order to obtain an expression for the total matrix diffusion one has to add the contribution from the pore and the surface diffusion.

3.4.1 Fick's first law - total matrix diffusion

An expression for the total steady state matrix diffusion is obtained by combining Equation 3-5 and Equation 3-11:

$$N_{tot} = -\left(D_w F_f + D_s \rho K_d\right)\frac{dC_p}{dx} \qquad 3\text{-}14$$

Then the effective diffusion coefficient, D_e, could be defined as:

$$D_e = D_w F_f + D_s \rho K_d \qquad 3\text{-}15$$

The equation is valid both for sorbing species that could be described by a linear isotherm and non-sorbing species. For non-sorbing species ρK_d equals zero.

3.4.2 Fick's second law - total matrix diffusion

An expression for the total transient matrix diffusion is obtained by combining Equation 3-7 and Equation 3-13:

$$\frac{\partial C_p}{\partial t} = \frac{D_w F_f + D_s \rho K_d}{\varepsilon + \rho K_d}\frac{\partial^2 C_p}{\partial x^2} \qquad 3\text{-}16$$

Also here the equation is valid both for sorbing species that could be described by a linear isotherm and non-sorbing species. Again ρK_d is set equal to zero for non-sorbing species. Using a linear isotherm is clearly a great simplification. At present, it is not clear how to correctly describe the surface diffusion.

3.5 Conduction

If a solution containing ions was placed in an electric field the cations would electro-migrate towards the anode and the anions would electro-migrate towards the anode. The current in the solution would the be:

$$I = e\frac{\sum_i N_i z_i}{t} \qquad 3\text{-}17$$

where I is the current (A), N_i the number of ions passing through a plane perpendicular to the electric field within the time t, z_i is the number of charge of the ions and e is the electron charge. The flux of ions ion passing through the plane would then be:

$$N_{tot} = -\frac{AF}{RT}\sum_i z_i C_{p,i} D_{w,i}\frac{dU}{dx} \qquad 3\text{-}18$$

where A is cross section area, F, R and T is respectively the Faraday constant, the gas constant and the temperature, $C_{p,i}$ is the ion concentration, $D_{w,i}$ the diffusivity of the ion in free liquid, and dU/dx is the potential gradient (V/m). By combining Equation 3-17 and Equation 3-18 the current in the solution could be calculated:

$$I = -\frac{AF^2}{RT}\sum_i z_i^2 C_{p,i} D_{w,i}\frac{dU}{dx} \qquad 3\text{-}19$$

as the Faraday constant is the product of the Avogadro constant and the electron charge. The current could also be calculated if the conductivity of the solution is known by using Ohm's law.

$$I = \kappa A\frac{dU}{dx} \qquad 3\text{-}20$$

where κ is the conductivity (S/m). By combining Equation 3-19 and Equation 3-20 one will get the Nernst-Einstein equation (Atkins, 1995) and the conductivity of a free solution, $\kappa_{w,}$ can be written as:

$$\kappa_w = \frac{F^2}{RT}\sum_i z_i^2 C_{p,i} D_{w,i} \qquad 3\text{-}21$$

The equation above has to be corrected if the conduction occurs in a porous medium. If the pore surfaces is uncharged and in no way attracts the current bearing ions the formation factor is added to Equation 3-21:

$$\kappa_p = \frac{F^2}{RT}F_f\sum_i z_i^2 C_{p,i} D_{w,i} \qquad 3\text{-}22$$

where κ_p is the conductivity of the porous medium. As pointed out in the discussion about sorption properties of rock, the pore surfaces are rarely uncharged. Therefore an electrical double layer will form where conduction could occur:

$$\kappa_s = \frac{F^2}{RT}\sum_i z_i^2 C_{p,i} \rho K_{d,i} D_{s,i} \qquad 3\text{-}23$$

where κ_s is the surface conductivity. The equation is valid for sorbing species that could be described by a linear Freundlich isotherm. The total rock conductivity, κ_r, is then the sum of the pore conductivity and the surface conductivity:

$$\kappa_r = \kappa_p + \kappa_s = \frac{F^2}{RT}\sum_i C_{p,i} z_i^2 \left(F_f D_{w,i} + \rho K_{d,i} D_{s,i}\right) \qquad 3\text{-}24$$

The ratio between the total conductivity of the rock and the conductivity in the free pore solution is:

$$\frac{\kappa_r}{\kappa_w} = \sum_i \frac{\left(F_f D_{w,i} + \rho K_{d,i} D_{s,i}\right)}{D_{w,i}} = F_f + \sum_i \frac{\rho K_{d,i} D_{s,i}}{D_{w,i}} \qquad 3\text{-}25$$

Equation 3-25 is valid only if the amount of sorbed ions is linearly proportional to the concentration in the pore water. As discussed in previous sections the amount of sorbed cations is to a large extent determined by the surface charge of the minerals. The sorption of the major cations, such as Na^+, K^+, and Ca^{2+}, that are of importance for the surface conduction as can therefore not be described by a linear isotherm. At present, it is not clear how to correctly describe the surface conduction. The influence of surface conduction in diorite at different pore water conductivities has been determined by Ohlsson et. al., 2001. By introducing a fluid of a known ionic strength in the pore system and then measuring the rock conductivity it was examined how κ_r/κ_w varied with the ion concentration. Figure 3-2 shows the result where the κ_r/κ_w ratio on the y-axis is normalised with the formation factor (which is independent of the pore water) and the ion concentration on the y-axis is expressed as the resistivity (that is the reciprocal of the conductivity) of the free pore water.

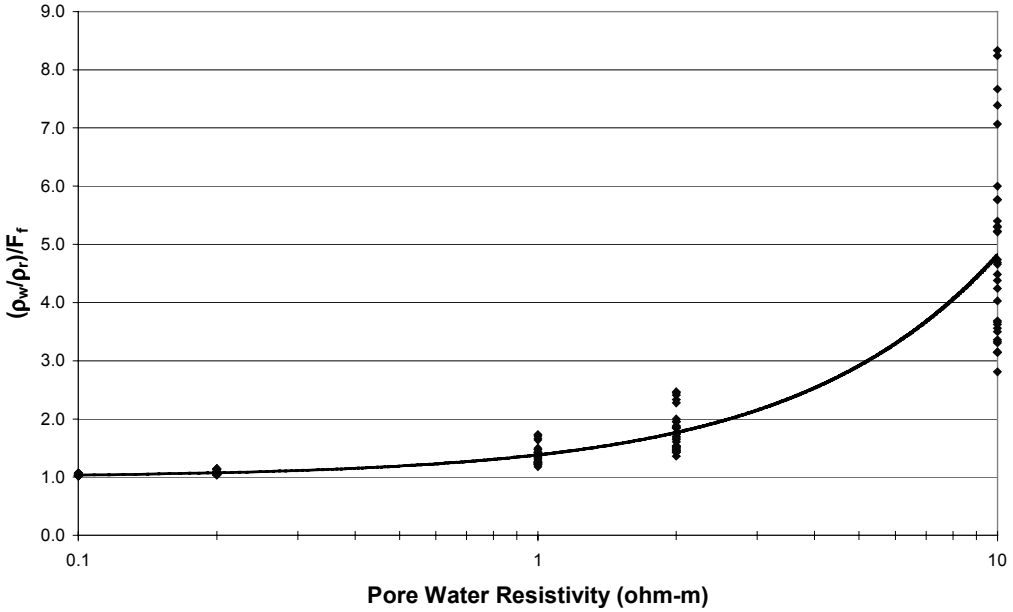

Figure 3-2 Influence on the rock conductivity by surface conductivity in diorite at different water conductivities. (From Ohlsson et. al., 2001.)

Figure 3-2 show that if the pore water conductivity is high, the current contribution from surface conduction is negligible. With decreasing pore water conductivity, the importance of surface conduction increases until the contribution from pore conduction could be neglected. At the resistivity level of the groundwater in Laxemar (around 1 ohm.m) the error introduced by the surface conduction is moderate. Therefore surface conduction has not been taken into account when obtaining the formation factor log and will not be furthered discussed in this report.

4 Theory of current and electric fields

4.1 Introduction

In dry state some minerals are conductive, such as pyrite, while others are insulators, such as quartz. Most rock contains water filled micropores and in the insulating minerals practically all current is transported by ions in these pores. Rock could be either isotropic, meaning that it has the same properties in all directions, or anisotropic, meaning that it has different properties in different directions. Rock is almost never homogenous in respect of resistivity, as it is normally a mixture of different minerals. In order to keep the theory simple, the discussion is restrained to homogenous conductors of isotropic media. An inhomogeneous conductor can be modelled by adding a number of homogenous blocks with different resistivities. The most important cases are shown below. For further reading Dakhnov, 1959, and Keller and Frischknecht, 1966, is recommended.

4.2 Cylindrical homogenous conductor

In Equation 4-1 the most commonly used form of Ohm's law is shown:

$$I = \frac{\Delta U}{R} \qquad 4\text{-}1$$

where I is the current (A), ΔU is the potential difference over the conductor (V) and R is the resistance of the conductor (ohm). If the conductor is cylindrical the current could be calculated by:

$$I = -\frac{\pi r^2}{\rho}\frac{dU}{dx} \qquad 4\text{-}2$$

where ρ is the resistivity of the conducting material (ohm.m), dU/dx is the potential gradient, and πr^2 is the cross section area of the cylinder (Figure 4-1).

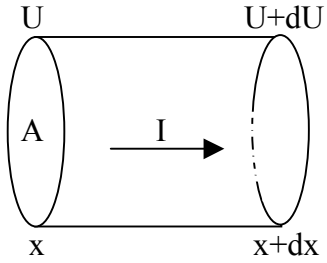

Figure 4-1 Cylindrical conductor.

The current could also be calculated by using the conductivity, that is the reciprocal of the resistivity, of the conducting material.

$$I = -\pi r^2 \kappa \frac{dU}{dx} \qquad 4\text{-}3$$

where κ is the conductivity (S/m). Both the resistivity and the conductivity are independent of the direction of the current flow in an isotropic homogenous conductor.

4.3 Homogenous conductor expanding infinitely

If a point electrode is placed in a homogenous conductor expanding infinitely in all directions, a spherical electric field will form around it. The current will flow perpendicular to the electric field, along the radius of the sphere. The direction of the current is normally symbolised by current lines (Figure 4-2).

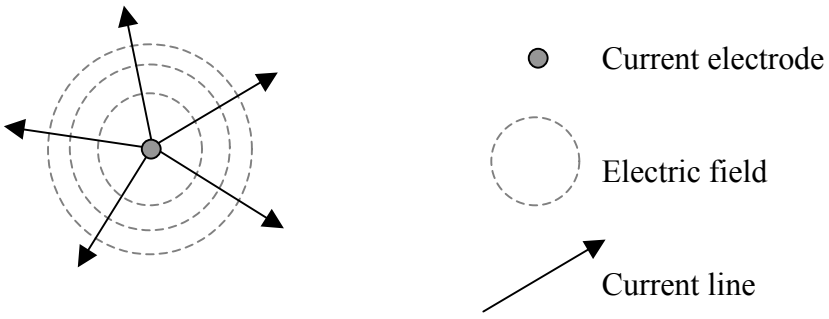

Figure 4-2 Electric field and current lines around a point electrode.

Kirchoff's first law states the continuity of the current lines as they pass through an initially uncharged three dimensional medium.

$$\frac{\partial^2 U}{\partial x^2} + \frac{\partial^2 U}{\partial y^2} + \frac{\partial^2 U}{\partial z^2} = 0 \qquad 4\text{-}4$$

This means that current can neither be created or disappear in the conductor. It should be noted that Kirchoff's law is not valid at a current electrode, which is initially charged. The current density in a media is the current divided by the cross section area

perpendicular to the current lines. For the case of a point electrode in a homogenous medium expanding infinitely in all dimensions the current density in any point is described by:

$$j = \frac{I}{4\pi r^2} \qquad 4\text{-}5$$

where r is the distance from the point electrode. If the point electrode had an infinitely small radius the current density would of course be infinitely great. Therefore a true point electrode does not exist. However, if the electrode is small compared to the volume of the electric field one could still talk about a point electrode. By applying Equation 4-3 to the spherical case and rearranging we would get:

$$dU = -\frac{\rho I}{4\pi}\frac{dr}{r^2} \qquad 4\text{-}6$$

By combining Equation 4-5 and Equation 4-6 the current density would be:

$$j = -\frac{1}{\rho}\frac{dU}{dr} \qquad 4\text{-}7$$

Equation 4-6 could be integrated from any point in space to a point infinitely far away, where the potential is assumed to be zero. This would mean that the potential at the point in space would be:

$$U = \frac{\rho I}{4\pi r} \qquad 4\text{-}8$$

where r is the distance between the point and the current electrode. It is not possible to have an electrode emitting electrons (the anode) without having another electrode collecting electrons (the cathode). These two electrodes will normally affect each other's electric field. In order to get a spherical electric field around current electrode A, the other current electrode, B, has to be placed infinitely far away so that it does not interfere. In many cases it is not possible to place one current electrode infinitely, or very, far away from the other current electrode. Figure 4-3 shows two current electrodes at a finite distance and an arbitrary point in the homogenous conductor.

Figure 4-3 Two oppositely charged electrodes and an arbitrary point in an homogenous medium.

The potential U_p, compared to the zero potential, at an arbitrary point with the distances r_A and r_B from A and B is:

$$U_P = \frac{\rho I}{4\pi}\left(\frac{1}{r_A} - \frac{1}{r_B}\right) = \frac{\rho I}{4\pi}\frac{r_A - r_B}{r_A r_B} \qquad 4\text{-}9$$

As it is only possible to measure potential differences, two potential electrodes, M and N, have to be used in a real case. If M and N are placed at the distances r_M and r_N from a point current electrode A (Figure 4-4) the potential difference will be:

$$\Delta U_{MN} = \frac{\rho I}{4\pi}\left(\frac{1}{r_m} - \frac{1}{r_n}\right) = \frac{\rho I}{4\pi}\frac{r_n - r_m}{r_m r_n} \qquad 4\text{-}10$$

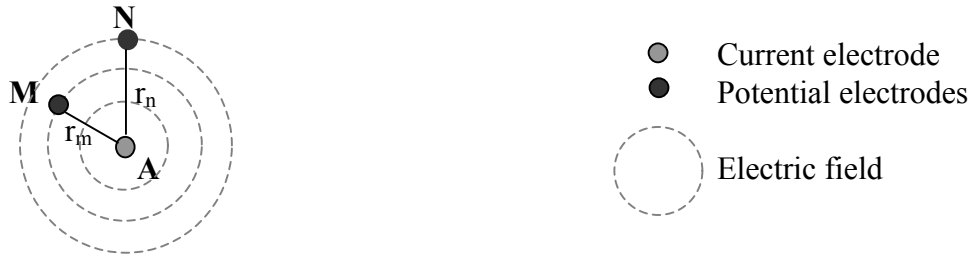

Figure 4-4 Two potential electrodes and a point current electrode.

Equation 4-10 is the same equation as Equation 4-9 except the distance indexes. The principle of reciprocity states that the measured potential difference will remain unchanged if the roles of the current electrodes and potential electrodes are interchanged. The general case involves two current electrodes and two potential electrodes (Figure 4-5).

Figure 4-5 Positive and negative current electrode and two potential electrodes.

The potential difference between M and N is:

$$\Delta U_{MN} = \frac{I\rho}{4\pi}\left(\frac{1}{r_{AM}} - \frac{1}{r_{BM}} - \frac{1}{r_{AN}} + \frac{1}{r_{BN}}\right) \qquad 4\text{-}11$$

4.4 Block modelling of non-homogenous conductor

As mentioned before rock is almost never homogenous in respect of resistivity. In rock there are normally resistivity gradients, for example where two different minerals are mixed and the ratio between the minerals is changed gradually, or resistivity boundaries between two media, for example at a water filled fracture in the rock. To simplify the calculations one may consider rock to be built up by different layers or blocks. The resistivity within each of these blocks or layers is homogenous but each block or layer has a specific resistivity. When measuring the resistivity in non-homogenous rock one usually uses linear arrays of current and potential electrodes in order to get simpler calculations when obtaining the resistivity.

4.4.1 One plane boundary, image point method

The simplest case of block modelling is when two homogenous conductors with different resistivities are separated by a flat boundary surface. This is the case when logging from the surface. The air can be considered as one block and the rock as the other. In this case the electrodes are placed at the boundary surface. To make the theory a bit more general one could place the electrode array within one conductor but still parallel to the surface (Figure 4-6). This case could apply if one was trying to log the rock resistivity under a thick overburden where the electrodes as placed deeply in the overburden but not at the rock surface. The case has a more theoretical than practical value. Surface rock resistivity measurements are often performed on outcrops or in trenches where the overburden has been removed. It is also common that the electrodes are placed in a relatively thin soil layer.

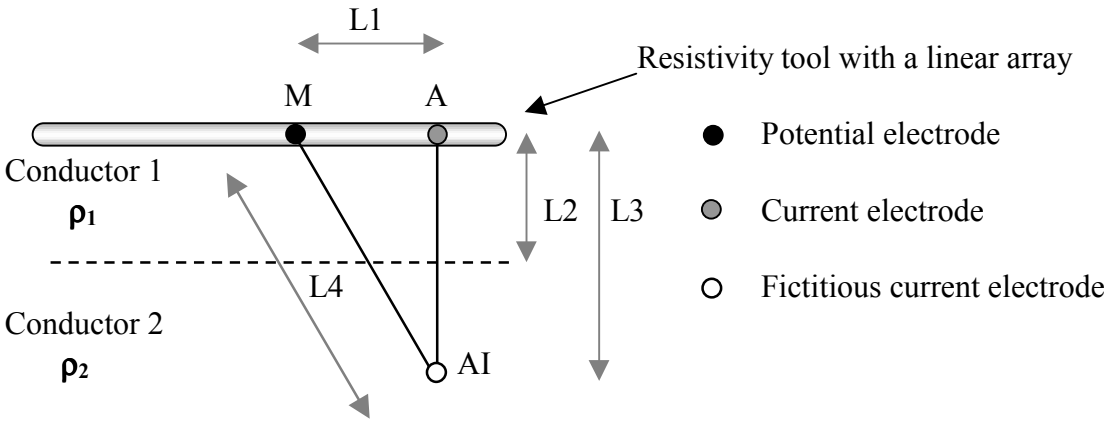

Figure 4-6 Set-up of a surface measurement where the electrode array is parallel to the surface but not at the surface.

According to the image point method the potential at an arbitrary point in conductor 1, is the same as if the whole body would have had the same resistivity except for an extra potential contribution. This extra contribution is taken to come from a second fictitious current source, AI, that is introduced at the image point of A through the boundary surface. The idea of the image method is to treat current as similar to light. At a boundary surface, light is reflected or transmitted. The current is treated to behave in analogy to this. The behaviour of light depends on the refraction index and in the same

manner the behaviour of current would depend on the resistivity in the conductors. In reality current does not behave like light and electrons are not reflected at a boundary surface. Still looking on it in this way, one can imagine a couple of current lines emanating from a current source near a boundary surface (Figure 4-7). A part of one line reflects at the surface and crosses the other lines. If one superimposes this reflecting line on the other lines, the result will be that the other lines change direction. As the current lines bend, the electric field is also affected. In reality it is the other way around. In the second conductor a secondary electric field is induced affecting the electric field in the first conductor which in turn affects the path of the current.

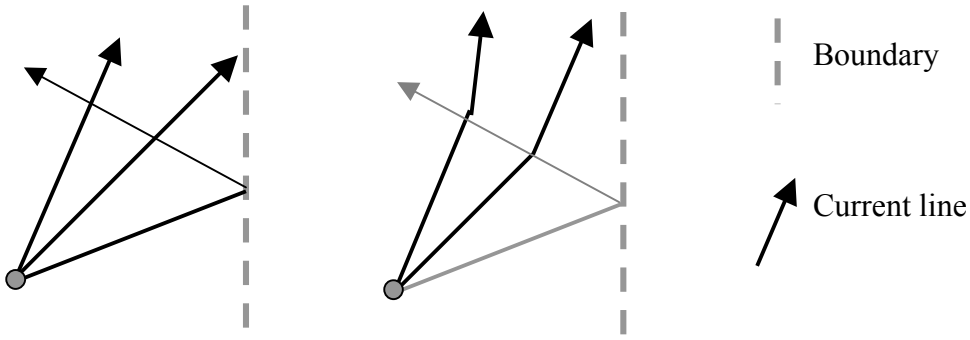

Figure 4-7 Current lines at a boundary surface illustrating the image point method.

The potential at M in Figure 4-6 could be calculated according to:

$$U_M = U_{M,A} + U_{M,AI} = \frac{\rho_1}{4\pi}\left(\frac{I_A}{L_1} + \frac{I_{AI}}{L_4}\right) \qquad 4\text{-}12$$

where $U_{M,A}$ and I_A is the potential and current origin from the current electrode and $U_{M,AI}$ and I_{AI} is the potential and current origin from the image electrode. The distances are shown in Figure 4-6. A point in conductor 2, for example at the image point of the current electrode, would only be subjected to the field origin from the current I_T transmitted through the boundary surface. The potential at AI, compared to the zero potential, would then be:

$$U_{AI} = \frac{\rho_2 I_T}{4\pi L_3} \qquad 4\text{-}13$$

where L_3 is the distance from the current electrode. If a point right between the current electrode and the image electrode, i.e. a point at the boundary surface, is chosen the boundary conditions that there must be continuity in potential and current density applies:

$$U_1\big|_s = U_2\big|_s \qquad 4\text{-}14$$

and

$$\frac{1}{\rho_1}\frac{dU_1}{dr}\bigg|_s = \frac{1}{\rho_2}\frac{dU_2}{dr}\bigg|_s \qquad 4\text{-}15$$

From this it can easily be shown that:

$$\rho_1\left(I + I_{AI}\right) = \rho_2 I_T \qquad 4\text{-}16$$

and:

$$I_T = I_A - I_{AI} \qquad 4\text{-}17$$

I.e. the current transmitted through the surface is the incoming current minus the reflected current, as expected. By combining Equation 4-16 and Equation 4-17:

$$I_{AI} = \frac{\rho_2 - \rho_1}{\rho_2 + \rho_1} I_A = k_{12} I_A \qquad 4\text{-}18$$

and

$$I_T = \left(1 - k_{12}\right) I_A = \frac{2\rho_1}{\rho_1 + \rho_2} I_A \qquad 4\text{-}19$$

where k_{12} is called the reflection coefficient and $(1\text{-}k_{12})$ is the transmission coefficient. By combining Equation 4-12 and Equation 4-18:

$$U_M = \frac{\rho_1 I_A}{4\pi}\left(\frac{1}{L_1} + \frac{\rho_2 - \rho_1}{\left(\rho_2 + \rho_1\right) L_4}\right) \qquad 4\text{-}20$$

By knowing the resistivity in conductor 1 and the potential U_M, the apparent resistivity in conductor 2 could be calculated using Equation 4-20.

In a more practical case when logging from the surface, where the electrodes are put directly on the rock surface and the air above is acting as a perfect isolator, the current would spread hemispherically through the rock. Taking into account the hemispherical surface area in Equation 4-8 the potential at a point in the conductor at the distance r from the current electrode (comparing to the zero potential) could be calculated according to:

$$U = \frac{\rho I}{2\pi r} \qquad 4\text{-}21$$

Equation 4-11 and Equation 4-21 are the starting point when calculating the apparent resistivity from surface measurements. This is further discussed in "Surface rock resistivity measurements".

4.5 Media with cylindrical coaxial boundaries

4.5.1 Introduction

This case is closely related to resistivity measurements in geophysical well logging. There are several problems involved when attempting to evaluate the rock resistivity from in-situ measurements. In an igneous rock/groundwater system the relatively conductive groundwater surrounding the measuring tool in the borehole will greatly disturb the rock resistivity measurements. This is especially a problem when using older tools, such as the ones SKB uses at present. Even though modern tools reduce the error arising when the borehole fluid is many orders of magnitude more electrically conductive than the surrounding rock, the issue is still of interest. Great efforts have been made to investigate the existing theory (Dakhnov, 1959) and apply it to the tools used by SKB.

Before performing well logging, a hole is drilled with an almost infinite depth comparing to its diameter. In the process of drilling, the rock close to the borehole may be affected. Micro fractures, altering the porosity of the rock matrix may be induced by the mechanical stress from the drilling and in addition the pores may be saturated with drilling mud, cooling water or filtrate. This zone is called the disturbed zone (or the invasion zone) and can be several millimetres thick in igneous rock (Autio et. al., 1999) and several centimetres thick in more porous sedimentary rock. The disturbance of the rock matrix and pore water decreases gradually with the distance from the borehole and at some distance the rock could be considered to be undisturbed.

In order to treat the problem with a reasonable simple theory some simplifications have to be made:

- The borehole and the rock surrounding the borehole are divided in three different infinitely long co-axial cylinders: the borehole, the disturbed zone, and the undisturbed rock (Figure 4-8).

- The medium in each cylinder is isotropic and homogenous. Therefore one has to find a representative mean value of the resistivity of the disturbed zone, where the resistivity in reality changes with the distance from the borehole.

This means that there are three isotropic homogenous cylinders. The inner cylinder, the borehole, has the outer radius r_0 and the resistivity ρ_0. The middle cylinder, the disturbed zone, has the outer radius r_d and the resistivity ρ_d. Finally the outer cylinder, the undisturbed rock, has the resistivity ρ_u and an infinite outer radius.

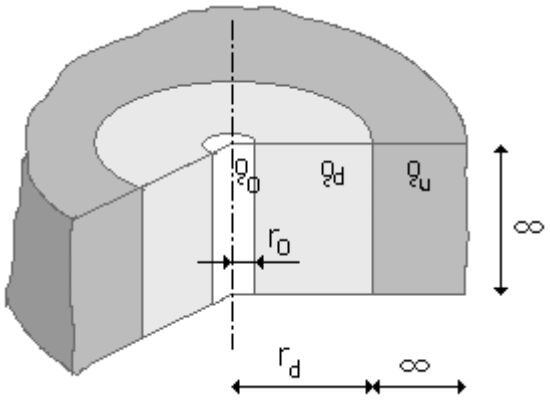

Figure 4-8 The borehole, the disturbed zone and the undisturbed rock.

The major drawback of the theory is that it works with homogenous cylinders that are infinitely long. Therefore it could only be used in rock that consists of layers of a thickness much larger than the borehole diameter. This is often not the case in fractured rock and rock where there are frequent changes in mineral composition.

4.5.2 Boundary conditions

When dealing with this case, cylindrical co-ordinates are better used, where the z-axis coincides with the borehole axis and the current electrode is placed in the origin. We shall also redefine our linear measurements in terms of borehole radius.

$$\begin{aligned} r &= r / r_0 \\ z &= z / r_0 \end{aligned} \qquad 4\text{-}22$$

Before solving the problem, a couple of boundary conditions have to be set up.

1. As in the case of one plane boundary, Kirchoff's first law has to be satisfied, here in form of Laplace's equation:

$$\nabla^2 U = 0 \qquad 4\text{-}23$$

2. As the distance from the current electrode approaches infinity, the potential approaches zero. This also means that the electric field becomes spherical when the distance from the current electrode approaches infinity.

$$U\Big|_{\sqrt{r^2+z^2}\to\infty} \to 0 \qquad 4\text{-}24$$

3. Very near the current electrode the potential is the same as it would have been in a homogenous conductor. This means that the electric field becomes spherical when the distance from the point current electrode approaches zero.

$$U\Big|_{\sqrt{r^2+z^2}\to 0} \to \frac{\rho_0 I}{4\pi r_0}\frac{1}{\sqrt{r^2+z^2}} \qquad 4\text{-}25$$

4. At the boundaries between the conductors there must be continuity in potential.

$$\begin{aligned} U_0\big|_{r,z=(1,z)} &= U_d\big|_{r,z=(1,z)} \\ U_d\big|_{r,z=(r_d,z)} &= U_u\big|_{r,z=(r_d,z)} \end{aligned} \qquad 4\text{-}26$$

where $U_{0,}$ U_d and U_u are the potentials in the borehole, the disturbed zone, and the undisturbed rock respectively.

5. At the boundaries between the conductors there must be continuity in the current density.

$$\begin{aligned} \frac{1}{\rho_0}\frac{dU_0}{dr}\bigg|_{r,z=(1,z)} &= \frac{1}{\rho_d}\frac{dU_d}{dr}\bigg|_{r,z=(1,z)} \\ \frac{1}{\rho_d}\frac{dU_d}{dr}\bigg|_{r,z=(r_d,z)} &= \frac{1}{\rho_u}\frac{dU_u}{dr}\bigg|_{r,z=(r_d,z)} \end{aligned} \qquad 4\text{-}27$$

6. The potential function is the same for negative values of z as for positive values of z as there is axial symmetry.

4.5.3 Solving the Laplace equation

As there is axial symmetry Equation 4-23, in cylindrical co-ordinates, reduces to:

$$\frac{\partial^2 U}{\partial r^2}+\frac{1}{r}\frac{\partial U}{\partial r}+\frac{\partial^2 U}{\partial z^2}=0 \qquad 4\text{-}28$$

By using Fourier's method of solving the differential equation, we assume that the solution is the product of two functions:

$$U = f(r)\phi(z) \qquad 4\text{-}29$$

where f(r) is only dependent on r and $\phi(z)$ is only dependent on z. If one differentiates Equation 4-29 and substitutes the result into Equation 4-28 and after that divide the outcome by Equation 4-29 one will get:

$$\frac{f''(r)}{f(r)}+\frac{1}{r}\frac{f'(r)}{f(r)}+\frac{\phi''(z)}{\phi(z)}=0 \qquad 4\text{-}30$$

When solving f(r) in Equation 4-30 both ϕ"(z) and $\phi(z)$ are independent of r and thus their ratio has to be constant.

$$\frac{\phi''(z)}{\phi(z)}=-m^2 \qquad 4\text{-}31$$

Equation 4-30 can now be written as a differential equation only dependent on r:

$$f''(r)+\frac{1}{r}f'(r)-m^2 f(r)=0 \qquad 4\text{-}32$$

At the same time Equation 4-31 can be written as a differential equation only dependent on z:

$$\phi''(z)+m^2\phi(z)=0 \qquad 4\text{-}33$$

The particular solution of Equation 4-32 will contain Bessel functions of zero order of the first and second kind, $I_0(mr)$ and $K_0(mr)$ for small arguments and the particular solution of Equation 4-33 will contain the functions sin(mz) and cos(mz). This means that the complete solution to Equation 4-28 will contain the products $I_0(mr)\sin(mz)$, $I_0(mr)\cos(mz)$, $K_0(mr)\sin(mz)$ and $K_0(mr)\cos(mz)$. According to boundary condition 6 there is axial symmetry and therefore the coefficients to the products containing sin(mz) have to be zero. Hence, the complete solution to Equation 4-28 is:

$$U_i=\int_0^\infty A_i(m)I_0(mr)\cos(mz)\,dm+\int_0^\infty B_i(m)K_0(mr)\cos(mz)\,dm \qquad 4\text{-}34$$

where $A_i(m)$ and $B_i(m)$ are functions of the parameter m and i is the index of cylinder. For the borehole one could get $B_0(m)$ by combining Equation 4-25, Equation 4-34, and the Weber-Lipschitz formula:

$$B_0(m)=\frac{\rho_0 I}{2\pi^2 r_0} \qquad 4\text{-}35$$

If new constants, $C_0(m)$, $C_d(m)$, $D_d(m)$, and $D_u(m)$, are created by dividing $A_0(m)$, $A_d(m)$, $B_d(m)$, and $B_u(m)$ with the right hand term in Equation 4-35, Equation 4-34 for the three different conductors will be:

$$U_0=\frac{\rho_0 I}{2\pi^2 r_0}\left[\int_0^\infty C_0(m)I_0(mr)\cos(mz)\,dm+\int_0^\infty K_0(mr)\cos(mz)\,dm\right] \qquad 4\text{-}36$$

$$U_d=\frac{\rho_d I}{2\pi^2 r_0}\left[\int_0^\infty C_d(m)I_0(mr)\cos(mz)\,dm+\int_0^\infty D_d(m)K_0(mr)\cos(mz)\,dm\right] \qquad 4\text{-}37$$

$$U_u=\frac{\rho_u I}{2\pi^2 r_0}\int_0^\infty D_u(m)K_0(mr)\cos(mz)\,dm \qquad 4\text{-}38$$

For the undisturbed rock the $A_i(m)$ term in Equation 4-34 has to be zero as $I_0(mr)$ becomes infinite for large values of r. Applying the boundary condition in Equation 4-26, keeping in mind that well radius r_0 equals one:

$$\int_0^\infty \left[\rho_0\left[C_0(m)I_0(m)+K_0(m)\right]-\rho_d\left[C_d(m)I_0(m)+D_d(m)K_0(m)\right]\right]\cdot \cos(mz)\,dm = 0 \qquad 4\text{-}39$$

The equation holds true for all z only if

$$\rho_0 C_0(m)I_0(m)+\rho_0 K_0(m)-\rho_d C_d(m)I_0(m)-\rho_d D_d(m)K_0(m)=0 \qquad 4\text{-}40$$

In the same manner for the boundary between the disturbed and undisturbed rock ($r = r_d$).

$$\rho_d C_d(m)I_0(mr_d)+\rho_d D_d(m)K_0(mr_d)-\rho_u D_u(m)K_0(mr_d)=0 \qquad 4\text{-}41$$

Before applying the boundary conditions in Equation 4-27, Equations 4-36, Equation 4-37, and Equation 4-38 have to be differentiated. In doing this one uses the Bessel function identity:

$$I_0'(m) = I_1(m) \qquad 4\text{-}42$$

and

$$K_0'(m) = -K_1(m) \qquad 4\text{-}43$$

By doing the same operations as with the potential boundary condition one will get:

$$C_0(m)I_1(m)-K_1(m)-C_d(m)I_1(m)+D_d(m)K_1(m)=0 \qquad 4\text{-}44$$

and

$$C_d(m)I_1(mr_d)-D_d(m)K_1(mr_d)+D_u(m)K_1(mr_u)=0 \qquad 4\text{-}45$$

An equation system with four equations (4-40, 4-41, 4-44, and 4-45) and four unknowns ($C_0(m)$, $C_d(m)$, $D_d(m)$, and D_u) could now be written as a matrix:

$$\begin{pmatrix} \rho_0 I_0(m) & -\rho_d I_0(m) & -\rho_d K_0(m) & 0 \\ 0 & \rho_d I_0(mr_d) & \rho_d K_0(mr_d) & -\rho_u K_0(mr_d) \\ I_1(m) & -I_1(m) & K_1(m) & 0 \\ 0 & I_1(mr_d) & -K_1(mr_d) & K_1(mr_d) \end{pmatrix} \begin{pmatrix} C_0(m) \\ C_d(m) \\ D_d(m) \\ D_u(m) \end{pmatrix} = \begin{pmatrix} -\rho_0 K_0(m) \\ 0 \\ K_1(m) \\ 0 \end{pmatrix} \qquad 4\text{-}46$$

When logging the rock resistivity a tool is wired down the borehole. Assuming that the electrode array is centred in the borehole it is only of interest to solve U_0 in Equation 4-36 at a point along the axis where r=0. As $I_0(mr) = I_0(0) = 1$ and

$$\int_0^{\infty} K_0(0)\cos(mz)\,dm = \frac{\pi}{2z} \qquad 4\text{-}47$$

Equation 4-36 then becomes

$$U_0\big|_{r=0} = \frac{\rho_0 I}{2\pi^2 r_0}\left[\int_0^{\infty} C_0(m)\cos(mz)\,dm + \frac{\pi}{2z}\right] \qquad 4\text{-}48$$

where C_0 could be calculated by solving the equation system in Equation 4-46. In order to shorten the solution of C_0 in Equation 4-46, the symbols are redefined as following:

$I_0(m) = I_{0m}$ $\quad I_0(mr_d) = I_{0mr}$ $\quad K_0(m) = K_{0m}$ $\quad K_0(mr_d) = K_{0mr}$

$I_1(m) = I_{1m}$ $\quad I_1(mr_d) = I_{1mr}$ $\quad K_1(m) = K_{1m}$ $\quad K_1(mr_d) = K_{0mr}$

C_0 then becomes:

$$C_0 = \frac{(\rho_d - \rho_0)\rho_d I_{0mr}K_{1m}K_{1mr}K_{0m} + K_{0mr}(I_{0m}K_{1m}K_{1mr}\rho_d(\rho_u - \rho_d)}{I_{0m}K_{1m}\rho_0(I_{0mr}K_{1mr}\rho_d + I_{1mr}K_{0mr}\rho_u) + I_{1m}(I_{0mr}K_{1mr}K_{0m}\rho_d{}^2}$$
$$\frac{+K_{0m}(-I_{1m}K_{1mr}\rho_d\rho_0 + I_{1mr}K_{1m}\rho_d\rho_u - I_{1mr}K_{1m}\rho_0\rho_u + I_{1m}K_{1mr}\rho_0\rho_u))}{+K_{0mr}(-I_{0m}K_{1mr}\rho_d{}^2 + I_{0m}K_{1mr}\rho_d\rho_0 + I_{0m}K_{1mr}\rho_d\rho_u + I_{1mr}K_{0m}\rho_d\rho_u - I_{0m}K_{1mr}\rho_0\rho_u))} \qquad 4\text{-}49$$

In Figure 4-9 $1000\cdot\cos(mz)$ where $z = 44.4$ and C_0 for different ρ_u/ρ_0 is plotted versus m. The value 44.4 (=1.6/0.038) is chosen as this is the value used later when obtaining correction factor curves for the borehole KLX02 in Laxemar, Sweden. The ρ_u/ρ_0 values used when calculating the C_0 curves are 50, 200, 1000, and 10,000 ohm.m.

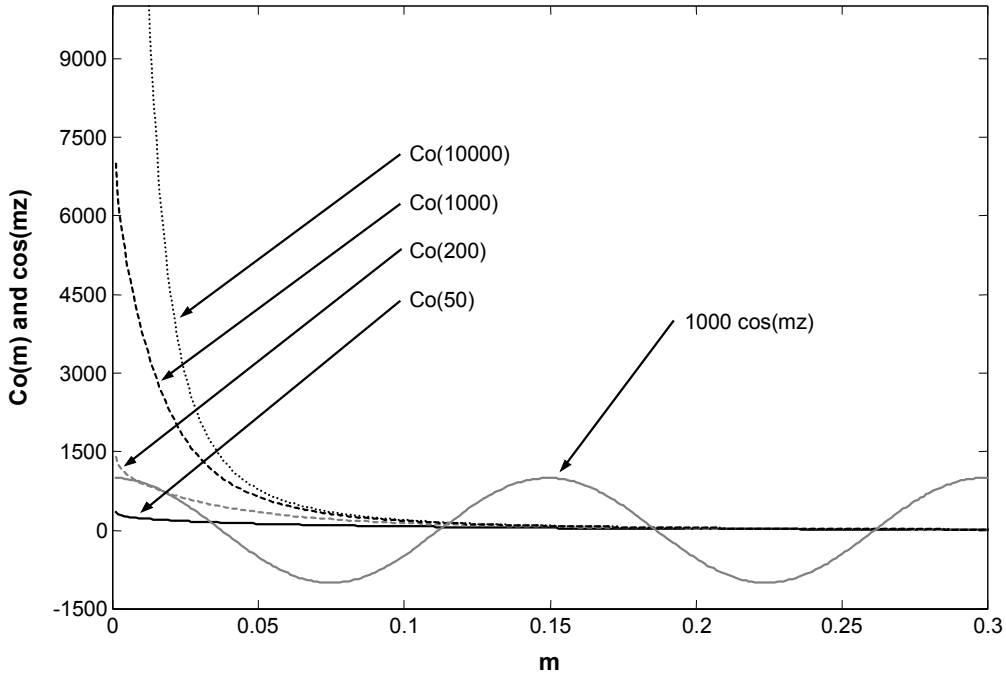

Figure 4-9 C_0 as a function of m and ρ_w/ρ_0 and cos(mz) as a function of m (here magnified by a factor thousand).

From Figure 4-9 one can see that $C_0 \cdot \cos(mz)$ approaches zero when m increases. Therefore one does not have to integrate the function to infinity. One can also show that the value of the function is smaller than that of $m^{-0.9}$ when m approaches zero. Therefore the lower and upper integration limit could be set to $1e^{-6}$ and 1 respectively when obtaining U_0 in Equation 4-48. It has been confirmed by using a much larger integration range that errors introduced when changing the integration range from $0 \rightarrow \infty$ to $1e^{-6} \rightarrow 1$ is negligible.

When m approaches zero the Bessel functions in Equation 4-46 approaches:

$$
\begin{aligned}
&I_0(mr) \rightarrow 1 \\
&K_0(mr) \rightarrow -\left(\ln\left(\frac{mr}{2}\right) + K \right) \\
&I_1(mr) \rightarrow \frac{mr}{2} \\
&K_1(mr) = \frac{1}{mr}
\end{aligned}
\qquad 4\text{-}50
$$

where K equals 0.577215. Equation 4-49 can therefore be simplified:

$$C_0 = \frac{(2(K(2\rho_0\rho_d - Km^2\rho_0\rho_d - 2\rho_d\rho_u + Km^2\rho_d\rho_u r_d^{\,2} + Km^2\rho_0\rho_u - Km^2\rho_0\rho_u r_d) +}{(4\rho_0\rho_d - 2Km^2\rho_0\rho_d - 2Km^2\rho_d\rho_u + K^2m^4\rho_d\rho_u r_d^{\,2} + 2Km^2\rho_0\rho_u -}$$
$$\frac{(2\rho_d^{\,2} - Km^2\rho_0\rho_d - 2\rho_d\rho_u + Km^2\rho_d\rho_u r_d^{\,2} + Km^2\rho_0\rho_u - Km^2\rho_0\rho_u r_d^{\,2})\ln\left[\frac{mr_d}{2}\right] +}{2Km^2\rho_0\rho_u r_d^{\,2} + m^2(2\rho_d^{\,2} - 2\rho_0\rho_d - 2\rho_d\rho_u + Km^2\rho_d\rho_u r_d^{\,2} +}$$
$$\frac{\ln\left[\frac{m}{2}\right](-2\rho_d^{\,2} + 2\rho_0\rho_d - Km^2\rho_0\rho_d + Km^2\rho_d\rho_u r_d^{\,2} + Km^2\rho_0\rho_u - Km^2\rho_0\rho_u r_d^{\,2} +}{2\rho_0\rho_u - 2\rho_0\rho_u r_d^{\,2})\ln\left[\frac{mr_d}{2}\right] + m^2\rho_d \ln\left[\frac{m}{2}\right](-2\rho_d +}$$
$$\frac{m^2(-\rho_0\rho_d + \rho_d\rho_u r_d^{\,2} + \rho_0\rho_u - \rho_0\rho_u r_d^{\,2})\ln\left[\frac{mr_d}{2}\right])))}{Km^2\rho_u r_d^{\,2} + m^2\rho_u r_d^{\,2}\ln\left[\frac{mr_d}{2}\right]))}$$

4-51

This means that one could calculate the potential at z using Equation 4-48 together with Equation 4-49 or Equation 4-51 for a given system having the known parameters ρ_d/ρ_0, ρ_u/ρ_0, r_d/r_0, and z/r_0. If the potential and all parameters but one are known, the unknown parameter, for example the undisturbed rock resistivity, could be calculated.

If the resistivity of the borehole fluid is smaller than that of the rock, which is the case when performing in-situ logging in igneous rock, the potential drop will be larger in the rock than in the borehole. Thus the electric field forming around the current electrode will not be spherical but elongated in the direction of the borehole. Numerical modelling, using Femlab® 3D has shown this. A small cylindrical current source, functioning as a point source, having the radius 0.5 and height 1 was placed in the centre of a cylinder having the radius 1 and the length 359 (the borehole). This cylinder was in turned placed in the centre of a sphere having the radius 180 (the rock). The resistivities of the cylinders were 1 while the resistivity of the sphere was varied (1, 10, 100, 1000, and 10,000). At the surface of the sphere the potential was defined as zero. The program calculated the potential in each point of the system and equipotentials were plotted in different colours. The results show that field becomes more elongated the greater the ratio between the rock resistivity and the borehole resistivity is (Figure 4-10).

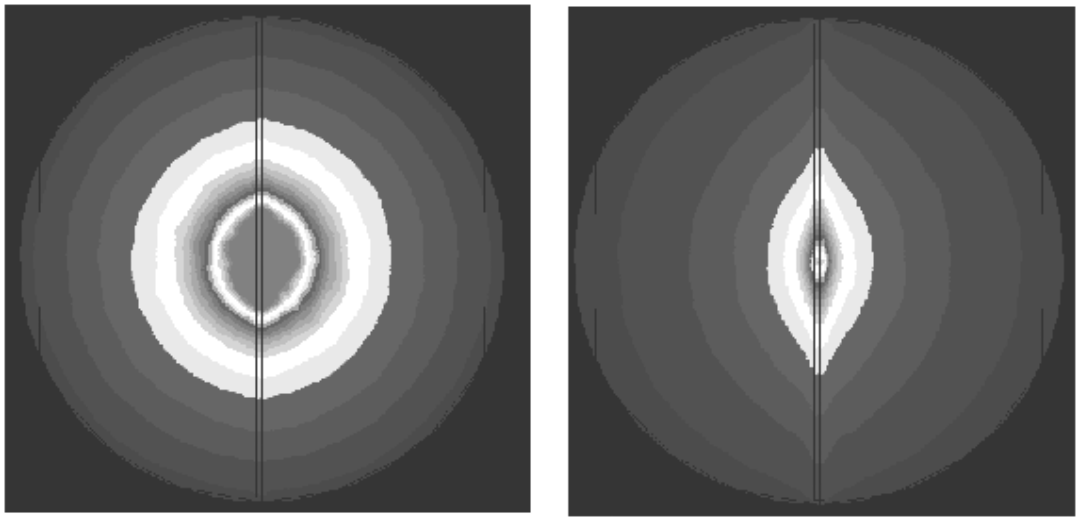

a) $\rho_u/\rho_0 = 10$ b) $\rho_u/\rho_0 = 100$

Figure 4-10 Equipotentials around a current source in a homogenous cylinder (the borehole) surrounded by a homogenous sphere (the undisturbed rock).

4.5.4 Creating correction factor curves

A practical example is when the resistivity of the borehole fluid is known as well as the potential drop form the current electrode to a point at a distance L from the current electrode. In geophysical well logging this method is called the normal log. In many cases the apparent resistivities, ρ_a, presented from these measurements have been obtained by using Ohms law for the spherical case:

$$\rho_a = \frac{4\pi L \Delta U}{I} \qquad 4\text{-}52$$

All data from the normal logging campaigns performed by SKB is presented in SICADA in this way. As seen in Figure 4-10 this will lead to an error, as the electric field is no spherical. It would be valuable to be able to recalculate an apparent resistivity into an undisturbed rock resistivity only by using a correction factor, C_{corr}.

$$\rho_u = C_{corr}\rho_a \qquad 4\text{-}53$$

By combining Equation 4-52, describing the potential drop in terms of apparent resistivity, and Equation 4-48 describing the potential drop in terms of true resistivities one will get Equation 4-54, keeping in mind that $z = L/r_0$ where L is the spacing and r_0 the borehole radius:

$$\frac{\rho_a I}{4\pi L} = \frac{\rho_0 I}{2\pi^2 r_0}\left[\int_0^\infty C_0(m)\cos\left(\frac{mL}{r_0}\right)dm + \frac{\pi r_0}{2L}\right] \qquad 4\text{-}54$$

Equation 4-54 could be simplified:

$$\rho_a = \rho_0 \left[1 + \frac{2L}{\pi r_0} \int_0^{\infty} C_0(m) \cos\left(\frac{mL}{r_0} \right) dm \right] \qquad 4\text{-}55$$

where C_0 is a function of ρ_u/ρ_0, $\rho_{d/}\rho_{0,}$ and r_d/r_0. When logging at a specific position, all the parameters ρ_0, ρ_d, $\rho_{u,}$ r_0, r_d, and L are constants and therefore an apparent resistivity could be calculated by Equation 4-55 for each set of parameters. By keeping L, r_0 and r_d constant and by varying ρ_u/ρ_0 and $\rho_{d/}\rho_0$ one can plot ρ_u/ρ_a versus ρ_a/ρ_0 (Figure 4-11).

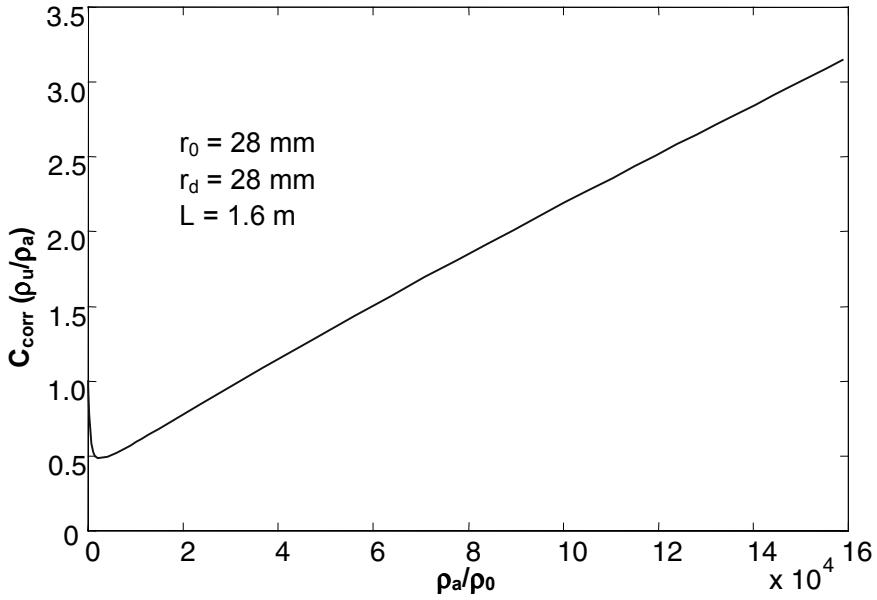

Figure 4-11 A correction factor curve.

Form Figure 4-11 and Equation 4-53 one can see that the y-axis of the plot equals the correction factor, C_{corr}. Both ρ_a and ρ_0 are easily obtained when performing in-situ logging with electrical methods. Examining the correction factor curve above one can see that r_d is set equal to r_0. This represents a case where no disturbed zone exists. If a disturbed zone exists or the system in some other way differs in geometry another correction factor curve has to be manufactured.

When drilling a core drilled borehole in crystalline rock the disturbed zone is very thin. Based on the disturbed zones in Autio et. al., 1999, a model disturbed zone 3 mm thick and three times less resistive than the undisturbed rock was used. Figure 4-12 shows that the correction factor curve does not change significantly when introducing the model disturbed zone.

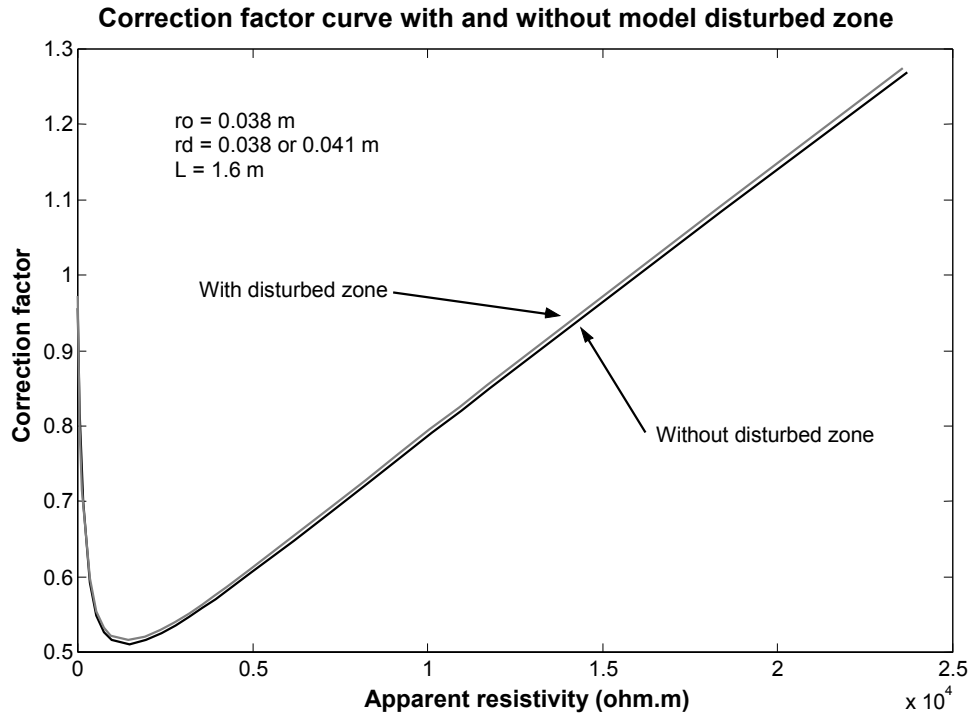

Figure 4-12 Correction factor curve with and without model disturbed zone.

At a first glance the correction factor curve above seems improbable, as there exists a minimum. When ρ_a/ρ_0 equals one the system is homogenous and the correction factor should be one. With increasing ρ_a/ρ_0 ratio the correction factor first decreases below one and reaches a minimum at some ratio. Further increase of the ρ_a/ρ_0 ratio will lead to an increase in the correction factor until it reaches one. This might lead to the idea that the electric field around the current electrode again becomes spherical. However as discussed above the numerical modelling showed that this was not the case (Figure 4-10). As of the shape of the correction factor curves was not obvious all equations and calculation where checked. Finding no errors in the analytical solution and no errors in the calculations further steps were taken to validate the correction factor curve. By using the numerical program Femlab® 3D the system used when obtaining Figure 4-10 was used to obtain numerical formation factor curves. Figure 4-13 shows correction factor curves for the same case from three different sources:

- Femlab - Solving the set-up used to create Figure 4-10 with Femlab® 3D. $L/r_0 \approx 57$ and $r_d/r_0 = 1$. Note that the current source was not a point source and that the "rock volume" surrounding the current source was not infinite.

- Matlab - The solution of Equation 4-55 by Matlab®. $L/r_0 = 57.1$ and $r_d/r_0 = 1$.

- Dakhnov - Curve based on values obtained from figure 81 in Dakhnov, 1959 (Appendix 1).

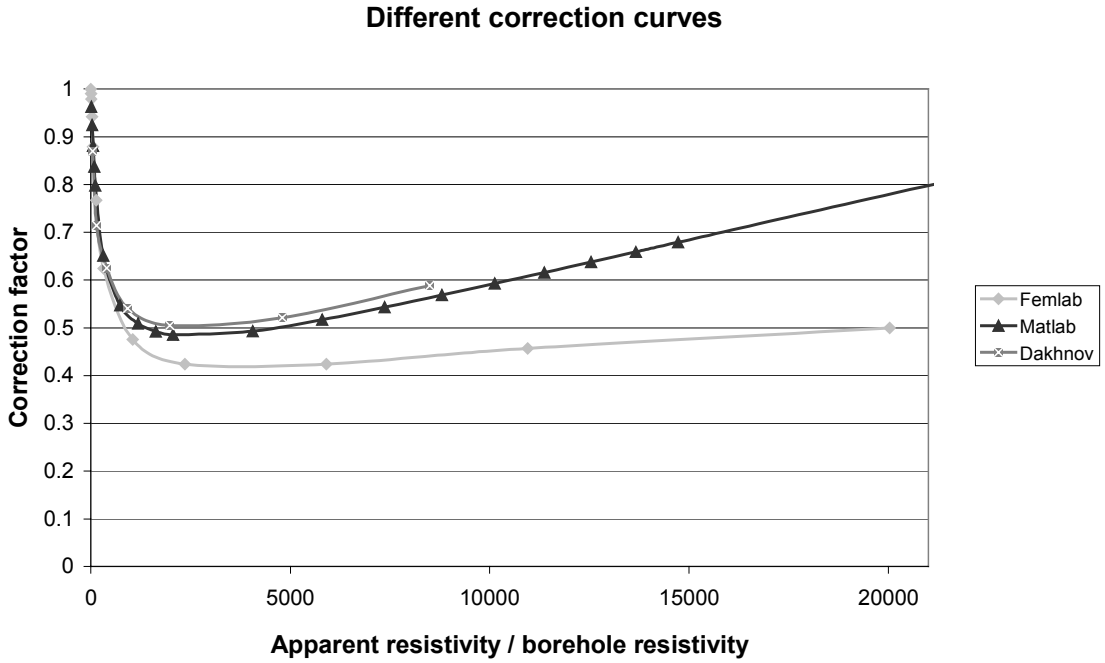

Figure 4-13 Three correction factor curves describing the same case.

The Dakhnov and Matlab curves are based on the same equations and should therefore coincide. However the data used when creating the Dakhnov curve was obtained by visual inspection of the diagram in Appendix 1 and small errors were most likely introduced. The Femlab curve deviates from the other two but has the same shape. The deviation is to a large extent due to the fact that the current source was not a point source and that a limited "rock volume" surrounding the current source had to be used. The error introduced by the limited "rock volume" became more severe when the ρ_u/ρ_0 ratio was increased as the field around the current source became elongated.

None of the correction factor curves above are able to correct experimental data in a reliable way. One reason for this is that the proposed model with three co-axial homogenous infinitely long cylinders and one point electrode does not represent the reality. Firstly the rock is seldom homogenous along the borehole even on a meter scale. Secondly the current electrode is often ring shaped and fitted on a cylindrical tool that in some cases is made of a highly conductive material, such as stainless steel (the electrodes are isolated from the tool suite). Therefore the tool in it self will disturb the measurements. For this reason an empirical correction factor curve was made for the SKB normal resistivity tool, based on data from logging campaigns performed in KLX02 in Laxemar, Sweden. Before presenting the empirical correction factor curve, the tools that were used to obtain the data it is based on are described (see Resistivity measurements of rock in-situ).

5 Formation factor measurements in laboratory

The formation factor of rock is traditionally measured by through, in or out diffusion experiments. Either a gas diffuses in the pores of a dried sample or a non-sorbing specie diffuses in the pore water in a saturated sample. As the surfaces of the mineral grains are negatively charged the non-sorbing specie in liquid diffusion experiments could be non-charged or negatively charged. It is important that the pH and ionic strength is controlled during the experiment. Some commonly used diffusing species could react during the experiment, as they may be sensitive to pH-changes, pe-changes, changes in ionic strength, UV-radiation, and so on. Therefore it is important to control the solutions in order to avoid these reactions. It is also important to make sure that outer circumstances, such as temperature and pressure, are constant throughout the experiment.

5.1 Liquid diffusion experiments

In a liquid through diffusion experiment a rock slice is placed between two chambers containing solutions of the same specie at different concentrations (Figure 5-1).

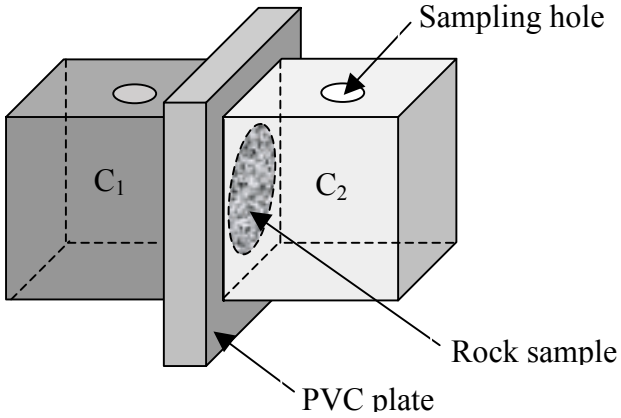

Figure 5-1 Experimental set-up of a liquid through diffusion experiment. (Drawn from Skagius, 1986).

The concentration C_1 in one chamber is very high while the other chamber initially contains no tracer. A small amount of the non-sorbing tracer, for example uranin, diffuses through the rock into the low concentration chamber. The amount diffusing through the rock is so small that the concentration in the high concentration chamber remains virtually constant. Samples are taken from the low concentration chamber and analysed in respect of concentration, for example by using a spectrophotometer. The concentration in the low concentration chamber, C_2, is plotted against the time in a breakthrough curve (Figure 5-2).

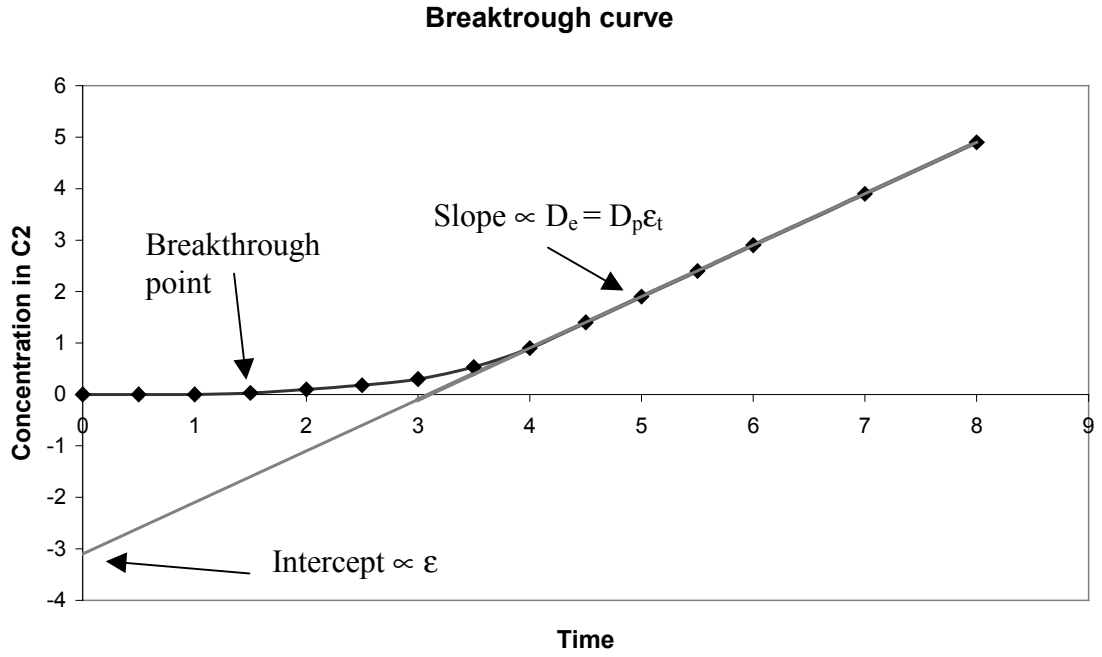

Figure 5-2 Principles of breakthrough curves from liquid through diffusion experiment with non-sorbing diffusing specie.

When time approaches infinity, the amount of diffusing specie that has diffused into the low concentration camber, Q, is:

$$Q = \frac{C_1 D_e}{L} t - \frac{C_1 L \varepsilon}{6} \qquad 5\text{-}1$$

Where L is the thickness of the sample (Crank, 1975). The effective diffusivity, D_e, could be calculated from the slope and the porosity, ε, from the intercept on the concentration axis of a breakthrough curve. If the diffusing specie is non-sorbing, the formation factor could be calculated from the effective diffusivity:

$$F_f = \frac{D_w}{D_e} \qquad 5\text{-}2$$

In a liquid in diffusion experiment a sample of the rock is placed in a solution containing the diffusing specie. The specie then diffuses into the pore water of the rock that initially was free of the specie. In a liquid out diffusion experiment a sample that is saturated with the diffusing specie is placed in a solution that initially is free of the specie. The concentrations in the solutions are monitored.

5.2 Electrical conductivity measurements

A new method of measuring the formation factor uses electro-migrating ions instead of diffusing species (Ohlsson, 2000). The pores in the rock sample are saturated with a NaCl solution of high ionic strength. This is achieved by placing the stones in the salt

solution of known composition for a long time. To speed up the saturation process the NaCl solution could be placed in a desiccator. After drying the rock sample in an oven it is also placed in the desiccator above the solution surface. The air is then evacuated using a vacuum pump. This will also evacuate the air or vapour in the micropores. The rock is then dropped into the solution and atmospheric pressure is restored forcing the solution to fill the micropores. After the saturation and equilibration the pore water has a known composition and conductivity. If an anode and a cathode where connected to the sample a potential gradient would be created. The anions and cations in the pore water would electro-migrates towards the anode and the cathode, carrying a current. Very soon the sample would become polarised and this would effect the current. Therefore alternating current is used and the frequency is high enough to ensure that the sample is not polarised. Care should be taken to use a frequency that minimises the capacitance effect. At frequencies below or around 100 Hz the capacitance effect is minor (Löfgren, 2001, Ildefonse and Pezard, 2001). By measuring the current and the potential drop over the sample the resistance could be obtained from Ohm's law. To prevent short-circuiting in the water film on the edge of the sample, the sample could be glued into a PVC-frame. To insure good connection copper electrodes could be used and a porous filter soaked with the salt solution could be placed between the electrode and the rock surface (Figure 5-3).

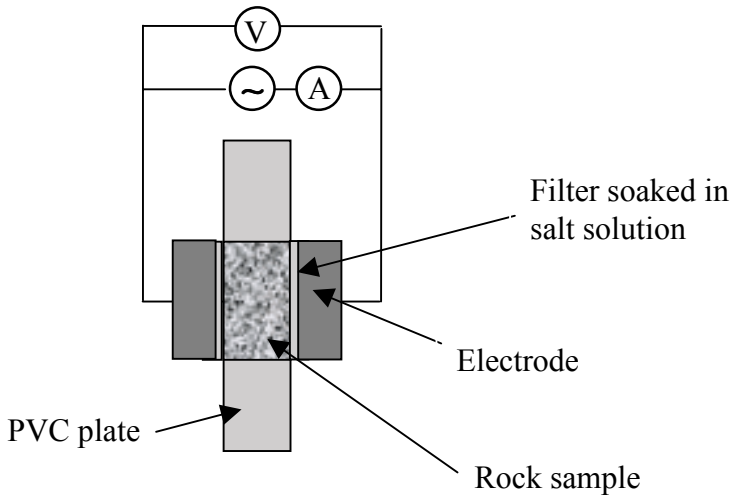

Figure 5-3 Experimental set-up of resistivity measurements.

By knowing the dimensions of the sample the rock conductivity, κ_r, could be calculated. As the pores are saturated with a salt solution with a known conductivity, κ_w, the formation factor could be obtained by Equation 3-25. As the pore water has a high ionic strength, the pore conduction contributes much more to the total conduction than surface conduction and Equation 3-25 could be simplified to:

$$F_f = \frac{\kappa_r}{\kappa_w} \qquad 5\text{-}3$$

The great advantage of the method is that the measurement is fast and does not require repeated sampling. However, before performing the measurements the samples have to be saturated for a couple or months but hundreds of samples could be saturated at the

same time only by placing them in a great vessel containing the salt solution. A disadvantage of the method is that it tends to give about two times higher formation factors than the through diffusion method (Ohlsson, 2000). In the comparison Ohlsson used uranin, which is a large organic molecule, in the through diffusion experiments while Na^+ and Cl^- ions carried the current in the electrical conductivity experiments. Different diffusing species are known to give slightly different formation factors due to anion-exclusion and size-exclusion effects. This may be an explanation to the deviation but the issue is under further investigation.

Another disadvantage with the electrical conductivity method is that current could be carried within the rock matrix. Here two cases emerge. The first is if the whole rock matrix is conductive. This could be investigated by measuring the dry rock conductivity. The dry rock conductivity for granitic rock is very low but if the rock is taken from an ore body it could be higher. If the current conducted in the rock matrix is higher or of the same magnitude as the current transported in the pores the electrical conductivity approach of measuring the formation factor is not applicable. The other case is if a minor amount of individual mineral grains are conductive. This may not affect the dry rock conductivity but these grains could "short circuit" the micropore system and apparently increase the constrictivity/tortuosity part of Equation 3-3. This could be tested by comparing the rock resistivity when using direct current as well as alternating current (Löfgren, 2001). If using direct current the constrictivity/tortuosity could not be overestimated due to electrically conductive minerals as the current is transported by ions (unless a number of electrochemical reactions occurred at the mineral surfaces). The comparison between the formation factors obtained by using direct as well as alternating current was done on three granite samples from Laxemar, Sweden, where no major difference could be seen (Löfgren, 2001, Löfgren and Neretnieks 2002). In these experiments special effort had to be made to avoid polarisation.

By using the electrical conductivity method enough samples could be analysed to perform formation factor logging on cores from deep boreholes. Possible one could also start investigating formation factor regions for different rock types and try to correlate the formation factor with texture and mineral content. This information would be valuable when trying to assess the matrix diffusion in rock not just around a borehole but between boreholes. Electrical conductivity measurements on laboratory could also be useful when validating in-situ resistivity measurements.

6 Resistivity measurements of rock in-situ

6.1 Introduction

Measuring electrical properties of rock in wells has been done since 1927 when Schlumberger developed the electrical coring log. Soon rock resistivity measurements became common when prospecting for minerals or oil. The most common methods were single-point resistance, normal and lateral. These tools were developed for detecting anomalies and not for quantitative rock resistivity measurements. The basic features of electrical logging could be shown by the example of locating water-bearing fractures in rock using the simplest equipment (Figure 6-1a). Two electrodes are connected to a power supply of constant voltage. One electrode is wired down the borehole while the other one remains on the surface. A bit simplified, the electrode in the borehole emits current that is conducted through the rock up to the electrode on the surface, thus creating a closed circuit. As both electrodes are connected to earth and the distance between them is great one does not consider that the current leaving the inhole electrode is directed toward the surface electrode but rather spreading out in all directions in the rock. If the inhole electrode is moved to a position in front of a fracture zone the current would not only be transported in the highly resistive rock but also in the electrically conductive groundwater flowing in the fractures. Therefore, the total resistance around the inhole electrode would decrease and the current would increase. This could be seen if one measures the current with an ampere-meter. By plotting the readout form the ampere-meter versus the depth of the inhole electrode, the most simplest electrical a log is created (Figure 6-1b). In order to avoid polarisation, alternating current is used rather than direct current.

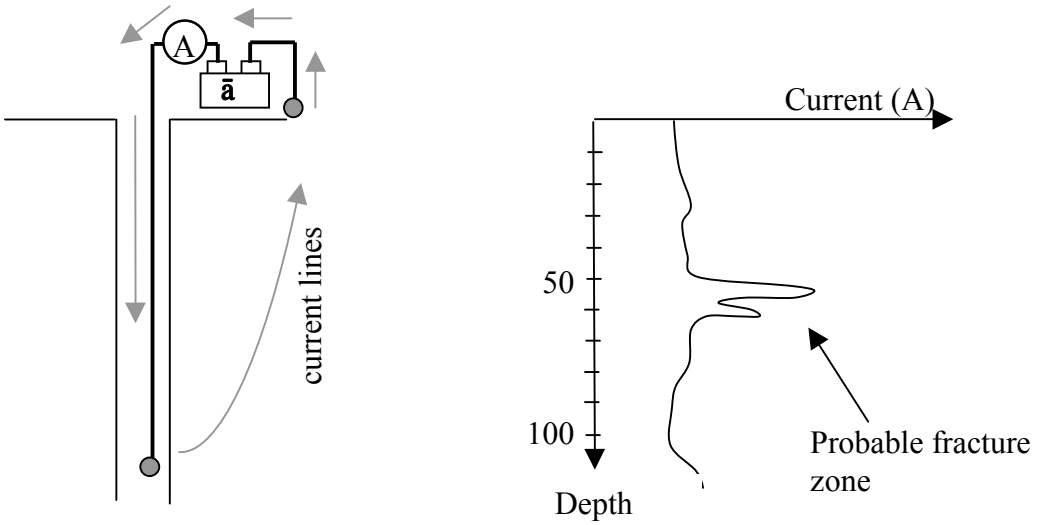

Figure 6-1 a) The most simple electrical logging equipment. b) The most simple electrical log.

From Figure 6-1b one could suspect that there is a water-bearing fracture zone between 50 to 60 meters. This anomaly could also be due to an electrically conductive ore formation, for example pyrite. In this type of logs, the qualitative logs, only changes in the readout is important and not the absolute values.

The same procedure could be carried out in sedimentary rock when locating oil-bearing formations. Oil may have a resistivity of the same magnitude as the resistivity of the surrounding sedimentary rock, and the anomalies could both be in forms of peeks or dips in the electrical log. If the electrical measurement is too imprecise and the noise is too great, anomalies due to oil reservoirs could remain undetected. Driven by the fact that better tools could locate more oil, coal, or whatever natural resource one was searching for, the technological advancement has been and still is fast in the area of equipment engineering. A breakthrough was the focused resistivity logs using guard electrodes forcing the current emitted by the current electrode to leave in a dish co-axial with the borehole. After the introduction of focused technique in 1950 the earlier, non-focused logs where more and more abandoned and are rarely used at present. Nowadays modern electrical log tools are quantitative, have a vertical resolution down to 10 cm, and are easy to use as specially developed software takes care of all the data gathering and processing.

In the following sections some logging tools that are or have been of importance are described. At present a number of companies manufactures electrical logging tools and every year new technology is introduced on the market. Therefore no attempt to cover the whole market has been made. The tools below are chosen as they give a good picture of the evolution of electrical logs and because they were innovative when they were introduced on the market. For further reading Desbrandes, 1985, and Keller and Frischknecht, 1966 is recommended. Tools used by SKB are also presented below together with some logs from campaigns performed in Sweden.

6.2 Single-point resistance array

The simplest borehole logging equipment is the single-point resistance array (also called single-electrode resistance). Two current electrodes, one remaining at the surface about 50 m from the borehole, and the other wired down in the borehole, are connected through an AC power supply (Figure 6-2).

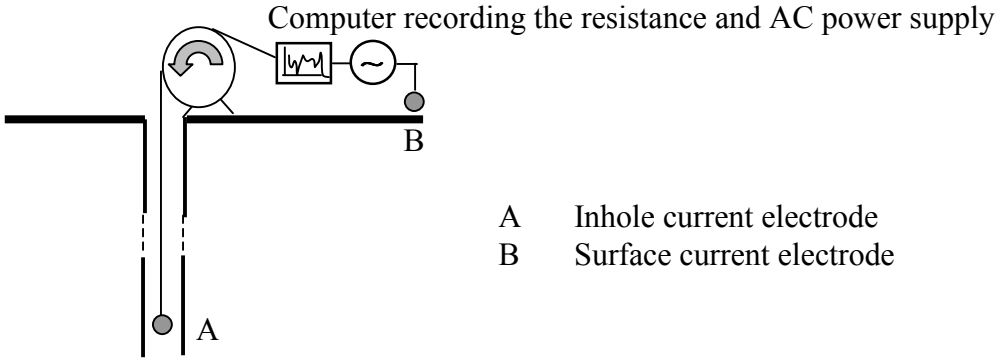

Figure 6-2 Set-up of single-point resistance. (Drawn from Keller and Fischknecht, 1966.)

The current and the voltage of the power source are measured and the resistance is calculated through Ohms law. All resistance of the circuit is taken to arise around the inhole electrode. In order to eliminate the contribution of the resistance between the surface electrode and the surface, a large contact area is used. In addition a secondary surface electrode may be placed 50 m from the primary surface electrode. As one makes sure that the potential between the two surface electrodes is zero when measuring, the resistance only becomes dependent on variations in the rock along the borehole. The approach of using two surface electrodes is however seldom used in general and not used by SKB. By assuming that the medium around the current electrode is homogenous the resistance is often recalculated by using Equation 4-8 and reported as resistivity. When drilling in sedimentary rock the borehole has to be filled with dense mud to be stabilised. In some special cases the mud has the same resistivity as the surrounding rock and the resistivity results could be considered to be quantitative. In most cases and especially when using groundwater as the borehole fluid the log is only qualitative and used for detecting anomalies. This is due to the fact that most of the current near the electrode will flow in the borehole fluid.

The single-point resistance is measured either continually or stepwise. SKB usually measures with a 0.1 m step with a maximum logging speed of 6 m/min. As the resistance is inversely proportional to the surface area perpendicular to the current flow, and the spherical surface area around the inhole electrode rapidly increases with distance from the electrode, the sample radius is only one or a couple of decimetres. Therefore a water-bearing fracture or some other local anomaly will have great impact on the results. A water-bearing fracture would lead to a dip from the base line in the resistivity log while a change in mineral composition may lead to a change in resistance and the value of the base line of the log will slightly decrease or increase.

In Figure 6-3 a single-point resistance log is shown from the section 350-400 m in KLX02 (here the resistance is recalculated to resistivity). From the core logging there has been established that rock type changes occur at 356-358 and 384-389 meters. In these sections the rock is designated as mafic volcanite while the surrounding rock is granite. From the core log one can see that section 384-389 contains more than 20

fractures quite evenly distributed (Figure 10-1). This is easily seen in the log below as a great dip. If the mafic volcanite had a resistivity that greatly differed from that of granite it would be undetectable because of the fracture zone. In the other mafic volcanite region (356-358 m) the situation is a bit more favourable as only a couple of fractures disturbs the measurements. Therefore it is possible to detect the resistivity change. Resistivity measurements with a quantitative log shows that the resistivity around 358 m is about five times higher than the resistivity of the granite a couple of meters from the mafic volcanite. This can also be seen from the single-point resistance log as a slight baseline shift. The single-point resistance log is better used for detecting water-bearing fractures than changes in mineralogy. The three marked dips around 364 m correspond very well to the fractures at 362.9 m + 363.1 m, 364.3 m, and 365.6 m detected in the core log. Core logging is described in Almén and Zellman, 1991.

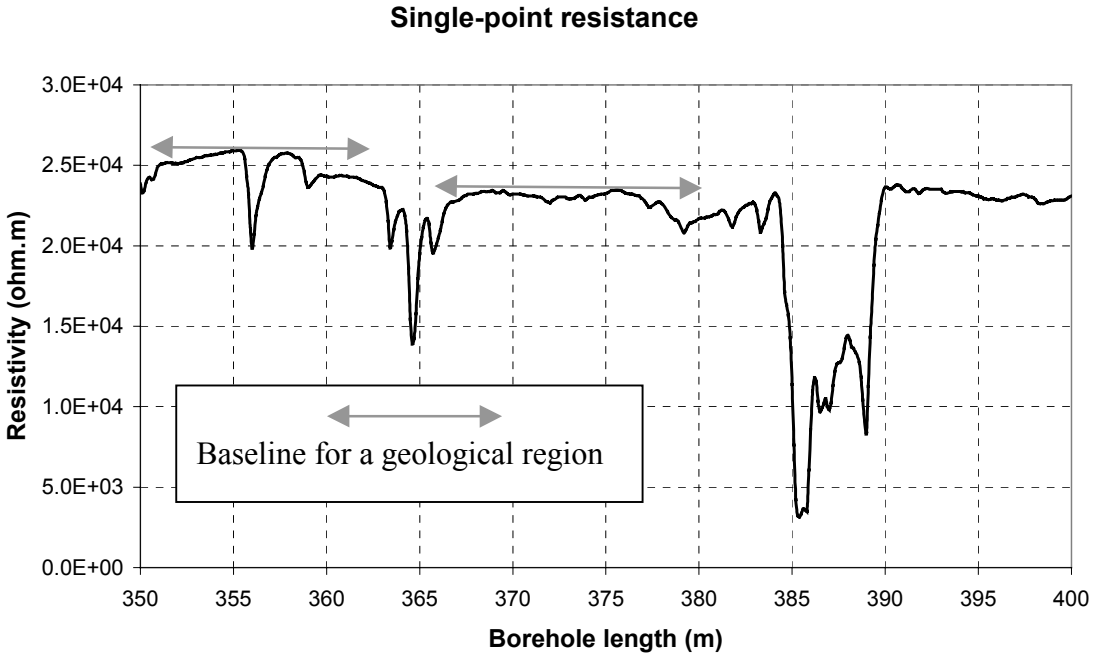

Figure 6-3 Single-point resistance log from KLX02 in Laxemar, Sweden. (Data from SICADA.)

Because of its simplicity, the single-point resistance could be stacked with other geophysical tools and measured secondarily in order to keep track of the depth. The measured anomalies could be used to correlate the depth to known anomalies.

6.3 Normal array

The set-up of the normal array is similar to that of the single-point resistance. Again two current electrodes are connected through an AC power supply (Figure 6-4). One electrode remains at the surface about 50 m from the borehole, and the other is wired down in the borehole. The potential between the two current electrodes is held constant at such a level that the current is acceptable for the equipment. The potential drop from the inhole current electrode to a point at a certain distance from the electrode is then measured. This is accomplished by wiring a potential electrode down the borehole at a

certain distance, L (called the spacing), from the current electrode. The inhole potential electrode is connected through a potentiometer to a potential electrode at the surface where the potential is zero by definition.

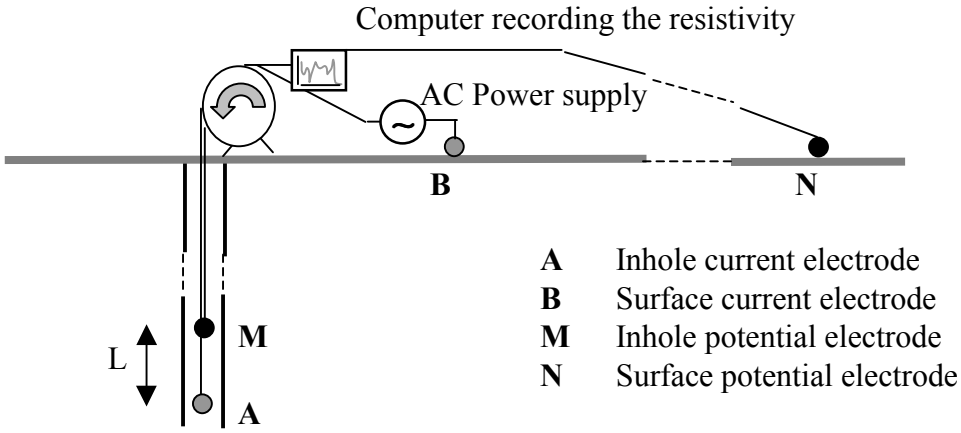

Figure 6-4 Set-up for normal resistivity log. (Drawn from Keller and Fischknecht, 1966.)

The potential drop from the current electrode A to the potential electrode M could be calculated by knowing the voltage of the power supply, ΔU_{AB}, the value of the potentiometer, ΔU_{MN}, and the potential drops from N to B, ΔU_{NB}:

$$\Delta U_{AM} = \Delta U_{AB} - \Delta U_{MN} - \Delta U_{NB} \qquad 6\text{-}1$$

ΔU_{NB} is normally taken to be zero as the electrodes are both connected to earth where the potential is zero. This may be controlled by using secondary surface electrodes as described above in "Single-point resistance". By assuming that the electrical field forming around the inhole current electrode is spherical the apparent resistivity could be calculated according to Equation 4-52. Deviations from the spherical field, due to the fact that the current density will be higher in the electrically conductive borehole fluid than in the resistive rock, could be corrected for in favourable cases that is shown later in this report. If the ratio between the rock resistivity and the borehole fluid resistivity is too great, which is often the case when logging in intrusive igneous rock using groundwater as the borehole fluid, the errors involved in correcting the apparent resistivity into rock resistivity are too great. In these cases the normal log can only be considered to be qualitative.

The configuration used by SKB is short normal, where the spacing is 0.4 m, and long normal (commonly called only normal), where the spacing is 1.6 meters. The investigation radius is between 0.6 and 2 times the spacing of the array. The potential between the two current electrodes is held constant at such a level that the current is within the region 5 mA to 30 mA. The (long) normal has a poor vertical resolution and therefore it is often not possible to detect minor point anomalies. This can be seen if comparing the normal log in Figure 6-5 with the single-point resistance log in Figure 6-3. The three anomalies, probably due to water-bearing fractures, around 364 m in KLX02 clearly shown by the single-point resistance log is shown as one wider

anomaly in the normal log. The poor vertical resolution, and at the same time the great investigation depth, makes the normal log less dependent on the borehole fluid. Therefore, it is easier to detect resistivity base line shifts with a normal log than with a single-point resistance. Again examining Figure 6-3 and Figure 6-5 one can see that the base line shifts, probably due to the mafic volcanite, is much easier to detect in the normal log than in the single-point resistance log. The short normal log has a better vertical resolution and a smaller investigation depth, making it close to the single-point resistance.

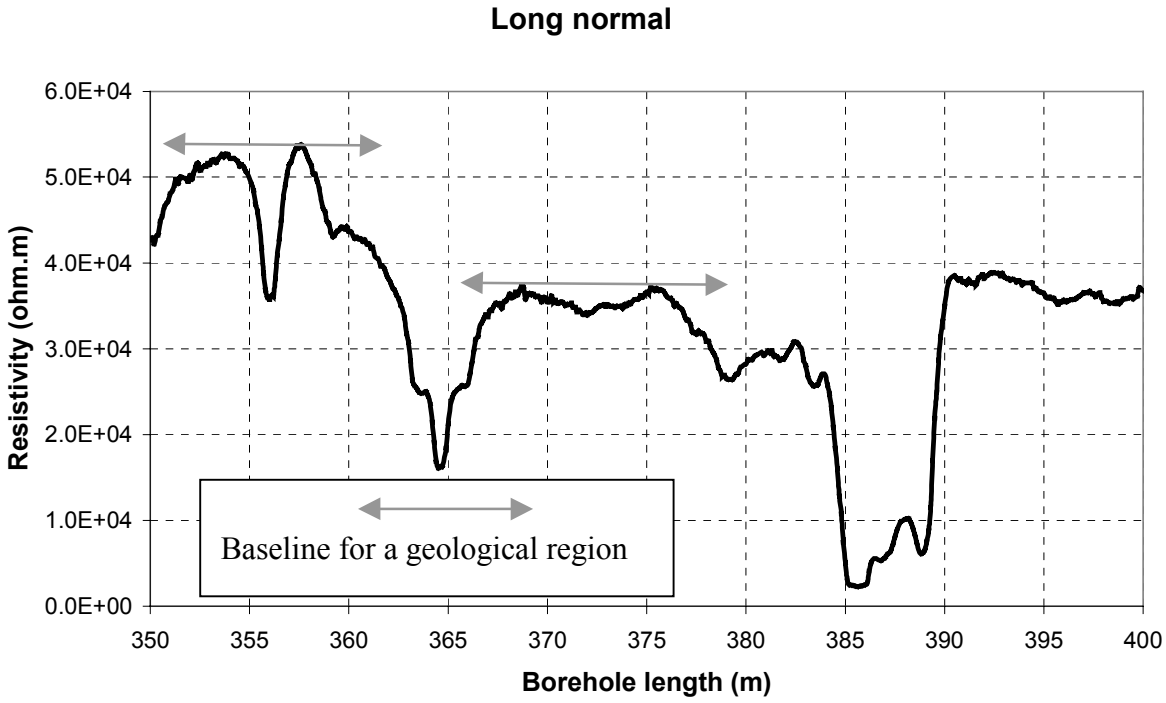

Figure 6-5 Normal log from KLX02 in Laxemar, Sweden. (Data from SICADA.)

6.4 Lateral array

In the lateral array, two potential electrodes are wired down the borehole together with the inhole current electrode (Figure 6-6). The potential gradient at a certain distance, L (called the spacing), from the inhole current electrode is measured. This is accomplished by measuring the potential drop between the two inhole potential electrodes placed closely on each side of the measuring point.

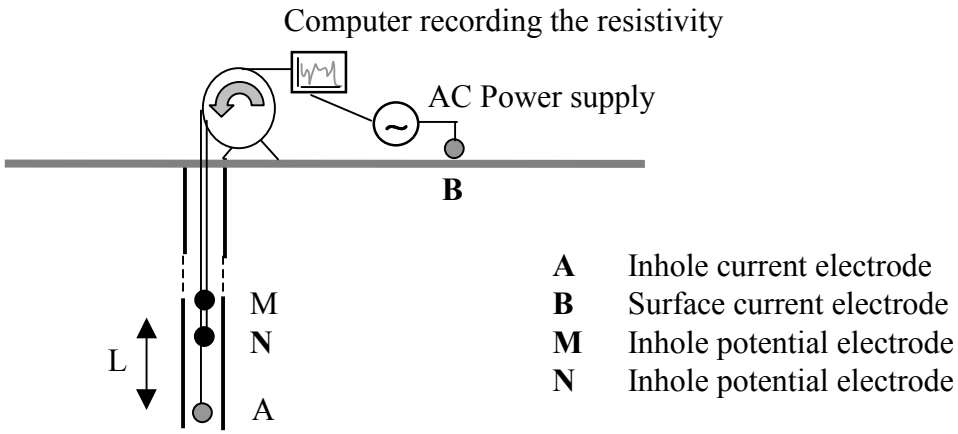

Figure 6-6 Set-up of lateral resistivity log. (Drawn from Keller and Fischknecht, 1966.)

The configuration used by SKB is 1.6 m - 0.1 m, meaning that the distance A-N is 1.6 m and the distance N-M is 0.1 m. This gives the spacing 1.65 m. Figure 6-7 shows a comparison of a lateral resistivity log with a normal resistivity log. Here one can see that the lateral log behaves like the single-point resistance. The vertical resolution is better than for the normal log while resistivity baseline shifts are harder to detect. When having a great rock resistivity to borehole fluid resistivity ratio, correcting the apparent resistivity into rock resistivity becomes impossible.

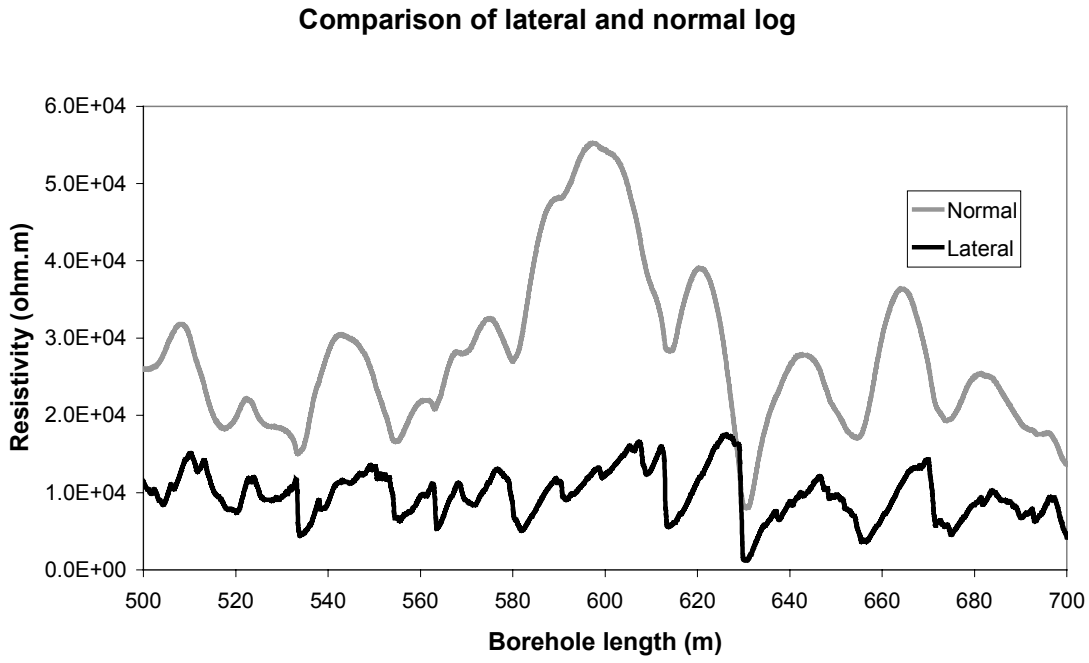

Figure 6-7 Lateral and normal log from KAS02 in Äspö, Sweden. (Data from SICADA.)

6.5 Combined resistivity probe use by SKB

SKB uses a probe that combines:

- Long normal (spacing 1.6 m)
- Short normal (spacing 0.4 m)
- Lateral (spacing 1.65 m)
- Single-point resistance
- Self-potential
- Borehole fluid resistivity
- Borehole fluid temperature

The probe, that is made of stainless steel, could be divided in there parts, the upper part with all the electronics, the middle part measuring rock resistivity and self-potential and the lower part measuring the resistivity and temperature of the borehole fluid. The rock resistivity measurements are not automatically corrected for self-potentials. The resistivity tool can be stacked with other geophysical tools in the WELLMAC system from SGAB. Some technical specifications of the are given below:

Supply voltage:	100 V AC, 300 kHz
	+15, -15 and +5 V DC
Max power supply:	5 W
Max electrode V:	100 V
Max electrode amp:	50 mA
Max cable length:	1500 m
Max Diameter:	42.4 mm
Length:	0.79 m (electronic part)
	2.38 m (rock resistivity and self-potential)
	0.64 m (borehole fluid resistivity and temperature)
Max log speed:	1 measurement/s (normally 6 m/min)
Max pressure:	150 bar
Max ambient temperature:	70°C (while operating)

A more extensive description of the system could be found in Rhén et al, 1995.

6.6 Focused logs

Focused logs usually use three or five inhole current electrodes (Figure 6-8). The centred electrode is normally called the current electrode while the surrounding two or four are called guard electrodes. If the surrounding medium is homogenous and if the current from each electrode was not affected by the fields emitted from the other electrode a spherical field would form around each of the electrodes (Figure 6-8 a). As all the electrodes have the same charge and emit current at the same time the current lines will be repelled in the real case. The current from the current electrode is therefore forced to leave in a horizontal dish co-axial with the borehole (Figure 6-8 b).

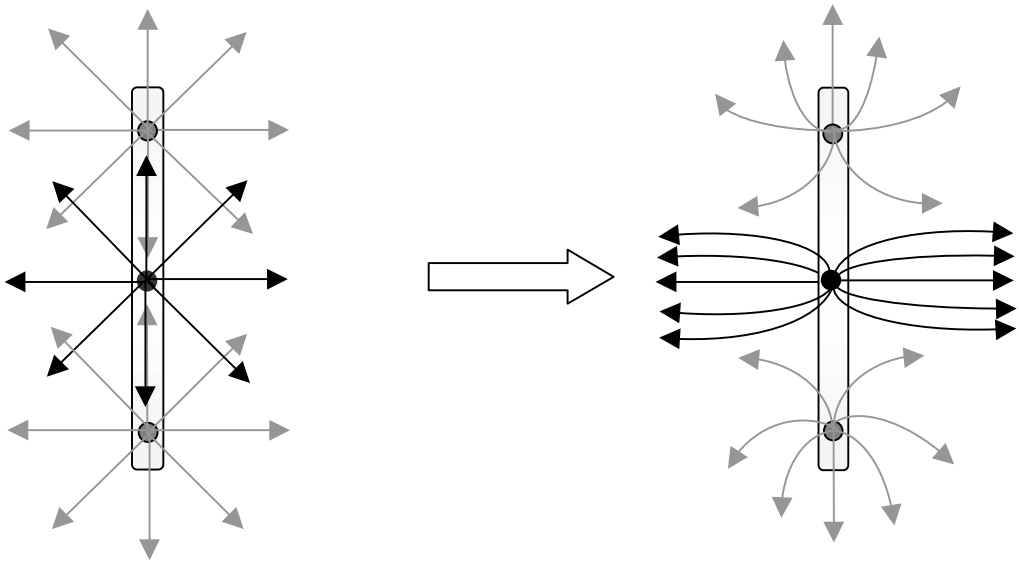

a b

Figure 6-8 a) Current lines from three electrodes emitting a spherical field. b) Resulting superimposed current lines.

As the current from the current electrode has to flow normally to the borehole, the measurements become more or less independent of the resistivity of the borehole fluid (as long as it is much lower than that of the rock). It also makes the measurements less dependent of the borehole diameter and the disturbed zone. To make sure than no current from the current electrode flows parallel to the borehole, most focused tools have two potential electrodes on each side of the current electrode (Figure 6-9). If there is a current flow parallel to the borehole there must also be a potential drop that could be detected with the potential electrodes. If this is the case a signal is sent to a computer controlling the power sources of the current electrode and the guard electrodes. The current is then increased or decreased in order to change the electric field to counteract the potential drop. When the potential drop is zero on each side of the current electrode, the measurement is made.

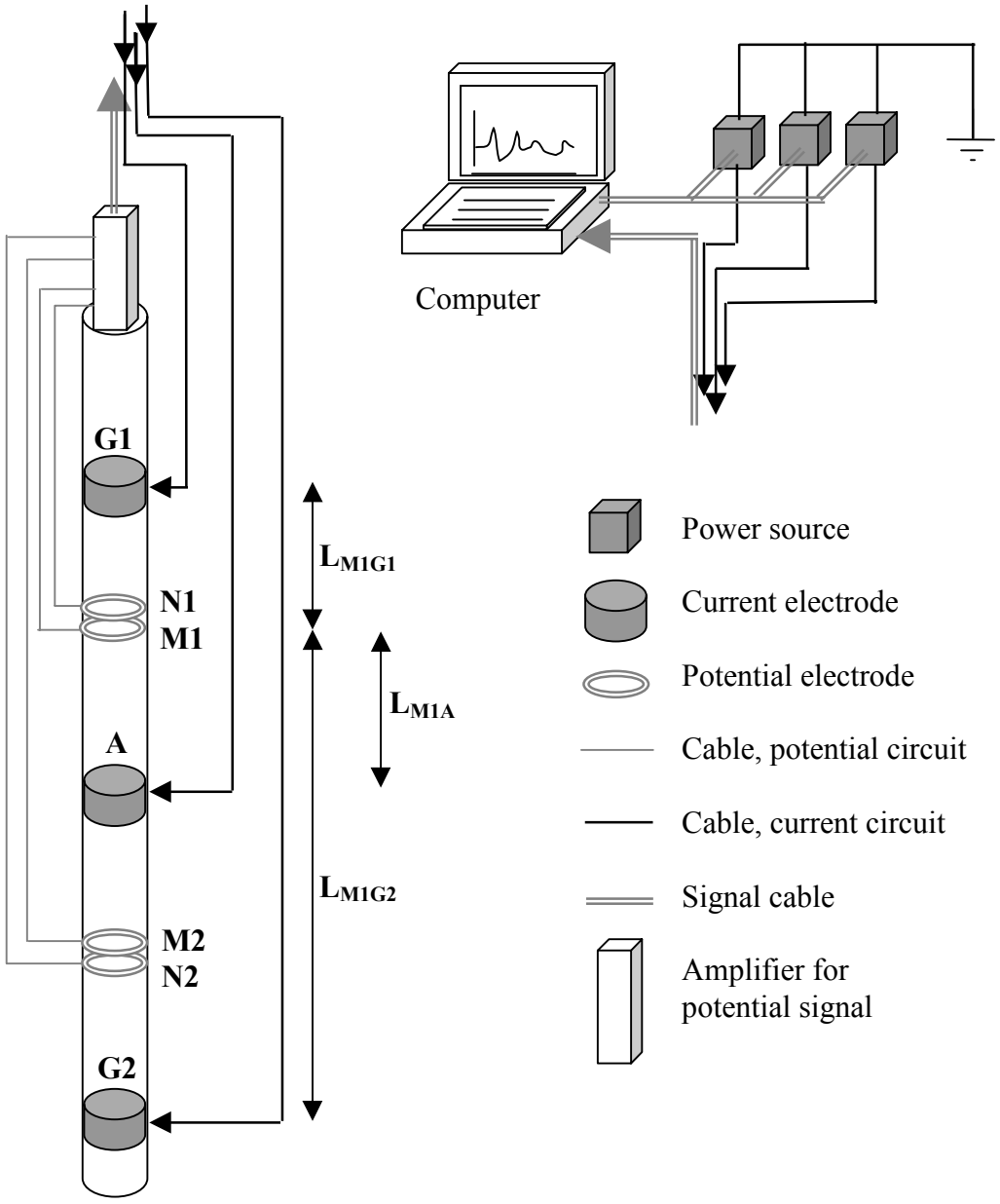

Figure 6-9 Principal sketch of a Laterolog 7.

The vertical resolution is a very important parameter in quantitative measurements. Focused tools have a vertical resolution of about the thickness of the current beam from the current electrode (Figure 6-8b). In igneous rock, water bearing fractures and fracture zones will lead to dramatic changes in the measured resistance. If a part of the current beam can flow in water in a fracture the total resistance will dramatically decrease leading to a misinterpretation of the rock resistivity. If the vertical resolution is too poor there is a chance that only few of the measured values are unaffected by fractures. It is recommended to choose a tool with a vertical resolution of at least half of the mean fracture interval and even better if one is also interested in the highly fractured zones. As an example the mean fracture interval in the borehole KLX02 is about half a meter. When logging with the normal resistivity log that has a resolution of about 3 m most of the values could not be used due to possible interactions of fractures. When logging

with a Dual-Laterolog with a vertical resolution of only a few decimetres most of the values could be used. Even in highly fractured zones some results could be obtained.

6.6.1 Theory of focused logs

The tool descried in Figure 6-9 is a Laterolog 7 with one current electrode, A, two guard electrodes, G1 and G2, and four potential electrodes, M1, N1, M2, and N2. The Dual-Laterolog, as an example, has four guard electrodes. However, it is sufficient to understand the theory of a seven electrode focused tool in order to understand the concept of all focused tools. For further reading Keller and Frischknecht, 1966, is recommended. In order to get a simple theory two approximations have to be made. The medium surrounding the tool is homogenous and isotropic and the electrodes are point electrodes. The total potential at M1, comparing to the zero potential, is the sum of the potential from the three current electrodes.

$$U_{M1} = U_{M1G1} + U_{M1A} + U_{M1G2} \qquad 6\text{-}2$$

Equation 4-8 can be combined with Equation 6-2:

$$U_{M1} = \frac{\rho}{4\pi}\left(\frac{I_{G1}}{L_{M1G1}} + \frac{I_A}{L_{M1A}} + \frac{I_{G2}}{L_{M1G2}}\right) \qquad 6\text{-}3$$

Where the I_{G1}, I_{G2} and I_A are the currents emitted by the electrodes and the distances are stated in Figure 6-9. In the same manner for N1:

$$U_{N1} = \frac{\rho}{4\pi}\left(\frac{I_{G1}}{L_{N1G1}} + \frac{I_A}{L_{N1A}} + \frac{I_{G2}}{L_{N1G2}}\right) \qquad 6\text{-}4$$

As the Laterolog is designed to eliminate any potential difference between M1 and N1 the potentials can be set to be equal:

$$U_{M1} = U_{N1} \qquad 6\text{-}5$$

If the focused tool is symmetric the current emitted by the guard electrodes will be equal, as the medium surrounding the tool is homogenous:

$$I_{G1} = I_{G2} \qquad 6\text{-}6$$

Then the total guard current is:

$$I_G = I_{G1} + I_{G2} = 2I_{G1} \qquad 6\text{-}7$$

Now the ratio between the current from the current electrode and from either of the guard electrodes can be calculated by combining Equation 6-3 to Equation 6-7:

$$\eta = \frac{2I_A}{I_G} = \frac{L_{M1G1}L_{M1G2}L_{N1G1}L_{N1G2}}{L_{M1A}L_{N1A}\left(L_{M1G2}L_{N1G2} - L_{M1G1}L_{N1G1}\right)} \qquad 6\text{-}8$$

By combining Equation 6-3 and Equation 6-8 the potential at M1 and M2 could be expressed by using only the current from A:

$$U_{M1} = U_{M2} = \frac{\rho I_A}{4\pi}\left[\frac{1}{L_{M1A}} + \eta\left(\frac{1}{L_{M1G1}} + \frac{1}{L_{M1G2}}\right)\right] \qquad 6\text{-}9$$

From this equation the resistivity can be calculated. By placing all the parameters constant for the tool in to a geometric factor, K, the apparent resistivity can be calculated by:

$$\rho_a = \frac{U_{M1}}{I_A} K \qquad 6\text{-}10$$

where K is :

$$K = \frac{4\pi}{\frac{1}{L_{M1A}} + \eta\left(\frac{1}{L_{M1G1}} + \frac{1}{L_{M1G2}}\right)} \qquad 6\text{-}11$$

The fact that the medium around the tool is not homogenous will affect the measurements. Firstly the current emitted by the guard electrodes will not be equal if there is a vertical variation in the resistivity as stated in Equation 6-6. As in the case for non-focused tools the problem of spherical field /cylindrical borehole will arise. This error is introduced in Equation 6-3 that is based on Ohms law for a spherical field. However, the field around the current electrode will not be directly affected by the borehole fluid and therefore the error introduced in Equation 6-3 and Equation 6-6 will only have a minor effect on the result. The deviation in apparent resistivity from the undisturbed rock resistivity is normally only a few percent or even less, slightly depending on the rock resistivity to borehole fluid resistivity ratio.

6.6.2 Laterolog 3

The first focused resistivity tool was the Laterolog 3 that had one current electrode with one guard electrode at each side. The potential was kept at the same level in the three electrodes making the current emitted from the current electrode to leave in hyperbolic lines. The technique was later abandon in the benefit of other focused logs.

6.6.3 Laterolog 7

The Laterolog 7 is described above. The thickness of the current beam is normally 0.8 m in larger tools (mostly used in the oil industry). The vertical resolution for quantitative measurements is approximately the same as the thickness of the current beam. Specialised tools can have a vertical resolution of only one decimetre. The deviation in apparent resistivity from the undisturbed rock resistivity is normally a few percent or less.

6.6.4 Laterolog 8

This log is very similar to Laterolog 7. The exception is that the thickness of the current beam (the zone where the current from the current electrode leaves) is 0.35 m. This makes it similar to the short normal array with the difference that the effect of the borehole fluid is almost entirely eliminated.

6.6.5 Dual-Laterolog

The Dual-Laterolog is similar to the Laterolog 7 but comprises an extra pair of guard electrodes (Figure 6-10). As in the Laterolog 7 the current from the current electrode, A, is sent out normal to the tool axis in a current beam. As described above this is assured by measuring the potential gradient on both sides of the current electrode with the potential electrode pairs M1-N1 and M2-N2. By adding the two extra guard electrodes, G12 and G22, which can change polarity, the field from G1 and G2 could either be enchanted or enfeebled. When the field is enchanted the current beam is forced to penetrate even deeper into the rock before it becomes dispersed due to inequalities in the power supply and rock matrix (Figure 6-10a). This is the case in the DLLd (Dual-Laterolog deep) that has a greater investigation radius and where the decree in current density mainly is due to the cylindrical geometry of the field. When G12 and G22 have an opposite polarity than G1 and G2 the field is enfeebled. Near the tool the field from G1 and G2 governs the direction of the current emitted by A while further away from the tool the field from G12 and G22 is attracting the current (Figure 6-10a). This is the case in the DLLs (Dual-Laterolog shallow) that has a smaller investigation radius where the decrease in current density with distance from the electrode is both due to the cylindrical and further out the more spherical geometry of the field. The DLLs is therefore more sensitive to the disturbed zone.

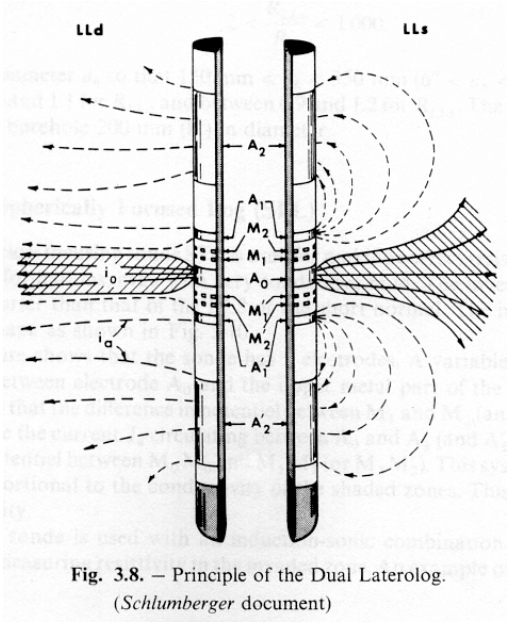

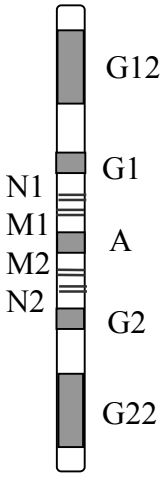

a b

Figure 6-10 a) Current lines from a Dual-Laterolog. (From Desbrandes, 1985). b) Electrode set-up of a Dual-Laterolog. The DLLd and DLLs mode can not be used at the same time.

The advantage of the Dual-Laterolog is that two resistivity measurements at different investigation radius can be made simultaneously. The disturbed zone may affect the measurements of the DDLd but this can be corrected for by using information from the DLLs. Before computers where commonly used, the resistivities of the disturbed zone and undisturbed rock were calculated by an equation system with two unknown parameters, the resistivities, and the two measurements:

$$\rho_{DLLs} = J_s\rho_d + (1 - J_s)\rho_u \qquad 6\text{-}12$$

$$\rho_{DLLd} = J_d\rho_d + (1 - J_d)\rho_u \qquad 6\text{-}13$$

where J_s and J_d are pseudo-geometrical factors provided by the Service Company. These factors, often given in charts, are both dependent on the geometry of the tool and the geometry of the borehole and the disturbed zone. At present the manufacturers of the resistivity tool often design software making all the corrections and calculations. The program may require additional input data concerning the disturbed zone. These data can be acquired using a microlog.

The Dual-Laterolog was primarily developed for the oil industry, where greater borehole diameters are used and the rock is sedimentary. Only recently, slimhole Dual-Laterologs has been developed for quantitative measurements in high resistivity rock. The slimhole Dual-Laterolog from Antares is a six-electrode tool and does not uses separate potential electrodes (M1, N1, M2, and N2 in Figure 6-10b) but measures the potential difference between A, G1, and G2 and a potential electrode at the surface. By making sure that all the potential differences are equal, the result is the same as if one would have used the separate potential electrode approach. The Antares Dual-Laterolog could be acquired with the tool diameter 38 mm and the quantitative measuring range 0.1-600,000 ohm.m. According to the manufacturer the error should not exceed 3% in the high performance region of 0.1-150,000 ohm.m. If measuring in rock with a resistivity above 600,000 ohm.m the error exceeds 20%. The vertical resolution should be 0.10 m, the maximum logging speed 25 m/min, the maximum pressure 250 MPa and the maximum temperature 75°C (Antares, 2000).

A demo logging was performed in the section 203-1400 m in the borehole KLX02. The tool used had a diameter of 43 mm and a quantitative range of 0.1-200,000 ohm.m where the high performance quantitative range was up to 50,000 ohm.m. The result from the section 350-400 m is shown in Figure 6-11.

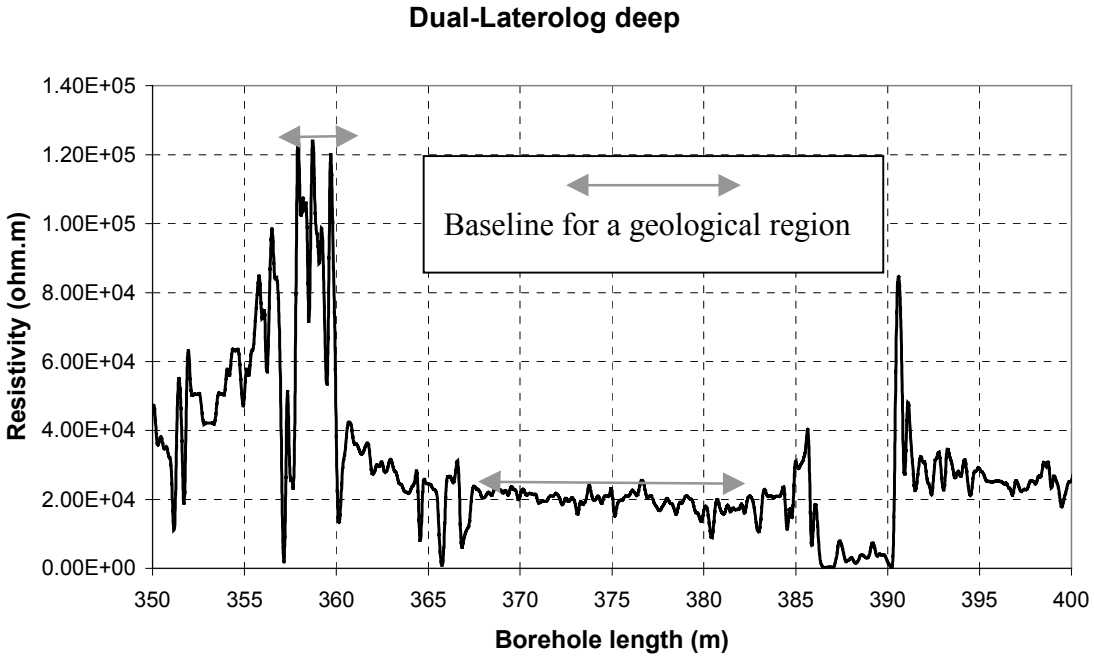

Figure 6-11 DLLd log from KLX02 in Laxemar, Sweden. (Data from Antares.)

Comparing the DLLd log with the single-point resistance (Figure 6-3) and the normal resistivity log (Figure 6-5) one can see that the DLLd combines the advantages of both. As in the single-point resistance log, fractures are very visible as dips in the DLLd log. The resistivity values associated with fractures should only be taken as qualitative. The three dips around 364 meters shown in the single-point resistance log are clearly shown also in the DLLd log. Here one can see a 1.5 m displacement on the borehole length axis as the dept calibration was not adequately performed before logging with the Dual-Laterolog. The high resistivity area around 350-360 m in the normal resistivity log is clearly seen also in Figure 6-11. Judging from the measurements the mafic volcanite (356-358 m according to the core logging) is 4-5 times as resistive as the surrounding granite. Figure 6-12 shows the section 350-364 m in KLX02. Here the borehole axis is corrected for the 1.5 m displacement. The black diamonds on the x-axis represent the location of the natural fractures located in the core logging. Here one can see the importance of vertical resolution.

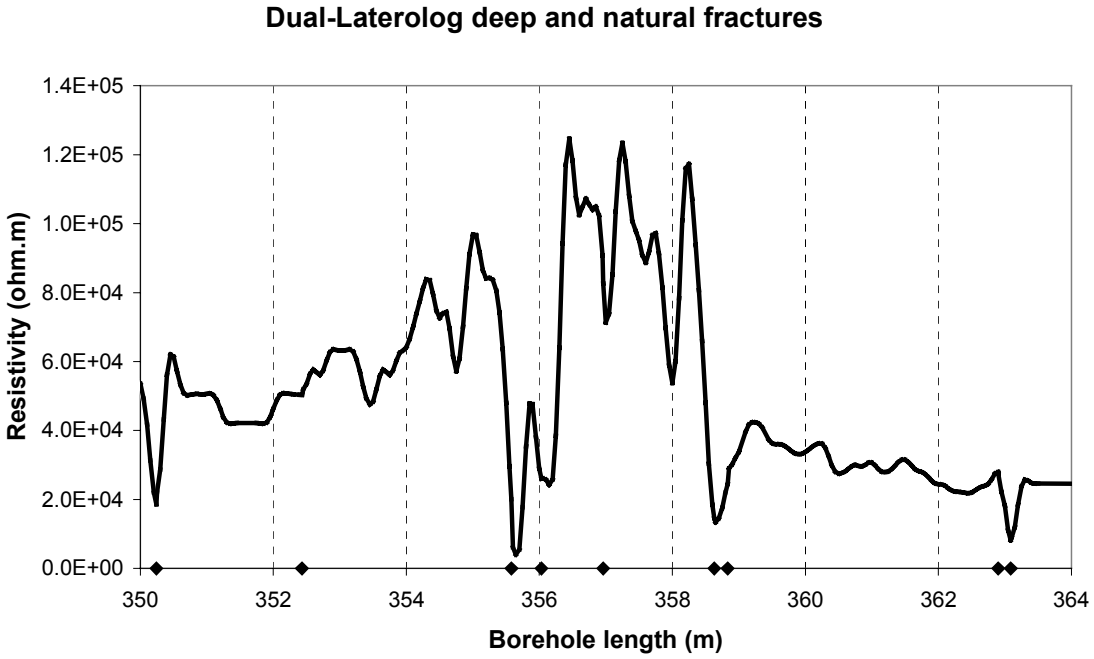

Figure 6-12 Dual-Laterolog deep (DLLd) and natural fractures (black diamonds) in KLX02 in Laxemar, Sweden. (Data from Antares and SICADA.)

In Figure 6-12 one can see that most of the natural fractures from the core logging coincide with resistivity dips in the in-situ log and this indicates that these fractures are water-bearing (or at least water filled). The fractures that do not coincide with resistivity dips are probable not water-bearing. The great dip at 358 m can not be accounted for without furthering examining the core. Due to the vertical resolution of only a few decimetres, high resistivities can be measured quantitatively between fractures (for example the peek at 356.5 m that is surrounded by two fractures). In conclusion the Dual-Laterolog is an excellent tool for measuring the rock resistivity quantitatively in fractured intrusive igneous rock.

6.7 Empirical correction factor curve for the normal log

Logging campaigns in KLX02 and KA3065A02 (Äspö, Sweden), among others, have shown that correction factor curves for the SKB normal resistivity log based on Equation 4-55 (Figure 4-12) are not applicable as they give too small correction factors at large ρ_a/ρ_0 ratios. One reason for this may be they are based on a model where a point electrode is placed directly in the borehole fluid. Furthermore the borehole fluid, the disturbed zone and the undisturbed rock are modelled as three infinitely long co-axial homogenous cylinders (Dakhnov, 1959). This is not the case in reality as a logging tool is used. The logging tool, which may be made of some highly conductive material, such as stainless steel, will fill most of the borehole surrounding the electrodes. In addition the current electrode fitted on the cylindrical tool is ring shaped and not a point electrode. Therefore the tool in it self will introduce a deviation from the Dakhnov model.

In logging campaigns performed in KLX02 three different resistivities of interest when making correction factor curves have been obtained. In 1993 the borehole fluid resistivity, ρ_0, and the apparent rock resistivity based on the normal log, ρ_a, was obtained. In 2000, quantitative rock resistivities were obtained by using Antares slimhole Dual-Laterolog. If the resistivities from the Dual-Laterolog are taken as true undisturbed rock resistivities, ρ_u, an empirical correction factor curve could be obtained by comparing ρ_a/ρ_0 and ρ_u/ρ_0 using Equation 4-53. When making the empirical correction factor curve, all in-data from these three logging campaigns where taken a "exact". I would have been preferred if the two rock resistivity logs had been obtained at the same time. It is important to point out that the vertical resolution is an issue when comparing ρ_a and ρ_u as the two rock resistivity tools responds differently to water-bearing fractures. For this reason only fracture free sections of 3.2 m, which approximately is the vertical resolution of the normal log, or greater were used. Between 213 and 1100 meters, 25 of these sections were found and ρ_a/ρ_0 and ρ_u/ρ_0 data from the midpoint of these sections were used (Figure 6-13). Below 1100 m the borehole fluid is too saline and therefore sections from this part of the borehole were not used.

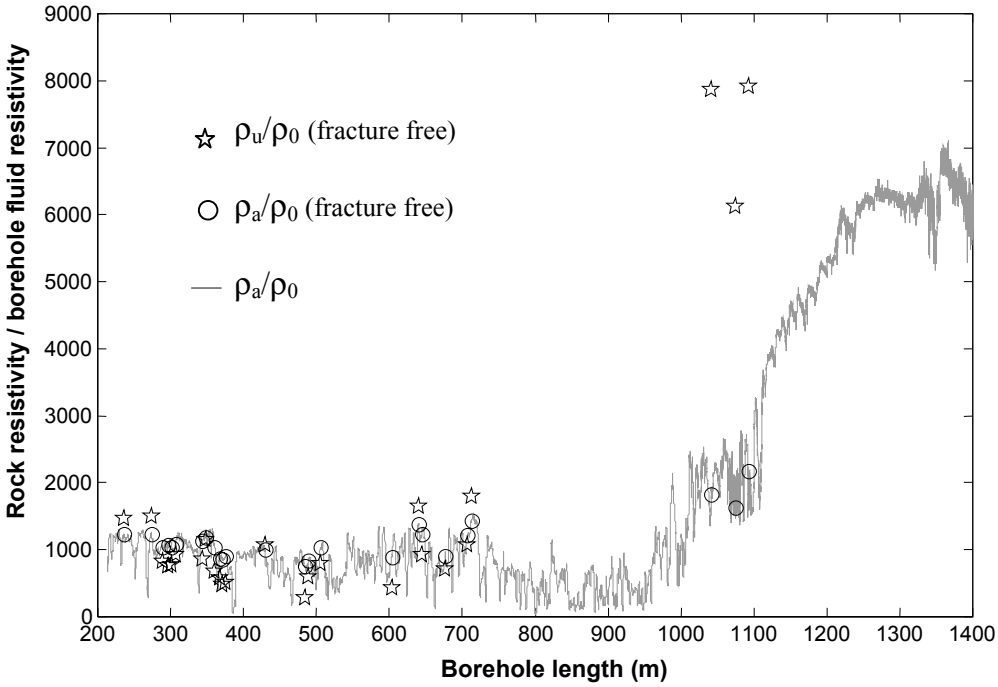

Figure 6-13 ρ_a/ρ_0 and ρ_u/ρ_0 data from KLX02 in Laxemar, Sweden.

From Figure 6-13 one can see that when ρ_a/ρ_0 is less than ~1100, ρ_u/ρ_0 is even lower leading to a correction factor less than one. When ρ_a/ρ_0 is higher than ~1100, ρ_u/ρ_0 is higher leading to a correction factor larger than one. As the correction factor should be one or close to one when the rock resistivity equals the borehole fluid resistivity, the empirical correction factor curve would probably have the same minimum as the correction factor curves in Figure 4-13.

In Figure 6-14 the correction factor for each section is calculated according to Equation 4-53 and plotted versus ρ_u/ρ_0 in a modified correction factor curve. A polynomial fitting has been made.

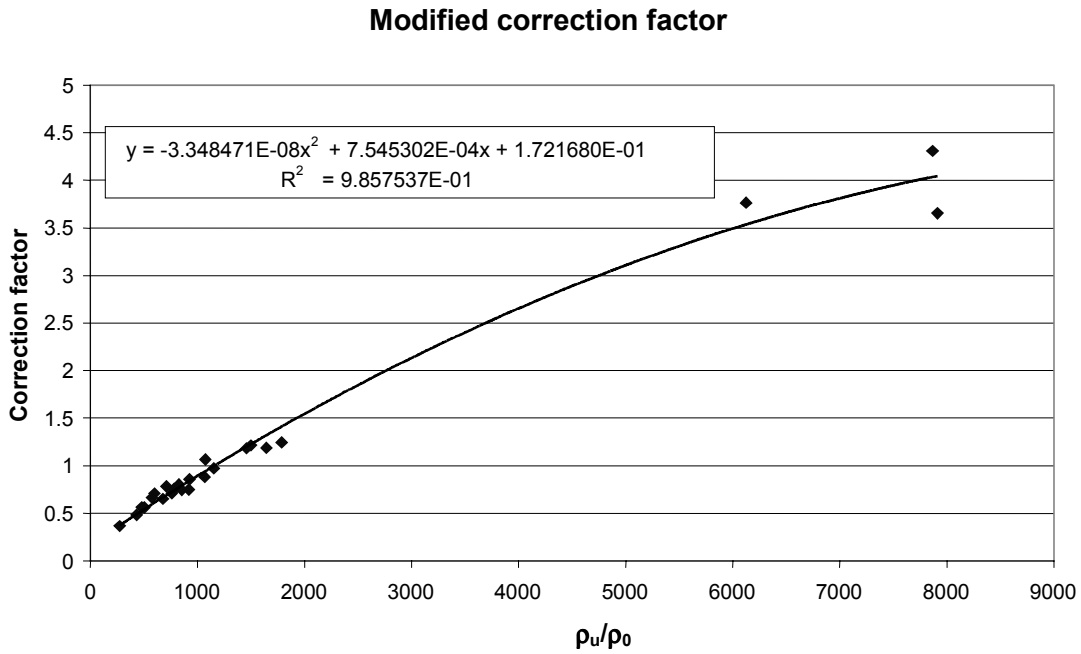

Figure 6-14 Modified correction factor.

In Figure 6-15 the polynomial function in Figure 6-14 has been used and ρ_u/ρ_0 on the x-axis has been recalculated to ρ_a/ρ_0. A polynomial fitting to the new curve has been made. The fitting is only valid in the ρ_a/ρ_0 range 500 to 2000.

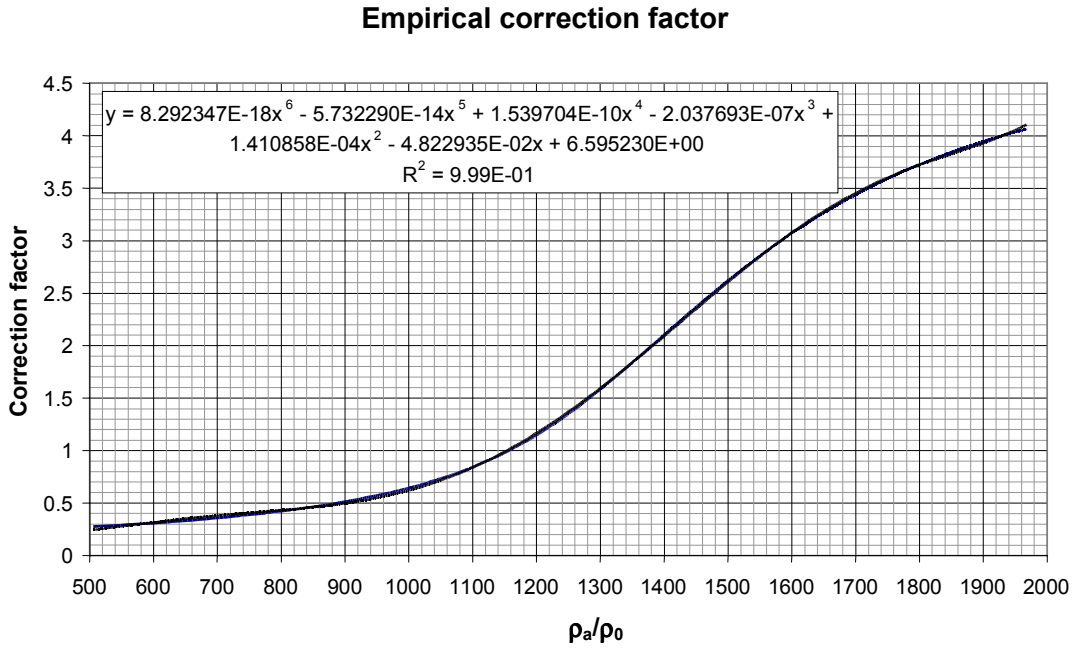

Figure 6-15 Empirical correction factor for the SKB normal log for 76 mm boreholes.

Here a warning is in place. If the borehole fluid has the same resistivity as the pore water, the real ρ_u/ρ_0 ratio would be in the order of 10^4 - 10^5. This would lead to a very large correction factor (Figure 6-14). Therefore the ρ_a/ρ_0 ratio would be so much smaller than the ρ_u/ρ_0 ratio that it may end up in the range valid for the correction factor curve. Therefore only a relatively small correction factor would be used. The resulting ρ_u/ρ_0 ratio would therefore be much less than the real ρ_u/ρ_0 ratio. The error arose as the borehole fluid was not much more resistive than the pore water or the natural groundwater. Before using the correction factor curve it must be determined that the borehole fluid is much more resistive than the natural groundwater. Methods of doing this are described in section 9.

In Figure 6-16 the normal log from section 350-400 m in KLX02 has been corrected according to the correction factor curve in Figure 6-15.

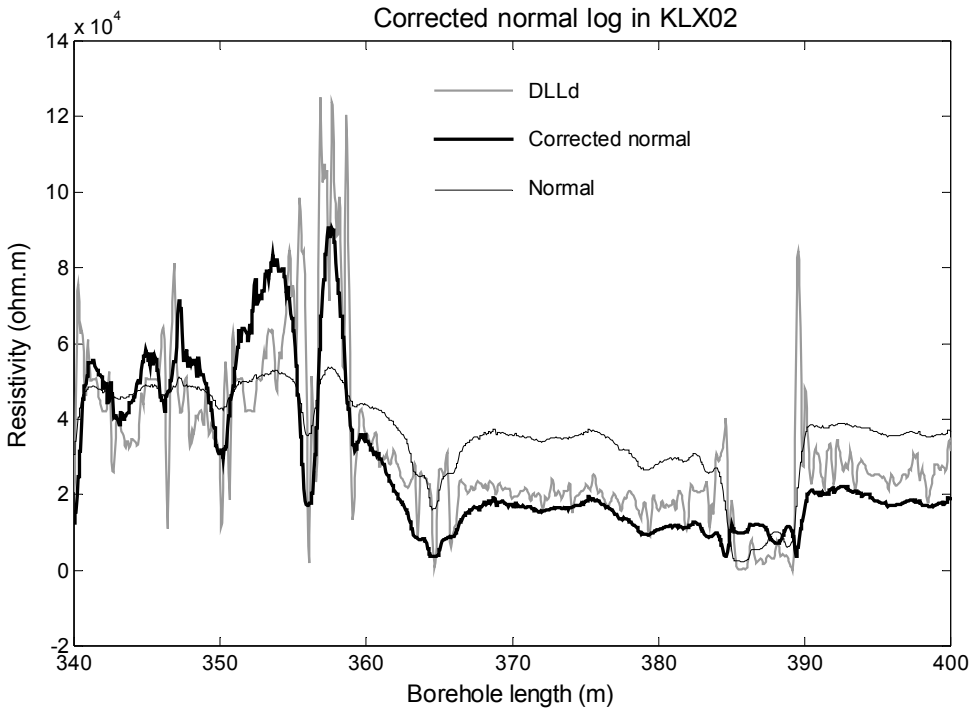

Figure 6-16 Corrected normal log in KLX02 in Laxemar, Sweden.

In Figure 6-16 one can see that the corrected normal log to a large extent coincides with the Dual-Laterolog deep. There are two main reasons why it is possible to achieve such a good correction of the normal log in this section. The first is that rock is relatively homogenous in respect of fractures and rock type changes. The second is that the borehole fluid mainly consists of surface water or water from the upper part of the rock that is ~25 times more resistive that the pore water.

If the borehole fluid is of the same order of magnitude as the pore water the correction factor will be much higher. In Figure 6-17 fracture free sections from the whole borehole have been sorted out and the correction factor from the midpoint of this sections has been plotted. As can be seen by Figure 9-3 the borehole fluid does not

consist of non-saline surface water below 1000 m but rather of a mixture of surface water and saline groundwater. At 1400 m the borehole fluid resistivity is of the same order of magnitude as that the pore water, judging from scooping formation factor calculations, and the correction factor becomes larger than 50.

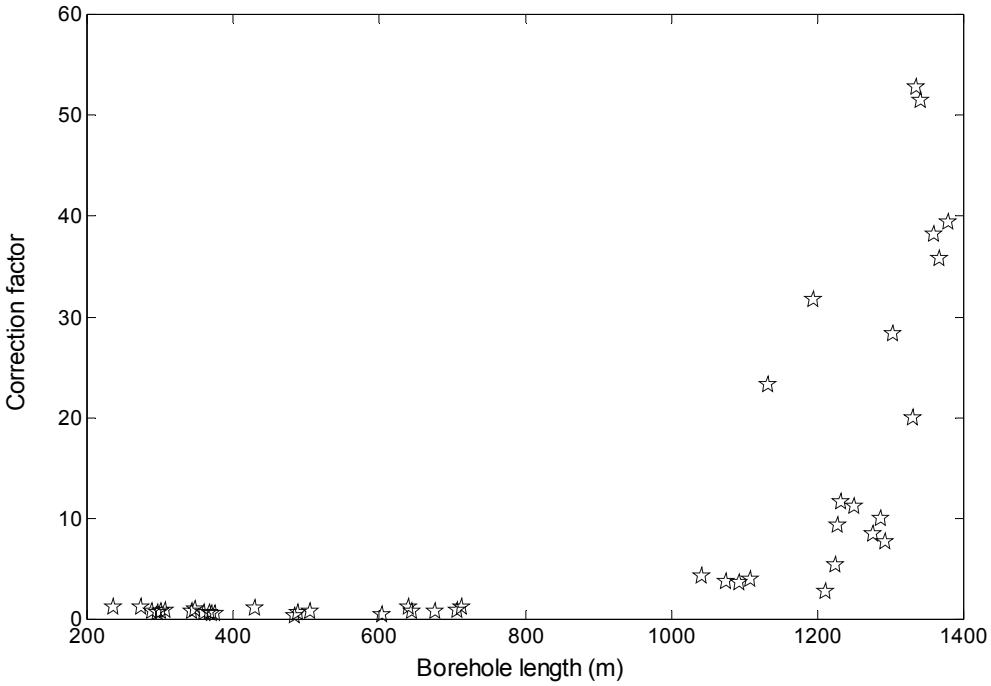

Figure 6-17 Empirical correction factors for whole KLX02 in Laxemar, Sweden.

To conclude the SKB normal log could be corrected successfully and give fairly quantitative values for a 76 mm borehole in saline regions if the rock is fairly homogenous and fracture free and if non-saline water is introduced as the borehole fluid.

6.8 Micrologs

Micrologs, both focused and non-focused are miniature logs often used to examine the disturbed zone. Their investigation radii are in the range of a couple of centimetres. Modern tools can have a vertical resolution on a centimetre scale and could therefore be interesting in trying to obtain the rock resistivity of altered rock around natural fractures. Many of these tools are however developed for the oil industry where large borehole diameters are used and therefore they do not fit in the 76 mm boreholes used by SKB.

6.8.1 Microlog

The microlog was introduced on the market in the early 1950s. They comprise button shaped electrodes held by pads. Hydraulic or spring arms press the pads against the rock (Figure 6-18). The electrodes are 25 or 50 mm apart and either normal or lateral arrays are used. As the investigation radius is very small (about 25 mm) only the resistivity of

the disturbed zone, ρ_d, can be measured. The resistivity measurements are also only qualitative. The advantage of the tool is that each porous and permeable layer is clearly detected.

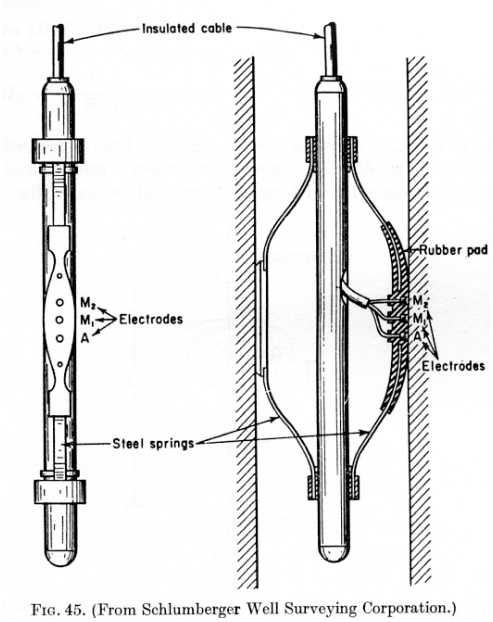

FIG. 45. (From Schlumberger Well Surveying Corporation.)

Figure 6-18 Set-up of a Microlog. (From Keller and Frischknecht, 1966.)

6.8.2 Microlaterolog

The Microlaterolog is similar to Laterolog 7 besides the fact that it is much smaller. The guard and potential electrodes are in shape of rings (Figure 6-19). The Microlaterolog gives excellent measurements of the resistivity of the disturbed zone and is often used together with the Microlog.

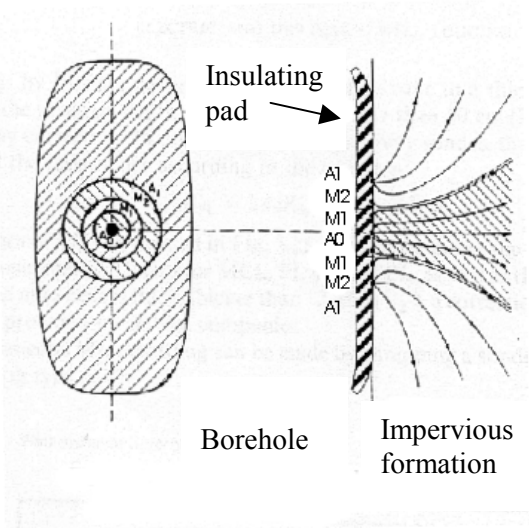

Figure 6-19 Set-up of Microlaterolog. (From Desbrandes, 1985 (image-enhanced).)

6.9 State-of-the-art tools

The aim of this report is not to cover the state-of-the-art tool commercially produced. The reason for this is that the progress of the slimhole technology (for boreholes as small as 56 mm or 76 mm in diameter) is commonly decades behind the state-of-the-art tools used in the oil industry at present. However, in order to give the reader an idea of the variety of techniques that could be used when measuring the rock resistivity, two completely different tools from two leading companies are shown below.

6.9.1 The High-Definition Lateral Log

The High-Definition Lateral Log (HDLL) from Baker Atlas is a fully digital array-type device utilising a single current electrode and 18 potential electrodes. From these 19 electrodes the HDLL acquires a great number of potentials and potential gradients, all of which are used to determine the formation resistivity at various depths of investigation of the rock (Figure 6-20). From these measurements, an array of normal and lateral curves can be constructed and a set of synthetic resistivity curves, for example focused curves, can be generated. The use of high-resolution electronics and special sensor mandrel construction, coupled with state-of-the-art inversion techniques, have enabled this tool to achieve a 30-45 cm vertical resolution and define disturbed zone resistivity profiles up to 3 meter in diameter (Baker Atlas, 1999).

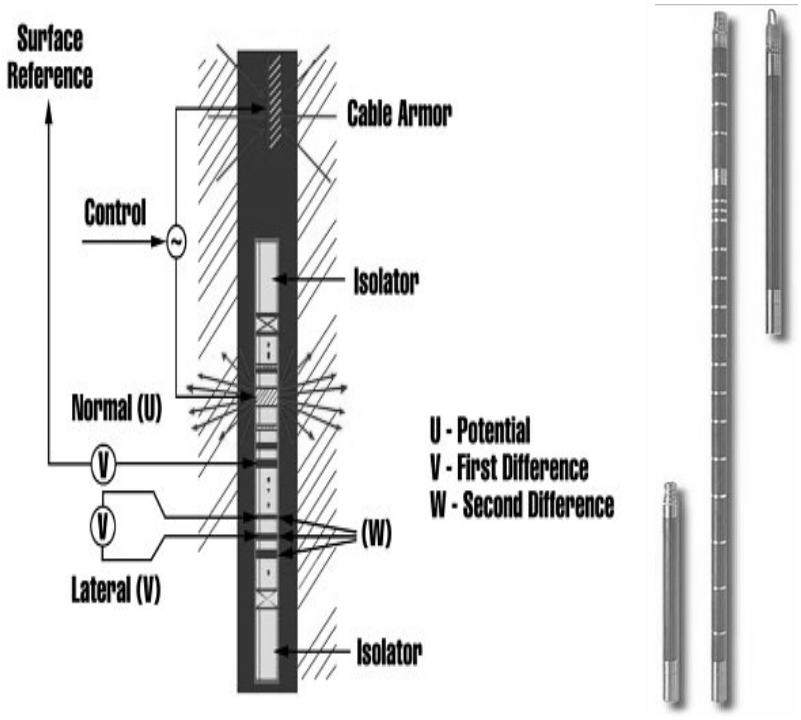

Figure 6-20 Set-up of HDLL. (From Baker Atlas, 1999.)

6.9.2 Resistivity-at-the-Bit Tool

With the Resistivity-at-the-Bit Tool (RAB) from Schlumberger (Figure 6-21) it is possible to measure the rock resistivity while drilling the hole. This assures that the resistivity of the pore water is not altered by a disturbed groundwater flow situation after drilling the hole. RAB measurements include bit resistivity, high-resolution "laterolog" resistivity with four depths of investigation, and gamma ray among other things. The resistivity could be measured quantitatively with a vertical resolution of around 0.1 m (Schlumberger Ltd, 2000).

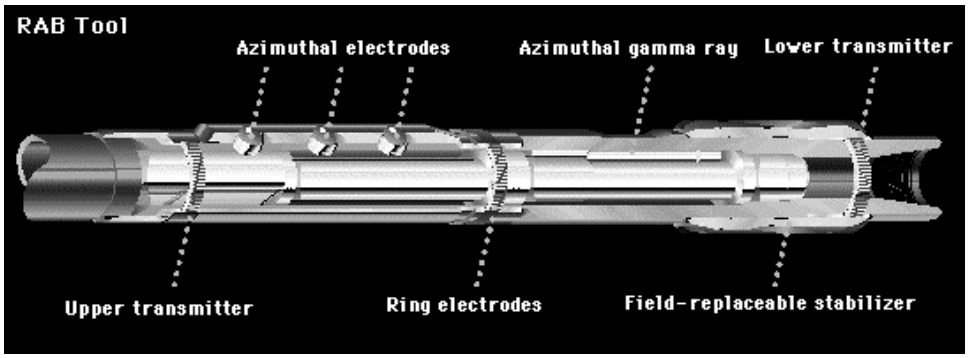

Figure 6-21 Set-up of RAB. (From Schlumberger Ltd, 2000.)

7 Surface rock resistivity measurements

7.1 Introduction

When measuring the resistivity of rock in order to acquire data for calculating the formation factor, surface methods are not so important. Weathering often alters the surface rock and the pore water is often strongly influenced by surface water (rainwater). However, when discussing methods of measuring rock resistivity one can not leave out surface measurements because they play an important role in characterising the rock before deciding to continue the investigation and drill a borehole (which is costly). There are various ways to set-up the electrode array when doing surface resistivity measurements and only those frequently used in geophysical surface surveys will be discussed here. The assumptions that are made are that the ground is flat and that there are no major self-potential differences. Furthermore the rock is also fairly homogenous; i.e. there are no or only small resistivity gradients in the surface plane and a couple of meters downwards. Modern equipment usually corrects for self-potentials by changing the flow direction of the current and then "zero out" any self-potentials. For further reading Parasnis, 1997, is recommended.

7.2 Wenner array

If the current electrodes (A and B) and the potential electrodes (M and N) are collinear and the distances between them are equal (Figure 7-1) Equation 4-11 reduces to:

$$\rho_a = 2\pi a \frac{\Delta U_{MN}}{I} \qquad 7\text{-}1$$

Where ρ_a is the apparent resistivity, a is the distance between the current electrodes and potential electrodes, ΔU_{MN} is the potential difference between the potential electrodes and I is the current.

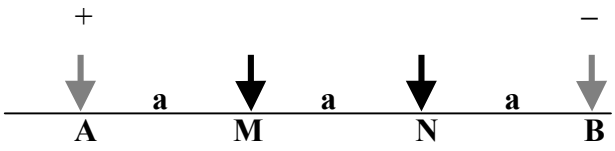

Figure 7-1 Set-up of Wenner array. (Drawn from Parasnis, 1997.)

7.3 Schlumberger array

This array is similar to the Wenner array but the current and potential electrodes are placed symmetrical round a centre (Figure 7-2). In this case Equation 4-11 reduces to:

$$\rho_a = \frac{\pi\left(L^2 + s^2\right)}{2s}\frac{\Delta U_{MN}}{I} \qquad 7\text{-}2$$

where s is the half of the distance between the current electrodes and L is half the distance between the potential electrodes. If the distance between the current electrodes is much greater than the distance between the potential electrodes (2L » 2s) the apparent resistivity can be calculated according to:

$$\rho_a \approx \frac{\pi L^2}{2s}\frac{\Delta U_{MN}}{I} \qquad 7\text{-}3$$

where $\pi L^2/2s$ is the array constant.

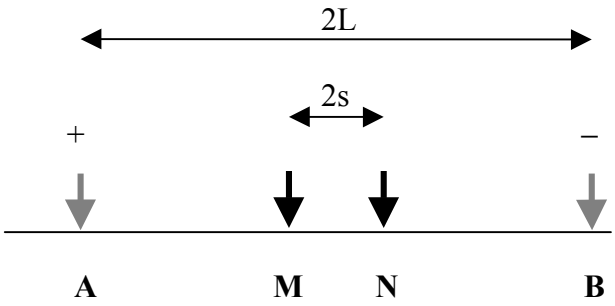

Figure 7-2 Set-up of Schlumberger array. (Drawn from Parasnis, 1997.)

7.4 Axial bipole-bipole array

In this array, which is also commonly referred to as the dipole-dipole array, the potential electrode pair is besides the current electrode pair but in the same line (Figure 7-3). If the distances between the potential electrodes and between current electrodes are the same, a, and the distance between the current electrode and potential electrode pairs is an integer of a, na, the apparent resistivity could be calculated according to:

$$\rho_a = \pi n\left(n+1\right)\left(n+2\right)a\frac{\Delta U_{MN}}{I} \qquad 7\text{-}4$$

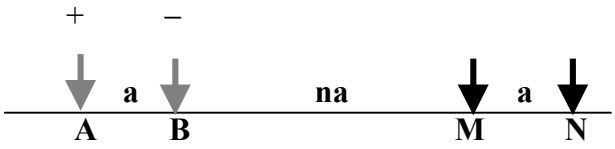

Figure 7-3 Set-up of Axial bipole-bipole array. (Drawn from Parasnis, 1997.)

7.5 Vertical electrical sounding

With vertical electrical sounding it is possible to determine the variation of rock resistivity in depth by using the same equipment as describes above. For rock resistivity measurements the method is strictly speaking only meaningful where the rock resistivity varies with depth without any lateral variations. These are the approximate conditions in sedimentary areas with gently dipping and flat-lying beds. The method is less favourable in moraine-covered Precambrian areas or areas of deep in-situ weathering with fresh rock underneath (Parasnis, 1997). It is however used in igneous and metamorphic rock covered with soil when studying the soil - rock interface and the groundwater situation. The general idea behind vertical electrical sounding is that as the current lines expand in the ground according to the figure below, the potential electrodes at different distances from the current electrodes encounters current lines that has passed through different depth (Figure 7-4).

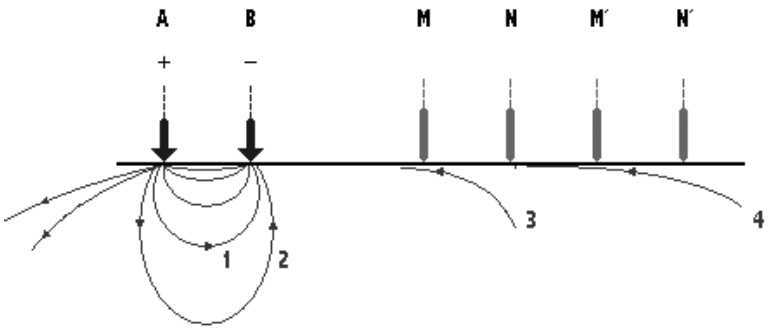

Figure 7-4 Set-up of and current lines in Vertical electrical sounding. (Drawn from Parasnis, 1997.)

Thus the potential difference $\Delta U_{M'N'}$ measured by the M'-N' potential electrode pair is more influenced by current that has passed through deeper rock than the potential difference ΔU_{MN} measured by the potential electrode pair M-N. As was shown in the theory part above it is possible calculate the apparent conductivity ρ_a from potential data. The mathematics involved here is more complicated but Slichter and Langer dealt with the problem in the Slicther-Langer theorem 1933. The most common arrays are Wenner sounding, Schlumberger sounding and axial bipole-bipole sounding.

8 Self-potentials

8.1 Introduction

Between two points in natural rock there may be a potential difference due to various reasons. This potential difference could easily be measured with a normal potentiometer with sufficient high impedance, and anomalies could later be interpreted as boundaries between different minerals or ore bodies. Self-potential methods are also of interest in geo-hydrology as the self-potential commonly is influenced by water flow. Self-potentials are not used in resistivity measurements but can disturb them as they introduce an additional potential. Before measuring the resistivity, the self-potentials between all the electrodes should be measured and "zeroed" out. The electrochemical mechanisms from which the self-potential origins are still under debate but some main aspects will be described below. For further reading Parasnis, 1997, is recommended.

8.2 Electrofiltration

Electrofiltration or streaming potential (zeta potential) is thought to origin from the fact that a potential difference is developed when a fluid containing ions flows in a capillary tube. This phenomenon was first studied in detail by Helmholtz and the basic ideas is that some of the ions could be adsorbed to the capillary wall in an ion-exchange reaction, releasing hydrogen or hydroxyl ions that have high ionic mobilities. This would result in unequal flow velocities of positive and negative ions. When applying this theory on self-potentials in rock the capillary tubes are the micro-pores and the pore-walls are negatively charged, able to release hydrogen ions in an ion-exchange reaction. Thus the flow rate of positive ions would be higher than that of the negative ions, as the ionic mobility of hydrogen ions are many times higher than that of anions or other cations, creating a potential difference. Self-potentials originating from electrofiltration are commonly negative, comparing with a point at the surface. The self-potentials that origin in the flow of water due to a pressure gradient is not sufficiently high to explain anomalies. In order for a self-potential anomaly to arise the water has to flow through a boundary between two rock media.

8.3 Electrolyte concentrations

Differences in electrolyte concentrations (concentrations of ions from dissolved salts) from place to place in the rock will produce a potential differences, just as in an electrolytic concentration cell. The current is carried with diffusing ions and eventually these potentials will vanish as the diffusion process equals out concentration differences.

8.4 Adsorption

Self-potential anomalies can occur when positive and negative ions adsorb to the mineral surface in the electric double layer but the details of the electrochemical mechanisms are not clear yet.

8.5 Mineral potentials

These potentials (also called sulphide potentials) are observed over conductive minerals. If an electric conductor, such as a conductive sulphide ore, is in contact with an ionic conducting electrolyte, such as the groundwater containing ions, there must be an electrochemical action at their boundary (Sato and Mooney, 1960). An electric conductive ore may liberate ions. An example is a sulphide, MeS, releasing ions according to:

$$MeS \longrightarrow Me^{2+} + S + 2e^{-} \qquad 8\text{-}1$$

There may also be more complicated reactions on the ore surface releasing ions such as OH^- and SO_4^-. If the concentration of the ions in the electrolyte is different at the top of the ore body from the concentration at the bottom, an ionic current will flow in the surrounding electrolyte while the electrons will flow through the ore body. The potential over the ore body will thus be different from the potential in its surroundings.

8.6 Method of self-potential measurements

It is quite easy to measure self-potentials in rock. The only equipment needed is a voltmeter with sufficiently high impedance and two non-polarisable electrodes, such as Pt-calomel electrodes or $Cu/CuSO_4$ electrodes. Ordinary metal electrodes will not do as there may be electrochemical reactions between the electrode and the groundwater creating an extra potential which disturbs the measurements. There are two major procedures for surface self-potential surveys. In the first one the electrodes, kept at a constant distance, advances along a line. This approximately gives the potential gradient along the line. In the other procedure one of the electrodes is kept as a base point while the other one is moved giving an self-potential map. In the self-potential tool that SKB uses for borehole measurements one electrode is kept at the surface while the other is wired down the borehole. The electrodes used are not non-polarisalbe so there is doubt if it is actually the self-potential that is measured. Figure 8-1 shows a self-potential log and a normal resistivity log from KAS02 in Äspö, Sweden. The figure shows that little detail information could be drawn from the self-potential log.

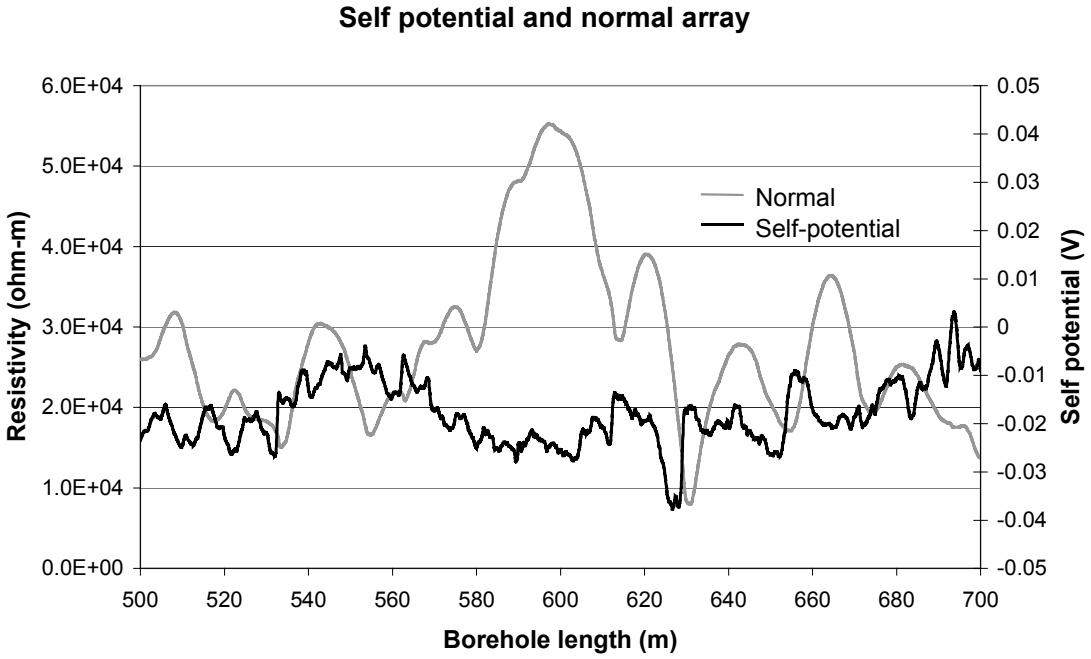

Figure 8-1 Self-potential and normal resistivity log from KAS02 in Äspö, Sweden. (Data from SICADA.)

9 Conductivity measurements of groundwater in-situ

9.1 Introduction

Due to plate tectonics, rock could have been subsided or be uplifted several kilometres many times since its creations (Stanfors et. al., 1999). Therefore water of various salinity, ranging from freshwater to seawater, could have infiltrated the rock. As the rock is porous, diffusion will quickly, on a geological time scale, smooth out sharp concentration gradients. When the rock is subsided or uplifted it will be subjected to different rock stresses. As a result metamorphosis will occur and fractures and fracture zones will form. During these processes fractures could be opened and closed, or sealed with precipitated minerals such as calcite. Open fractures may work as hydraulic conductors and the electrical conductivity of the groundwater at different depth is strongly associated with the flow situation in the rock.

9.2 Historical perspective of groundwater in the Baltic Sea region

Glacial periods greatly affect the salinity of the groundwater in the upper part of the rock. At great depth very old saline water may be found that has a long turnover time as a result of resistance to mixing due to the high density. In the latest glacial period affecting Sweden, a thick ice layer was covering the Baltic Sea region (Figure 9-1a). When the ice began to retreat, the melt water formed a non-saline lake, The Baltic Ice Lake (Figure 9-1b). Freshwater infiltrated the rock that had been subsided by the thick ice layer. As the ice retreated further a channel opened and seawater from the Atlantic Ocean was allowed to mix with the former lake creating the Yoldia sea, a bay of the Atlantic Ocean (Figure 9-1c). Now saline water, denser than freshwater, could infiltrate the rock. When the ice retreated further, the land rose above the see level. Again a lake with freshwater, the Ancylus Lake, was created (Figure 9-1d). When most of the glaciers had melted the sea level of the Atlantic Ocean rose faster than the land in southern Scandinavia. Saline water from the Atlantic Ocean was introduced through a narrow passage between present Sweden and Denmark, giving rise to the Littorina Sea (Figure 9-1e). In the northern parts of the Baltic region the uplift was still substantial and as a result the surface area of the Littorina Sea decreased. At present the water in the Baltic Sea is brackish, with a salinity gradient from south to north, as a result of inflow of freshwater from rivers in north and saline water from the Atlantic Ocean in south (Figure 9-1f). For further reading on the shoreline in Sweden during the Weichsel glacial period and on historical evolution of the Baltic Sea, Morén and Påsse, 2001 and Påsse, 2001 is recommended.

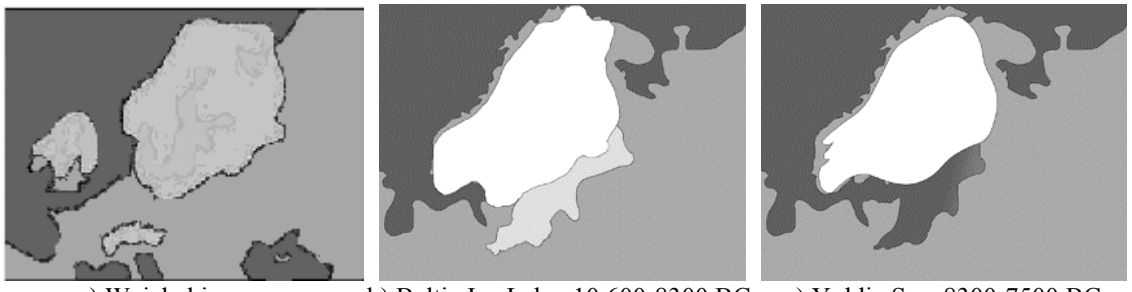

a) Weichel ice age b) Baltic Ice Lake, 10.600-8300 BC c) Yoldia Sea, 8300-7500 BC

d) Ancylus Lake, 7500-6000 BC e) Littorina Sea, 5 800-500 BC e) Baltic Sea, present time

Figure 9-1 Historical evolution of the Baltic Sea. (Data from Björk, 1995 and Mörner, 1995. Figures from Taraxacum miljö media, 2000.)

Taking the historical situation into account it is easy to understand that the groundwater situation in rock near the cost line of the Baltic Sea is complicated. For further reading on groundwater chemistry Gascoyne and Wikberg, 1999, is recommended.

9.3 Difficulties in groundwater measurements

When measuring the salinity or conductivity of groundwater in rock, a borehole has to be drilled. During and after the drilling, water is pumped in and out of the borehole to cool the drill or flush the borehole, thus the natural flow situation will be disturbed. Pumping is also needed when performing some measurements, for example when obtaining water chemistry data or when performing hydraulic conductivity tests. It is important to realise that when trying to characterise a groundwater system at depth one is never able to characterise the natural system that existed before the drilling. When a borehole is drilled it will be filled with groundwater, externally introduced water and mud from the drilling. This mixture is referred to as the borehole fluid. Even after the mud has settled and the externally introduced water has been flushed out, the borehole fluid will is not likely to represent the groundwater at a corresponding depth. One reason is that as a result of the pumping groundwater from deeper parts of the rock could have been transported up the borehole. Even when no pumping is performed the situation will be disturbed as the borehole functions as a hydraulic conductor and short-circuit different parts of the borehole.

Figure 9-2 shows a hypothetical and exaggerated case where the groundwater situation has changed due to the borehole and extensive pumping. The salinity is represented in Figure 9-2a by different shades of grey where the darker represent more saline groundwater. The arrows represent groundwater flow in fractures and the borehole.

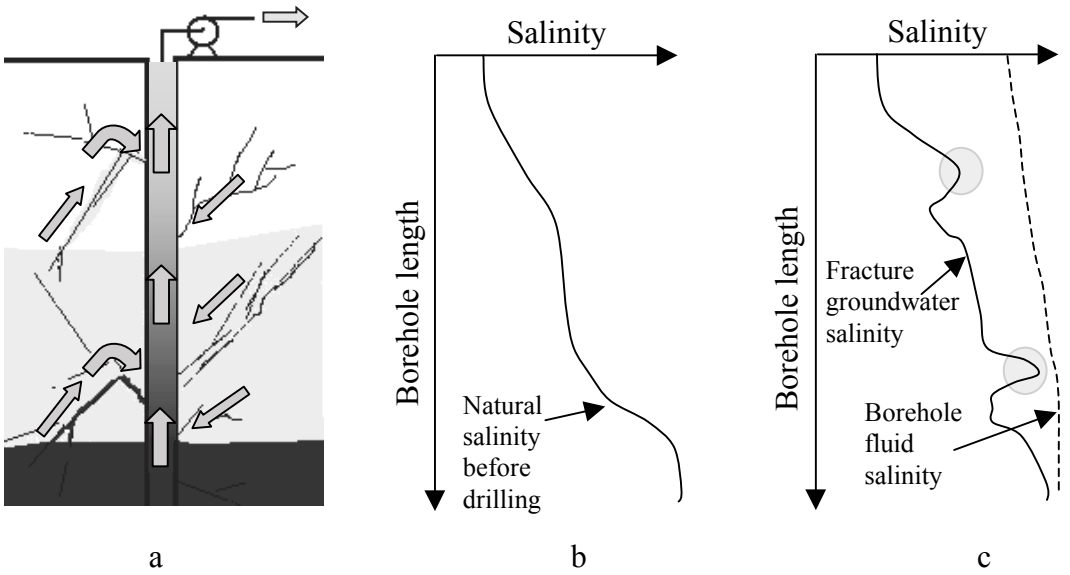

Figure 9-2 a) Disturbed flow situation of a borehole. b) Salinity before drilling. c) Salinity measured after drilling and pumping.

In this case the groundwater in the deepest part of the borehole is saline and the surface water is non-saline. The groundwater in-between is brackish. The natural salinity curve before the drilling shown in Figure 9-2b is expected to be quite smooth as groundwater typically flows only a few meters per year at depth and will have time to equilibrate with the pore water in the surrounding rock. Figure 9-2 c shows salinity peeks in the fracture groundwater salinity log (marked with grey rings) that corresponds to major water bearing fractures where water has been transported from deeper parts of the rock due to the pumping. It also shows that the borehole fluid salinity is higher than the natural salinity in the entire borehole as saline water is pumped up the borehole. Here it is important to point out that each operation and each borehole affect the natural flow situation in a unique way. In some prioritised deep boreholes SKB will sample the groundwater during the drilling phase in order to get a first strike of the groundwater chemistry. By packing off the end section of the borehole the groundwater can be sampled and analysed at the surface. Steps are taken to avoid mixing with water introduced in the drilling or with groundwater from other parts of the borehole (SKB, 2001).

9.4 Borehole fluid conductivity and temperature log

The borehole fluid electrical conductivity is measured by wiring down a liquid conductivity tool in the borehole. The borehole fluid is introduced in an isolated channel and the conductivity is measured directly with a conductivity meter. In this channel the temperature of the fluid is also measured and these data are used when calculating the apparent salinity of the borehole fluid. The conductivity of the borehole fluid could be

used when correcting the apparent rock resistivities from the normal resistivity tool and also for detecting major salinity gradients and water bearing fracture zones. Great inflow of fracture water in the borehole from fracture zones may change the conductivity of the borehole fluid in that region of the borehole. If to much time elapses from the drilling to the measurements, local salinity gradient in the fracture water may not be detected due to mixing. In some cases the resistivity of the borehole fluid is more influenced by surface water than by fracture water, especially if the water flows down the borehole and out through fractures. In these case one can not even obtain the order of magnitude of the conductivity of the groundwater naturally existing at that depth.

Figure 9-3 shows a borehole fluid resistivity/conductivity log from KLX02. Later measurements strongly indicate that the low conductivity zone above 900 m is due to surface water or water from the upper part of the rock naturally flowing down the borehole (Rouhiainen, 2001). The main part of the hole was drilled in October-December 1992 and the borehole fluid resistivity logging was performed in July 1993. Still some local resistivity/conductivity differences are shown, possibly indicating fracture zones.

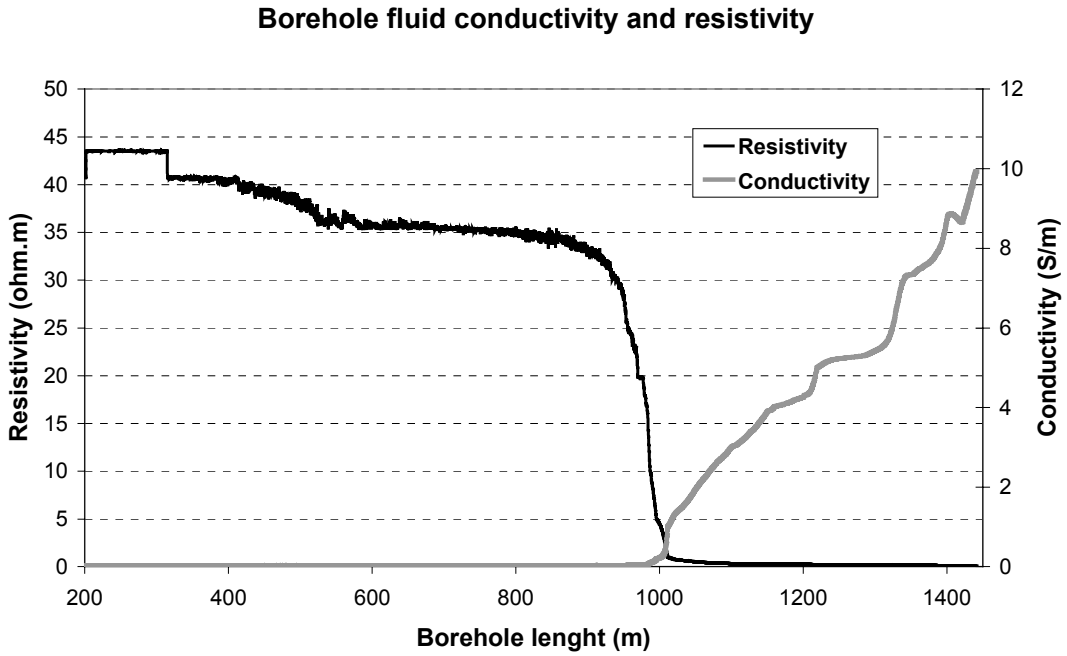

Figure 9-3 Borehole fluid conductivity/resistivity log from KLX02 in Laxemar, Sweden. (Data from SICADA.)

The borehole fluid conductivity tool used by SKB is a part of a resistivity system described in section 6.5.

9.5 Fracture specific EC measurements

The Posiva difference flow meter is able to measure the water flow in or out of fractures in a small section of a borehole. The temperature and the electrical conductivity of the

fracture water could also be measured. A small section, typically 0.5 or 3 m, of the borehole is sealed off by using rubber disks (Figure 9-4) assuring that the measurements are not affected by water from other parts of the borehole. The tool comprises a separate channel for water flowing along the borehole and therefore the pressure build-up over the rubber disks is negligible.

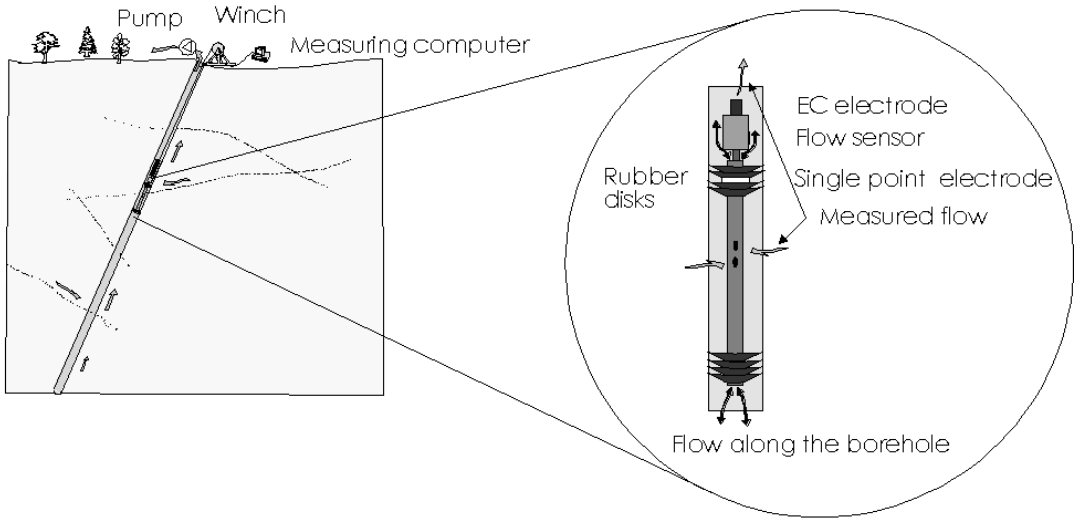

Figure 9-4 Schematic drawing of the Posiva difference flow meter. (From Rouhiainen, 2001.)

When performing detailed flow logging, a thermal dilution or a thermal pulse detector is used for measuring the flow rate of the water flowing in or out of fractures in the section. The measuring range for the former detector is 2-5000 ml/min and the latter is 0.1-10 ml/min. At the same time the temperature and the electrical conductivity (EC) of the water passing the flow detector is measured. Either the natural flow is measured without pumping or a drawdown is used. The tool could typically be moved in steps of 0.1 m and one measurement takes about 10 seconds. As the tool moves to another position the rubber disks may leak and therefore borehole fluid intrudes the section. As mentioned above the borehole fluid seldom represent the groundwater in the rock at a corresponding depth. The measured EC (called Background EC) could therefore not be used quantitatively. In order to obtain quantitative EC data a drawdown is used. Water is pumped out of the borehole and a pressure gradient from the rock to the borehole is formed along the borehole. If the section contains a water-bearing fracture, water will therefore flow from the fracture into the section, past the detector and up the borehole. This water is called fracture specific groundwater. In order to assure that all the water that flow through the detector origins from the fracture the tool has to halt. From the measured flow a computer calculates how long it would take for the fracture specific groundwater to fill up the section volume (typically 500 ml) three times. If the time is unreasonably long the tool moves to another fracture and if the time is reasonable the tool is halted this time. While the tool has halted the EC is measured continually (this EC could be called the transient EC). Figure 9-5 shows two different transient EC plots from KLX02.

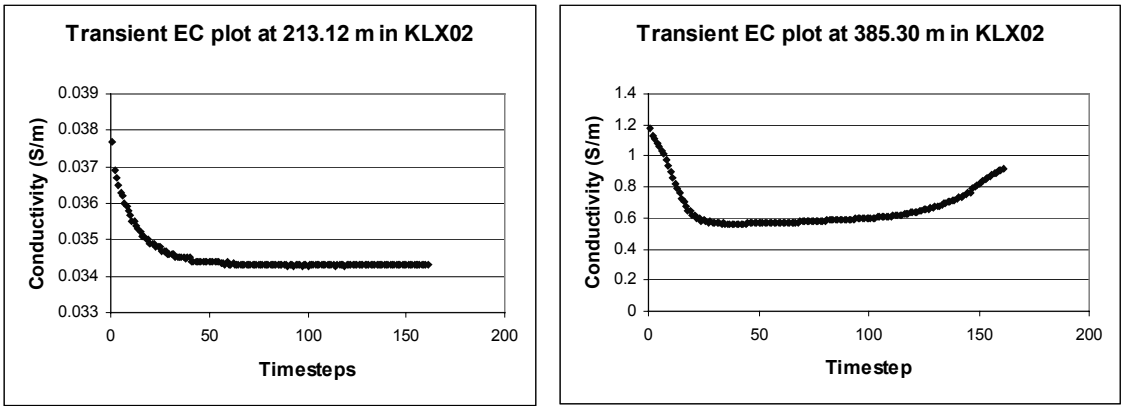

Figure 9-5 Two different transient EC plots form KLX02 in Laxemar, Sweden. To the left a successful measurement. To the right an unsuccessful measurements where leakage probable occurred (Data from Rouhiainen, 2001).

Before the measurements extensive pumping has usually been performed in-order to flush the fractures from groundwater affected by the borehole fluid. In this case it meant that the borehole fluid had origin from deeper parts of the rock and therefore was more saline. Initially the transient EC is greatly affected by the water introduced in the section before the tool halted. As mentioned above leakage is common when the tool is moved and therefore this water is more or less influenced by the borehole fluid. As time pass the transient EC is more and more affected by the fracture specific groundwater and at the end the EC (called fracture specific EC) should be constant (Figure 9-5, left plot). The right plot in Figure 9-5 does not show this behaviour. Probably there has been some leakage that, for some reason, increased with time. The end value should therefore not be used. The plot indicates however that the fracture specific EC is around or below 0.6 S/m. In Figure 9-6 the fracture specific EC, the background EC and the flow in the section 250 - 300 m in the borehole KLX02 is shown. The logging was performed during spring 2000 in a campaign by SKB.

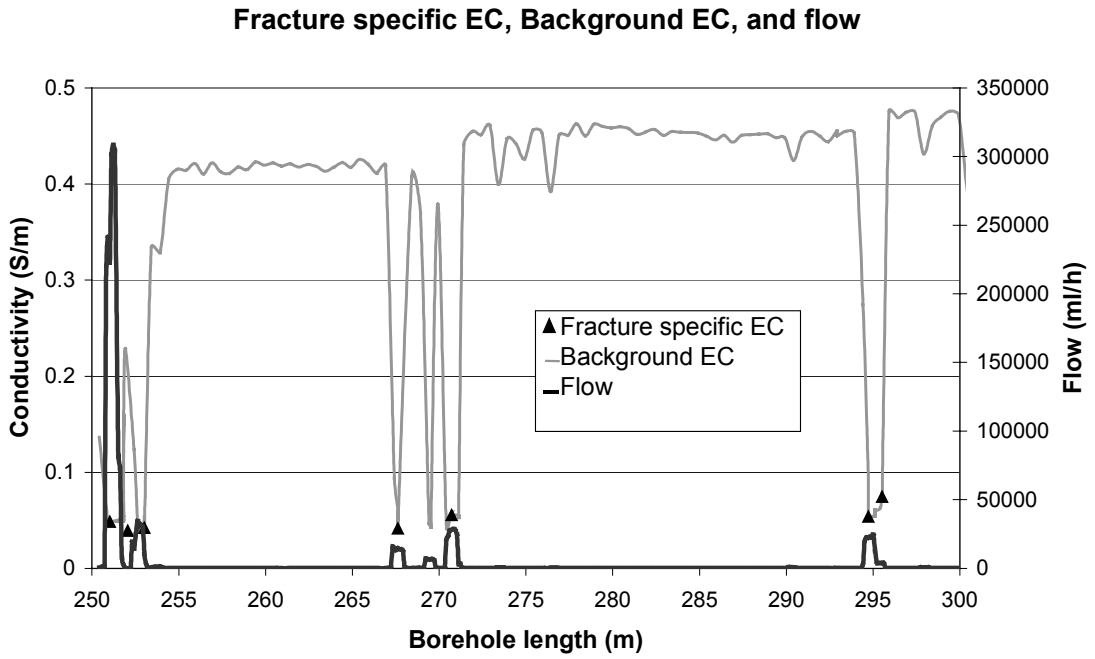

Figure 9-6 Fracture specific EC, background EC, and flow (22 m drawdown) in KLX02 in Laxemar, Sweden. (Data from Rouhiainen, 2001.)

From Figure 9-6 one can see that the fracture specific EC is fairly constant around 0.05 S/m. One can also see that the background EC is fairly stable at around 0.45 S/m in regions a couple of meters away major water-bearing fractures. This clearly shows that one can not use the background EC quantitatively. At this section the electrical conductivity of the fracture specific groundwater from seven fractures were measured. In this case the one could make the assumption that the groundwater conductivity is constant or varies linearly with depth.

If some values, for example the two around 295 m in Figure 2-6, had deviated in magnitude from the others more measurements around 295 m would be required. Generally if more measurements are required one has measure the fracture specific EC in fractures with a lower flow. This may lead to practical problems at these measurements would require longer time and the detectors may require a minimum flow larger than this flow. It is important that the tool is designed to meet the requirement of being able to measure at low flows.

10 Obtaining formation factor logs in-situ

10.1 Introduction

In saline areas the formation factor could be obtained from the pore water conductivity and the undisturbed rock conductivity according to Equation 5-3. This equation does not take surface conduction into account and is therefore only valid in regions where the groundwater conductivity is high (higher than around 5 S/m according to Figure 3-2). In areas with moderate conductivity (~1 S/m) the error should not become too great. In low conductivity areas surface diffusion has to be taken into account. At present the knowledge of how to do this is limited and therefore formation factor logging in-situ by electrical methods is not yet applicable in low conductivity areas. All in-situ logs necessary for obtaining a formation factor log have been obtained by SKB in the borehole KLX02 in Laxemar, Sweden. Essential logs are:

- Core log
- Fracture specific, background and transient EC logs from the Difference flow meter.
- Rock resistivity log from the Dual-Laterolog.

Other useful logs are:

- Flow log from the Difference flow meter.
- Caliper
- Nuclear geophysics logs
- Borehole camera

Data exist for most part of the 1700 m deep borehole but for this exercise the section 350 m to 400 m was chosen. It should be kept in mind that the aim of this report is to display the methodology behind formation factor logging and not to obtain numerical results. Before one start working with the different logs it is important that they are corrected for possible displacements of the borehole length axis. Here the borehole length axis of all the important logs has been adjusted so that they correspond with the core log. It would be valuable to have some well-defined physical markings in the borehole that could be detected when logging in order to simplify this task. Otherwise there is a chance that the borehole length axes of the logs are wrongfully adjusted in order to fit the expected outcome. SKB has developed a tool that creates notches on the borehole wall. When logging a separate calliper tool can detect the location of these notches and in this way controlled measurements of the borehole length can be achieved.

10.2 Creating the formation factor log

10.2.1 Examining the rock resistivity log

The rock resistivity log was obtained in a logging campaign performed by SKB during September 2000 using the Antares slimhole Dual-Laterolog, which gave accurate results that needed no corrections (Figure 6-11). The resistivity log is greatly affected by water-bearing fractures and cavities. In order to detect these fractures and cavities the natural fracture (also called natural joint) log from the core log, the DIFF-flow log and caliper log were used (Figure 10-1).

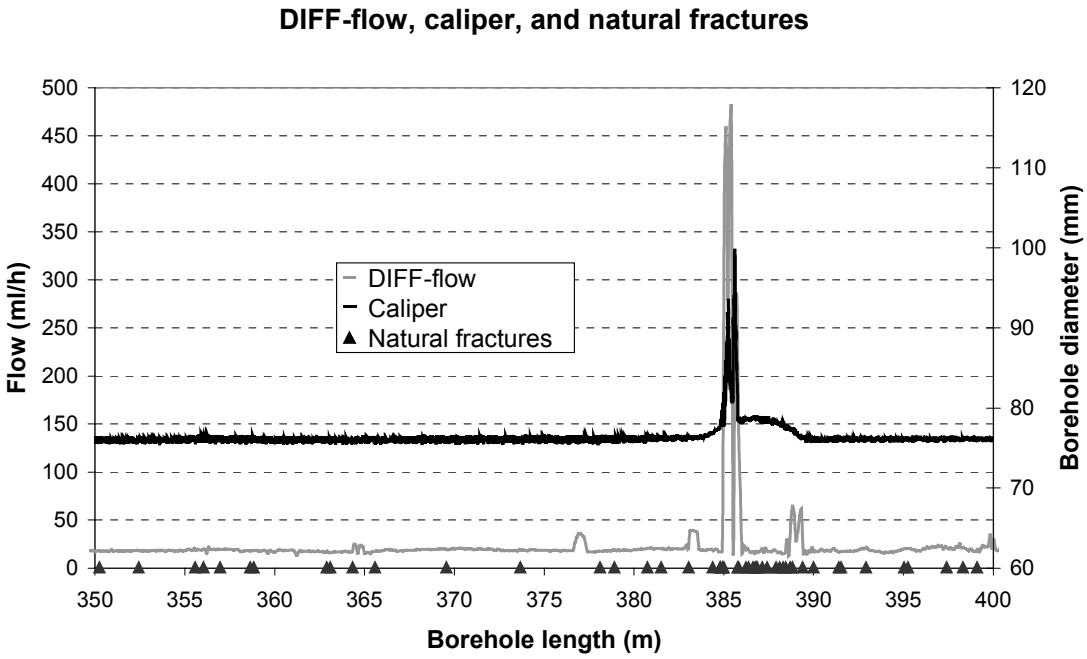

Figure 10-1 DIFF-flow (22 m drawdown), caliper, and natural fractures from the core logging. (Data from SICADA and Rouhiainen, 2001.)

From the caliper log in Figure 10-1 one can see that there are no major deviation in the borehole diameter except at 384-390 m where there is also a major fracture zone. From the DIFF-flow log one can see that there are no major groundwater flows, with exception of the fracture zone at 384-390 m where the flow clearly is higher than the quantitative detection level of 120 ml/h.

As no anomalies that where not accounted for in the core log was detected in the flow or caliper logs, the location of free water that could cause resistivity anomalies should fairly correspond with the fractures in the core log. As water could fill dead end fractures all fractures, not only the hydraulically conductive one, have to be taken into account. There may also be an alteration zone around some of the fractures where the rock has weathered. As the rock resistivity tool delivers a huge amount of data it is often affordable to delete all data point within some distance from any fracture. If this is done automatically it is recommended to delete all point within 30 cm from a fracture

although the manufacturer (Antares) claims that the vertical resolution of the tool is only 10 cm. If necessary, one could avoid an excessive loss of data by examining anomalies individually.

An undisturbed rock resistivity log is obtained from the rock resistivity log when data possibly disturbed by free water is deleted. (Figure 10-2).

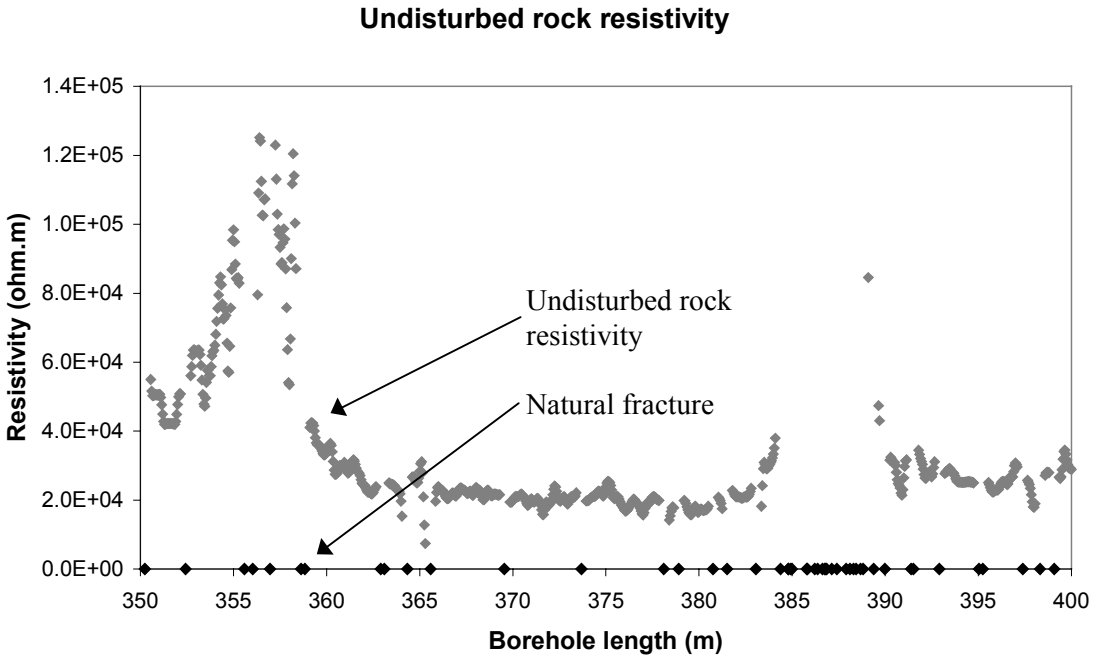

Figure 10-2 Undisturbed rock resistivity in KLX02 in Laxemar, Sweden after automatic filtering of data. (Data from SICADA and logging campaign performed by SKB during September 2000.)

Comparing Figure 10-2 with 6-11 one can see that almost all resistivity dips have been deleted. At 365 m one can see that two or three resistivity data probably affected by fractures has remained undeleted. As these resistivities probably do not represent the undisturbed rock they could be deleted manually. In indistinct cases the core could be re-examined.

10.2.2 Examining the groundwater conductivity

The groundwater conductivity was obtained in a logging campaign performed by SKB during spring 2000 using the Posiva difference flow meter (Rouhiainen, 2001). As only the electric conductivity of the groundwater from a few fractures has been measured there is a question how to interpolate these data for the rock between these fractures. The entity needed when performing formation factor logging is not the free groundwater conductivity but the pore water conductivity. Therefore the question if the free groundwater is in equilibrium with the pore water that was brought up previous is very relevant. In some section it feels quite safe to assume constant groundwater conductivity or to make a linear interpolation (Figure 9-6). In other sections there is no fracture specific EC measured. The best way to deal with this problem would be to perform

additional measurements. If this could not be done a rather uncertain estimation has to be made. No fracture specific EC data exists from section 350 m - 400 m and therefore such estimation had to be made. Figure 10-3 shows the EC in KLX02.

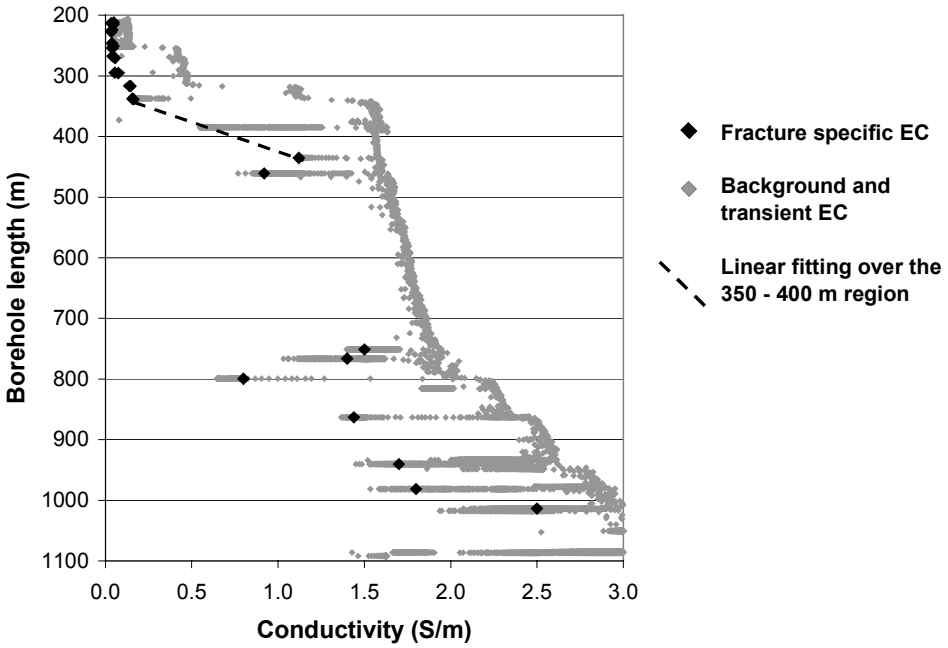

Figure 10-3 Electrical conductivities of groundwater in KLX02 in Laxemar, Sweden. (Data from Rouhiainen, 2001)

The black diamonds in Figure 10-3 represents fracture specific EC while the grey diamonds represents background and transient EC. At 385.3 m an attempt was made to measure the fracture specific EC (Figure 9-5) but due to leakage the value had to be dismissed. However, the transient EC log indicates that the fracture specific EC at 385 m should be around or below 0.6 S/m. A linear fitting was made between the nearest values on each side of the section (at 339 m and 435 m), crossing 0.6 S/m at 385 m. This is represented by the broken line in Figure 10-3. The fitting was used as an approximation of the pore water conductivity in the section.

As an alternative a low groundwater conductivity value corresponding to that of the upper part of the rock could have been used in the whole section. The electrical conductivity of the rock would then be due to surface conduction. The fact that the in-situ rock conductivity log corresponds fairly well to the surface conductivity log measured on unstressed bore core samples in the laboratory support this approach (Löfgren, 2001). A third alternative would have been to assume that the pore water was in equilibrium with the non-saline borehole fluid (Figure 9-3). In this case the current would also have been transported by surface conduction.

This shows the necessity of obtaining reliable data on groundwater electrical conductivity and to perform measurements as soon as possible after the borehole is drilled. In this case it could be argued that there is no way of knowing what pore water

conductivity that should be used when obtaining the formation factor and that quantitative formation factors could not be obtained. Once again it should be reminded that this report focus on the methodology and not on results.

10.3 Examining the formation factor log

A formation factor log was obtained by using the linear fitting of the pore water conductivity shown in Figure 10-3 and the undisturbed rock resistivity log. The formation factor log is shown in Figure 10-4.

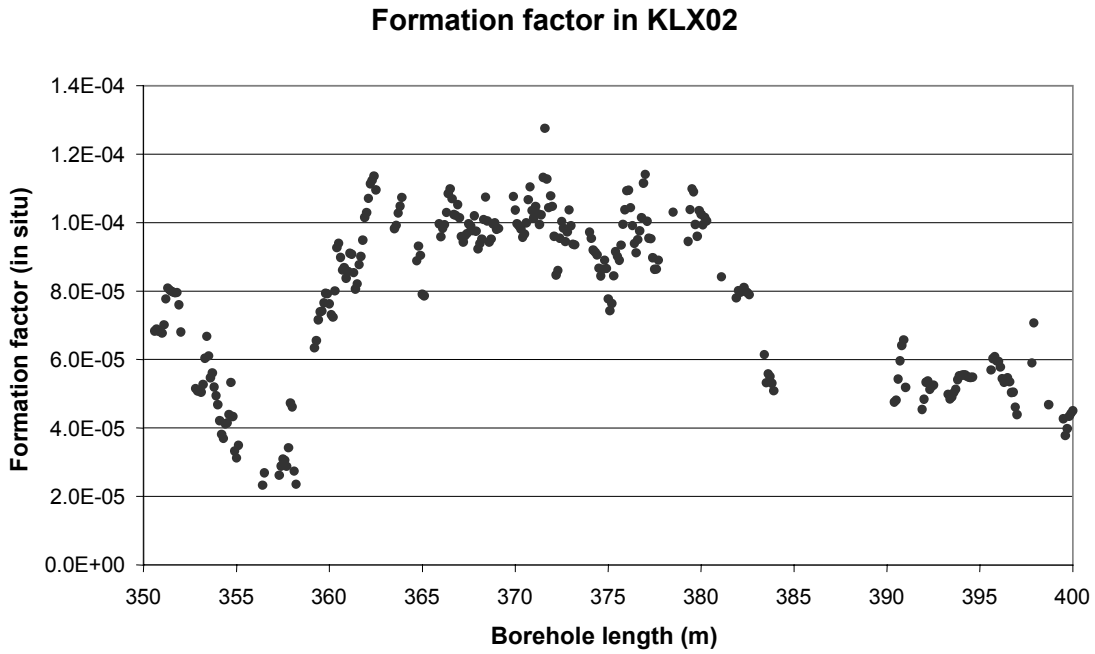

Figure 10-4 Formation factor log in KLX02 in Laxemar, Sweden.

A major change in the formation factor should be associated with a major change in the rock matrix, such as a rock type change. Therefore one could suspect that there is a rock type change at the dip around 357 m in Figure 10-4. The core confirms that there are two sections designated as mafic volcanite, one between 356-358 m and the other between 384-389 m, surrounded by granite. The second rock type change is partly disguised as the rock is heavily fractured.

It is important to have independent methods where anomalies due to for example rock type changes corresponds to the anomalies in the formation factor log. The core is invaluable for this purpose. If the borehole is percussion drilled, rock type changes and fractures could be detected with a borehole camera. Tools based on nuclear geophysics, such as the gamma-gamma log, can also be used. Figure 10-5 shows the gamma-gamma log from KLX02.

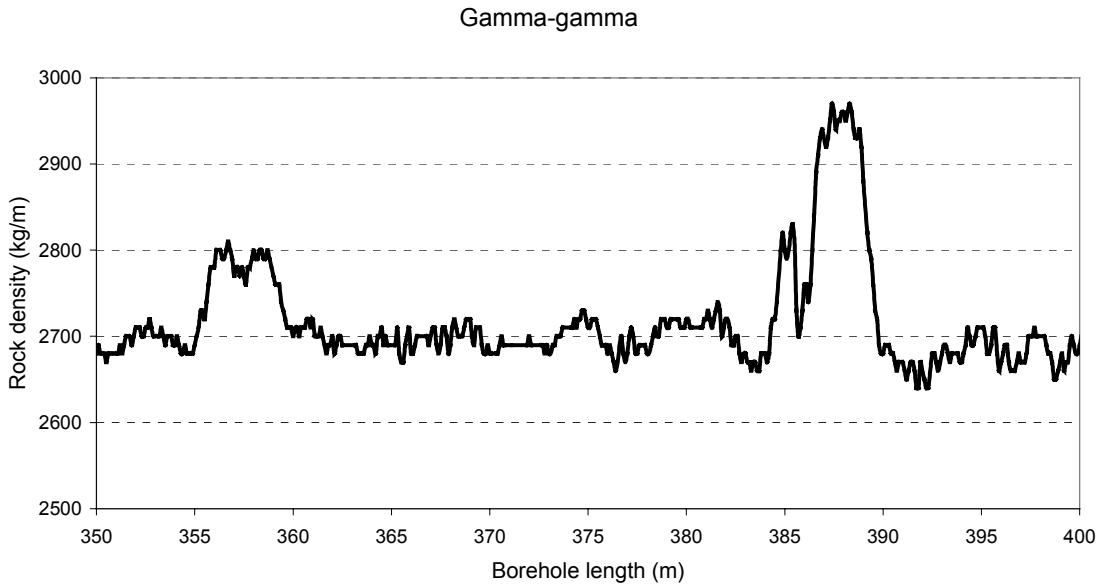

Figure 10-5 Gamma-gamma in KLX02 in Laxemar, Sweden. (Data from SICADA.)

In the gamma-gamma log one can clearly see the same anomalies corresponding to the two sections of mafic volcanite. Nuclear geophysics tools and borehole camera are briefly described in Almén and Zellman, 1991.

10.4 Validating in-situ results with laboratory measurements

As the in-situ formation factor logging is a new method it is important to validate the in-situ result by performing measurements in the laboratory on the core. Even if one would choose to take a sample only from every tenth meter it would still add up to 100 samples in a 1000 m deep borehole. Therefore it would be recommended to measure the formation factor of most of these samples with electrical methods. This was done in the section 350 m - 400 m in KLX02. Figure 10-6 shows a comparison of the formation factor log obtained in-situ with the formation factor log obtained in the laboratory.

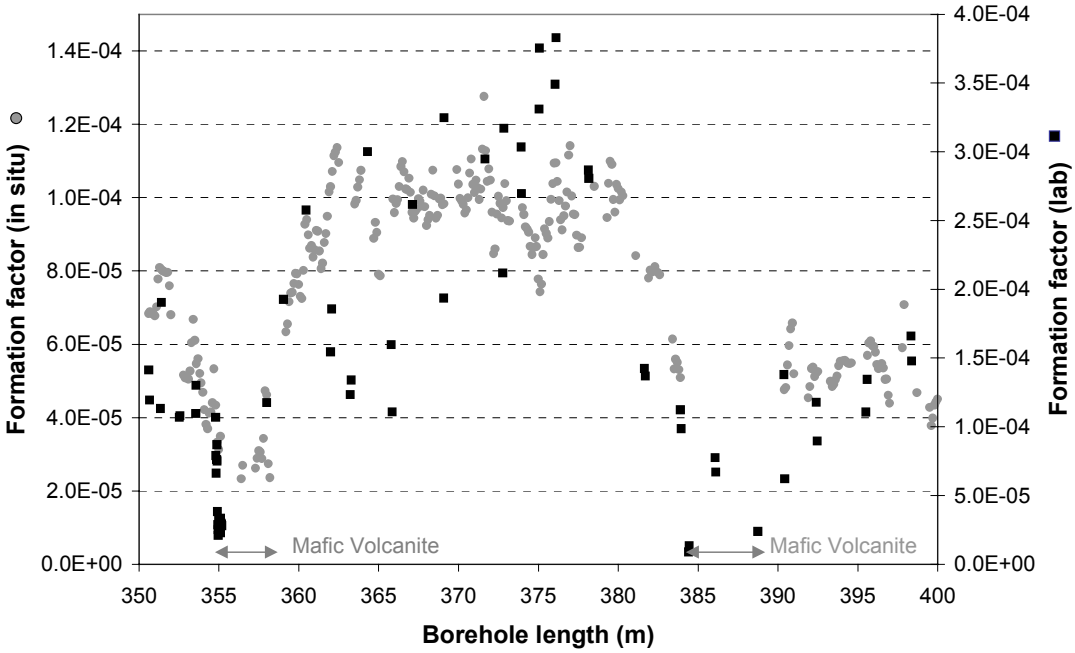

Figure 10-6 Comparison on in-situ formation factor (grey rings) and laboratory formation factor (black squares) in KLX02 in Laxemar, Sweden. Not the different scale on the y-axes.

The two curves clearly follow each other and geological features, such as the rock type changes, are visible. Note that the two logs have different scales. On average the in-situ formation factors are around 35 % of the laboratory formation factor values. This is consistent with the fact that the core samples are unstressed and possible slightly altered by the drilling. Here it should however be remembered that the pore water conductivity was estimated based on a linear fitting of the groundwater conductivity and that the value 35% easily could change if choosing another way of fitting the data. If choosing the constant pore water conductivity value of 0.16 S/m (the fracture specific EC at 339 m) the in-situ and laboratory formation factor logs would almost coincide if not accounting for surface conduction. At this low salinity surface conductivity would on the other hand probably play an essential role. If choosing the constant value 1.12 S/m (the fracture specific EC at 435 m) the in-situ values would be around 20 % of the laboratory values. However, using a constant value makes it impossible to fit the curves at both ends of the section. This again points out the necessity to obtain a sufficient number of fracture specific EC measurements.

The relatively high spread in the laboratory formation factor may be due to the fact that many core pieces were chosen because they where already parted in about 1 dm pieces by natural fractures. When cutting them into 1.5 cm samples not enough care was taken to avoid rock which might had been naturally altered by flowing water. Therefore there may be a slight overestimation of some formation factors obtained in laboratory. In future it is recommended to use core pieces that has not been naturally altered by flowing water.

11 Discussion and conclusions

When starting the writing of this report, one formation factor log had been obtained from the borehole KAS02 in Äspö, Sweden by using data from SICADA. The rock resistivity data had been obtained with a normal resistivity tool and the pore water resistivity data had been obtained from the borehole fluid. The influence of water-bearing fractures on the rock resistivity data had not been taken into account. Even by using this poor set-up a qualitative log was obtained where the result, with a bit of fortune, were in the same order of magnitude as results from formation factor measurements performed in the laboratory (Ohlsson et. al, 2001). Therefore a project was started to make quantitative formation factor logging in-situ a reality. At present the project has gone much furthered, encouraged by new equipment and promising results. When performing formation factor logging in-situ there are four main difficulties to overcome:

- Obtaining quantitative undisturbed rock resistivities
- Obtaining quantitative pore water resistivities
- Correcting the data for surface diffusion
- Obtaining formation factor data of altered rock surrounding fractures

In addition the results are preferable validated by formation factor logging on the core in the laboratory. If the borehole is percussion drilled, independent geophysical logs could be used to investigate anomalies.

11.1 Obtaining quantitative undisturbed rock resistivities

There are two key factors when obtaining quantitative undisturbed rock resistivity data. The first is that the tool gives accurate data when logging in fracture free zones. The normal resistivity log currently used by SKB should in general be considered as qualitative even if the tool in some special cases could be considered as quantitative. A breakthrough for the project was when a company manufacturing focused slimhole rock resistivity tools was found. The Antares Dual-Laterolog provides apparent rock resistivity data that directly could be used as quantitative rock resistivity data. A successful demonstration logging was made in the borehole KLX02 in Laxemar, Sweden. The second key factor is the vertical resolution of the logging tool. The vertical resolution of the normal resistivity tool is a few meters. Therefore the apparent rock resistivity may be highly influenced by water-bearing fractures in the measured section. When trying to sort out data that could have been affected by these fractures a situation arose where almost no data could be used. When using the Dual-Laterolog with a vertical resolution of one or a few decimetres this was not a problem. By combining data from the core log, the DIFF-flow log and the caliper log fractures and other water filled cavities could be identified. Without making an optimisation all resistivity data

within 0.3 m from a fracture were sorted out. This meant that some data not affected by the fractures was unnecessarily sorted out. However, enough data remained to make an undisturbed rock resistivity log for the section 350-400 m in KLX02. The exception was at the fracture zone at 384-390 m where the fracture frequency was too great. The result shows that the problem of obtaining quantitative undisturbed rock resistivities between major fracture zones has been solved.

Still the issue exists of how electrically conductive minerals will affect the rock resistivity (or rather the apparent formation factor obtained from the rock resistivity). Experiments suggest that this is not a problem in granitic rock where electrically conductive minerals are not abundant (Löfgren, 2001). In ore bodies, however, this may be a problem. Therefore it is valuable to examine the mineralogy of the rock from the core when performing formation factor logging by electrical methods.

11.2 Obtaining quantitative pore water resistivities

Obtaining the pore water conductivity is the great uncertainty when performing in-situ formation factor logging with electrical methods. At present there is no way of measuring this entity directly in-situ. Neither are there any ways of saturating the rock with a solution of a known resistivity, as when performing laboratory measurements. When obtaining the first formation factor log, the resistivity of the borehole fluid resistivity was used as an approximation of the pore water resistivity at a corresponding depth. This approximation was abandoned (Löfgren et. al., 2000), when a new tool was introduced on the market. The Posiva difference flow meter can measure the electrical resistivity of groundwater pumped out of fractures. Due to extensive pumping in the process of drilling and after drilling the borehole, the flow situation has been disturbed and it is therefore not likely that the fracture water is in equilibrium with the surrounding pore water. However, the groundwater gradients seem to be small over large sections and therefore this might not be such a great problem. Clearly more work is needed on this issue.

It is also important that all measurements are made as soon as possible after the drilling of the bore hole as the groundwater flow and chemistry is likely to deviate more from the natural case with time.

11.3 Correcting the data for surface conduction

As seen by Figure 3-2 the formation factor could be overestimated due to the surface conduction. There is an idea that the surface conductivity should be within a limited range for a specific rock type. If this range better could be determined empirically one could set a lower conductivity value for the groundwater in areas which could be logged by electrical methods. A study with this purpose has been undertaken. If the method should be used in areas with even lower groundwater conductivities a greater

understanding of surface conductivity in geological materials is vital. Clearly more research is needed on the subject.

11.4 Obtaining formation factor data from altered rock surrounding fractures

A drawback of the method is that one can not measure the formation factor around fractures. If radionuclides would be released form the repository, matrix diffusion would only be important around the fractures. It is likely that there are no major changes in the rock type around a fracture if the rock is not altered. Therefore the formation factor measured only 30 cm away may very well represent the rock at the fracture. However, around some fractures weathering processes have altered the rock. It is commonly noticed that there is an increase in porosity in this altered zone, which typically has an extension of a few centimetres in the rock. There is no reason why the formation factor of the alteration zone at the borehole could not be logged by electrical methods. It is only a matter of finding a tool with a higher vertical resolution and logging with a high vertical precision. Such tools exist on the market at present but most of them do not fit in the 76 mm boreholes used by SKB. The centimetre of rock closest to the water-bearing fracture would probably be very hard to log though, as the free water will disturb the logging.

11.5 Validating the results

As formation factor logging in-situ is a new method the results are preferable validated. Measuring the formation factor on core samples in the laboratory could do this. A few samples could be measured by standard through diffusion experiments and maybe 50 or 100 samples by electrical methods. The electrical approach was used in the section 350 m - 400 m in KLX02 (Figure 10-6) with good results. As the in-situ formation factor is expected to be only 20% - 70% of the laboratory formation factor (Skagius, 1986) it is hard to determine if there is a small systematic error in the in-situ formation factor. However larger errors could easily be detected. If the borehole is percussion drilled formation factor anomalies could qualitatively be validated by independent geophysical in-situ logs such as the gamma-gamma log or the borehole camera.

11.6 End statement

To conclude, formation factor logging in-situ by electrical methods is a very promising alternative when obtaining data for matrix diffusion calculations. It should be used as complement to traditional through diffusion experiments and electrical methods in the laboratory. In accuracy the method could not compete with laboratory measurements as one could expect an error of some tenth of a percent or more. On the other hand laboratory experiments are performed on unstressed samples, giving rise to the same magnitude of error. The main advantage of the method is the number of data it produces. Thousands of quantitative or semi-quantitative measurements could be

obtained in only a few weeks. This could lead to a much better understanding of how the formation factor varies in space and with rock type. A few years ago when this project started, the idea of obtaining quantitative formation factor logs in-situ was considered quite speculative. This report shows that the method is no longer speculative but instead quite doable but also that some issues deserve more attention.

References

Almén, K-E., Zellman, O., 1991. Äspö Hard Rock Laboratory. Field investigation methodology and instruments used in the pre-investigation phase, 1986-1990, SKB TR 91-21, Svensk Kärnbränslehantering AB.

Andersson, J., Almén, K-E., Ericsson, L.O., Fredriksson, A., Karlsson, F,. Stanfors, R., Ström, A., 1997. Parametrar av betydelse att bestämma vid geovetenskaplig platsundersökning. SKB R 97-03, Svensk Kärnbränslehantering AB.

Antares Datensysteme GmbH, 2000. Stuhr, Germany. Catalogue for Log acquisition system, HydroBase logging software, logging instruments.

Archie, G.E., 1942. The electrical resistivity log as an aid in determining some reservoir characteristics. J. Pet. Technol. 5, 1-8.

A**tkins, P. W., 1995.** Physical chemistry, 5th Ed., Oxford University Press, , p 834-850.

Autio, J., Kirkkomäti, T., Siitari-Kauppi, M., Timonen, J., Laajalahti, M., Aaltonen, T., Maaranen, J., 1999. Äspö Hard Rock Laboratory. Use of the ^{14}C-PMMA and HE-gas methods to characterise excavation disturbance in crystalline rock, Swedish SKB IPR-99-18, Svensk Kärnbränslehantering AB.

Baker Atlas / Baker Hughes Inc., 1999. Houston, Texas, U.S.A. Internet homepage: http://www.bakerhughes.com/ July 1999.

Björk, S., 1995. A review of the history of the Baltic sea 13.0-8.0 ka BP. Journal of Contaminant Hydrology, Vol 27, pp. 19-40.

Bryant, S., Pallatt, N., 1996. Predicting formation factor and resistivity index in simple sandstone. Journal of Petroleum Science and Engineering. Vol. 115, pp. 169-179.

Crank, J., 1975. The Mathematics of Diffusion, 2nd Ed. Oxford University Press.

Dakhnov V.N., 1959. Geophysical well logging, Moscow 1959. Translated by Keller. V., 1962. In Quaterly of the Colorado School of Mines. Vol. 57, No. 2.

Desbrandes, R., 1985. Encyclopedia of well logging. Translated by Brace, G., 1985. Graham & Trotman Ltd.

Femlab® Version 2.00, Comsol AB, Stockholm, Sweden

Fredén, C., 1998. Theme editor of Jord och berg, Sveriges nationalatlas, Sveriges Nationalatlas Förlag.

Gascoyne, M., Wikberg, P., 1999. Guest editors of Geochemistry of the Äspö Hard Rock Laboratory, Sweden, Applied Geochemistry Vol. 14, No. 7, Pergamon Press.

Ildefonse, B., Pezard, P., 2001. Electrical properties of slow-spreading ridge gabbros from ODP Site 735, Southwest Indian Ridge. Tectonophysics Vol. 330, pp. 69-92.

Keller, G.V., Frischknecht, F.C., 1966. Electrical methods in geophysical prospecting. Pergamon Press.

Löfgren, M., Ohlsson, Y. Neretnieks, I., 2000. Formation factor determinations by *in-situ* resistivity logging. In proceedings of 24th Symposium on the Scientific Basis for Nuclear Waste Management, August 27-31, 2000, Sydney.

Löfgren, M., 2001. Formation factor logging in igneous rock by electrical methods. Licentiate thesis at the Royal Institute of Technology, Stockholm, Sweden. ISBN 91-7283-207-x.

Löfgren, M., Neretnieks, I., 2002. Formation factor loggings by electrical methods. Comparison of formation factors logs obtained in-situ and in the laboratory. Accepted for publications in Journal of Contaminant Hydrology.

Matlab® Version 5.3.0, The Mathworks, Inc. Natick, Massachusetts, USA

Morén, L., Påsse, T., 2001. Climate and shoreline in Sweden during Weichsel and the next 150.000 years. SKB TR-01-19, Svensk Kärnbränslehantering AB.

Mullin, J.W., 1993. Crystallization, 3rd Ed. Butterworth-Heinemann.

Mörner, N.-A., 1995. The Baltic ice lake - Yoldia sea transition. Journal of Contaminant Hydrology, Vol 27, pp 95-98.

Neretnieks, I., 1980. Diffusion in the rock matrix: An important factor in radionuclide retardation?. Journal of Geophysical Research. Vol. 85, No. B8, pp. 4379-4397.

Ohlsson, Y., Neretnieks, I., 1995. Literature survey of matrix diffusion theory and of experiments and data including natural analogues. SKB TR 95-12, Svensk Kärnbränslehantering AB.

Ohlsson Y., 2000. Studies of Ionic Diffusion in Crystalline Rock. Doctoral thesis at the Royal Institute of Technology, Stockholm, Sweden. ISBN 91-7283-025-5.

Ohlsson, Y., Löfgren, M., Neretnieks, I., 2001. Rock matrix diffusivity determinations by *in-situ* electrical conductivity measurements. Journal of Contaminant Hydrology, Vol 47, pp. 117-125.

Parasnis, D. S., 1997. Principles of applied geophysics, 5th Ed. Chapman and Hall.

Påsse, T., 2001. An empirical model of glacio-isostatic movements and shore-level displacement in Fennoscandia. SKB R 01-41, Svensk Kärnbränslehantering AB.

Press, F., Siever, R., 1998. Understanding earth, 2nd Ed. W. H. Freeman and Company.

Rhén, I., Stanfors, R., Wikberg, P., Forsmark, T., 1995. Comparative study between the cored test borehole KA3191F and the first 200 m extension of the TBM tunnel. SKB Progress Report 95-12, Svensk Kärnbränslehantering AB.

Rouhiainen, P., 2001. Difference flow measurements in the borehole KLX02 at Laxemar. SKB IPR 01-06, Svensk Kärnbränslehantering AB.

Sato, M., Mooney, H.M., 1960. The electrochemical mechanism of sulphide self-potentials.

Schlumberger Ltd., 2000. New York, New Tork, U.S.A.
Internet homepage: http://www.slb.com/ October 2000-10-18

Schön, J.H., 1996. Physical properties of rock: fundamentals and principles of petrophysics. Pergamon Press

SICADA. Site Characterisation Database System of Swedish Nuclear Fuel and Waste Management Co., SKB.

Skagius, K., 1986. Diffusion of dissolved species in the matrix of some Swedish crystalline rocks. Doctoral thesis at the Royal Institute of Technology, Stockholm, Sweden.

SKB, 2001. Platsundersökningar. Undersökningsmetoder och generellt genomförandeprogram. SKB R-01-10, Svensk Kärnbränslehantering AB.

Stanfors, R., Rhén, I., Tullborn, E-L., Wikberg, P., 1999. Overview of geological and hydrogeological conditions of the Äspö hard rock laboratory site. Applied Geochemistry Vol. 14, No. 7, p 819-834.

Stumm, W., Morgan, J.J., 1996. Aquatic chemistry, chemical equilibria and rates in natural waters. John Wiley and sons, Inc.

Taraxacum miljö media, 2000-10-18 Hässelby, Sweden
Internet homepage: http://www.taraxacum.com/ October 2000

Appendix 1

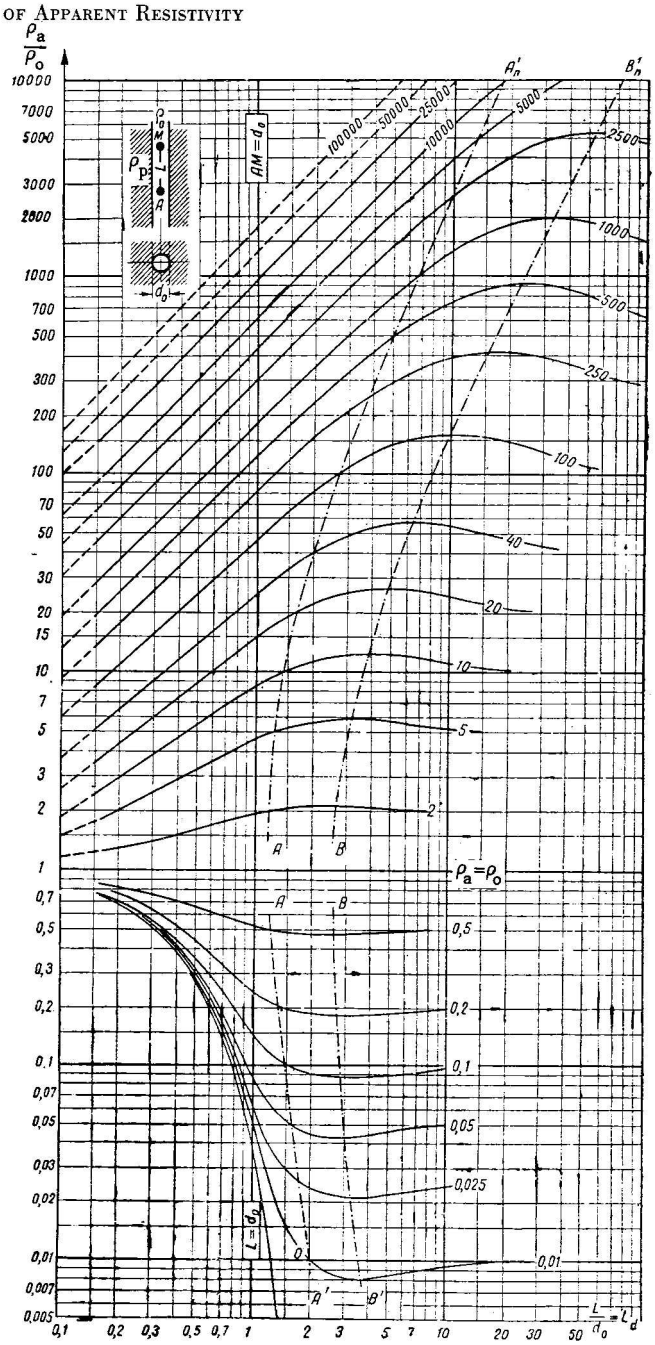

Figure 81. Departure curves for the normal array for ρ_a/ρ_0 as a function of L/d_0, with parametric values of ρ_P/ρ_0. The line AA′ is the locus of points at which the apparent resistivity equals rock resistivity. The line BB′ is the locus of the maxima or minima for each departure curve.

Correction chart for the normal array from Dakhnov, 1959. $L/(2r_0)$ is on the x-axis, ρ_a/ρ_0 is on the y-axis, and ρ_u/ρ_0 is the parametric value of the departure curves. No disturbed zone is taken into account.